
Budapest University of Technology and Economics

# DIPLOMA WORK

## FRICTIONAL SLIDING IN LIMIT STATE ANALASIS CODES OF MASONRY ARCHES

**YU MENG** (G6IELY)

*SUPERVISOR:*

DR. KATALIN BAGI, FULL PROFESSOR

DEPARTMENT OF STRUCTURAL MECHANICS

## Acknowledgements

The author is indebted to Dr Katalin Bagi for her active supervision, super patience and enthusiasm regarding such an interesting topic.

The author thanks Dr Peter Gorog for giving valuable technical advice about the program Archie-M and program RING.

The author thanks Mr. Shipeng Chen for the advice of program 3DEC and Mr. Xiaobao Hui for the use of program Archie-M and LimitState:RING.

Finally, by no means least, the author would like to thank her family and friends for their continued support and encouragement.

## Abstract

The most important computational programs available for the assessment of masonry arches are Archie-M, LimitState:RING and 3DEC. The first two programs based on limit state analysis are widely applied in the engineering practice and have a huge efficiency.

The diploma work to be presented simulated single span masonry arches with the three programs, where 3DEC was used as virtual reality. In 3DEC, each voussoir of the arch was represented as a deformable block jointed by dry contacts. Rotation and sliding of the masonry blocks as well as their deformations are allowed. 3DEC uses Coulomb friction models, which was non-associated since the dilation degree was set to zero, but RIGN uses an associated friction model, and Archie-M completely excludes from the analysis the possibility of sliding. The importance of effects like sliding, material crushing and block deformability had to be assessed by comparing the results provided by 3DEC, Archie-M and RING.

Arches with different geometries and different material properties behave differently. Three investigated variable parameters in this thesis are: i) number of blocks, ii) angle of embrace; iii) contact friction angle. In order to gain an understanding of the behavior of the arches themselves, no attempts were made to model the effects of fill, spandrel walls or any other construction details.

Each model was equilibrated under gravity first, and then a full width vertical “concentrated load” was applied to the arch. Failure loads and failure modes were investigated and recorded, and critical loads and their critical positions were detected. Arch behaviors in different parameters were concluded and the results in Archie-M, RING and 3DEC were compared.

Archie-M does not include sliding failure but RING does, and this led to differences in the failure modes. RING produced closer results to 3DEC than Archie-M modelling, not only for failure load, but also for failure mode.

*KEYWORDS*: Single span masonry arches, limit state analysis, discrete element method, frictional sliding, 3DEC, Archie-M, RING

# Content

# 1 Literature Overview

Masonry structures consist of individual units, like bricks, stones and so on, and joints between them. The joints can be dry or mortared. Masonry arch structures have a long history and an extensive use. Arch is the earliest and greatest invention in the field of architecture. The arch has been long used in masonry structures, most commonly in masonry bridges, masonry gates and aqueducts. *Figure 1.1* shows some examples.

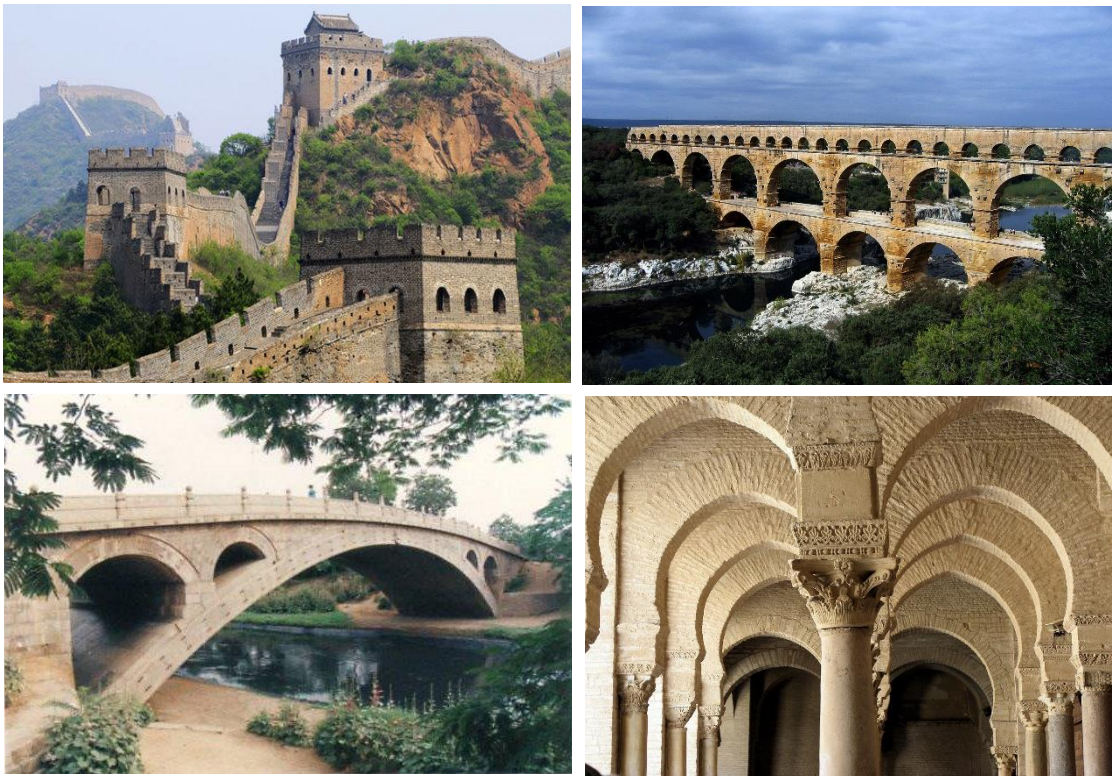

**Figure 1.1 Typical masonry arch structures: (a) semi-circular arches of brick construction at the Great Wall, China, 220-206 BC; (b) multiple arches of the Pont du Gard in Roman Gaul (modern in France); (c) segmental arch bridge of stone construction in Anji Bridge, China, 595-605; (d) Horseshoe arches in the 9th-century Mosque of Uqba, in Kairoua, Tunisia (https://hyperallergic.com/219284/the-great-wall-of-china-is-falling-apart/; https://www.pinterest.com/pin/352899320782715670/; http://stone-bridge.blogspot.com/2006/07/zhaozhous-bridge.html; https://www.pinterest.com/pin/505669864387506101/ )**

There are various types of arches, for example, triangular arch, lancet arch, equilateral pointed arch, shouldered flat arch, elliptical arch and Ogee arch (see *Figure 1.2*). In this thesis, I will discuss semi-circular arch and segmental arch, which are most widely used types in the world.

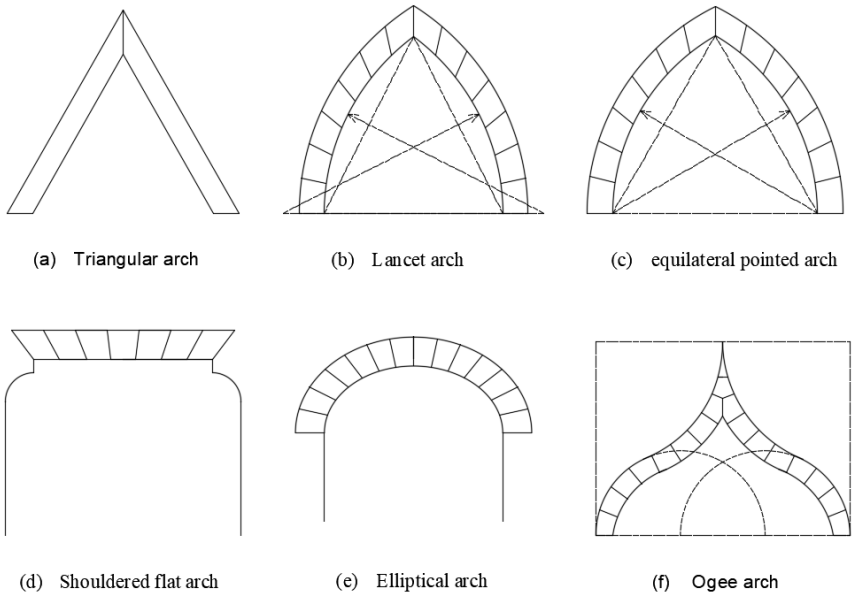


**Figure 1.2 Some types of arches**

Although masonry structures have been constructed and developed for a long time, their analysis is still a puzzle for engineers. Sometimes it appears nearly impossible to fully and correctly simulate and analyze an arch structure as the conditions may be so complicated. Masonry is a material with a discontinuous body (individual units and joints) and special mechanical properties (very high compression and very low tension), so that the behavior is totally different from that of elastic materials. *Figure 1.3* shows this property vividly with a highly localized stress percolation visible.

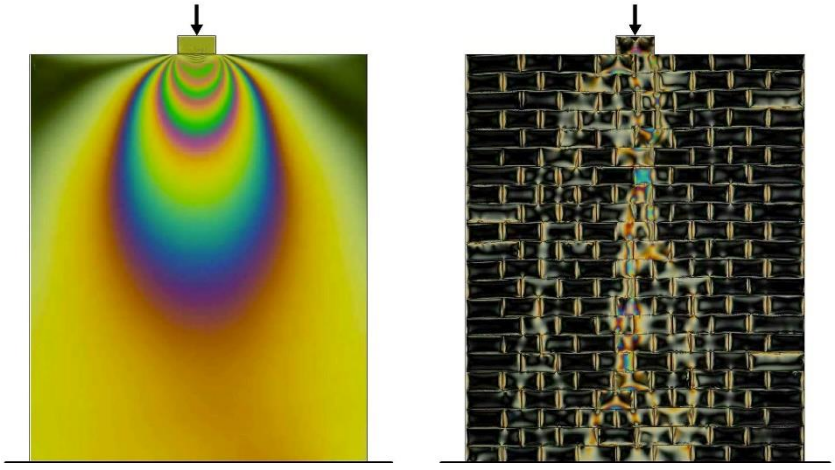

**Figure 1.3 A comparison between the stress diffusion in an elastic body (on the left) and a model of masonry (on the right) (Wikipedia)**

## *1.1 Heyman's Theory of Masonry Arches*

Heyman's theory of masonry structures is a very popular and recognized modern method to analyze the behavior of masonry arches. It was based on the limit analysis

of plastic structures (Selvam, 1993) and the idea Kooharian (1952) proposed, and was introduced by Heyman in a paper entitled "The Stone Skeleton" (1966). Heyman's theory puts emphasis on the question if the given structure can balance the given load or to find the range of load the structures can stand. Heyman analyzed the plasticity behavior of stone structures and made three assumptions about the material:

*(i) Stone has no tensile strength;*
*(ii) Stone has an infinite compressive strength;*
*(iii) Sliding failure cannot occur.*
*(Heyman, 1968)*

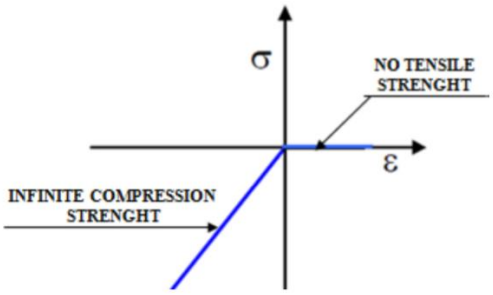


**Figure 1.4 Heyman's first two hypotheses (Lucio, 2014)**

There is also an implicit assumption that stone blocks have infinite stiffness, which assures that the geometry of structures remains the same for any load. Although the assumptions were for stone, they can be used for all the masonry materials.

### *1.1.1 Static Theorem*

According to Kooharian (1952), "*It states that collapse will not occur in the structure if at each stage of loading, a safe, statically admissible state can be found*."

The static theorem, also called safe theorem, aims to find an upper bound value of loading that can maintain the equilibrium of the structure. Firstly, there should be an equilibrium state such as the internal forces equilibrate the external forces, and the thrust line, which shows the path of the resultants of the compressive forces, should be within the cross-section of the arch. Once the thrust line passes outside of the cross-section, we say the arch collapses, as that means tensile stresses should appear in the arch, which it cannot resist.

When the thrust line is just at a surface point, a hinge develops at that point. Hinges appear at the intrados or extrados. When the number of hinges is big enough, a mechanism of collapse develops. For arches, usually four hinges make the structure fail. At collapse the arch forms a 4-bar mechanism.

Usually, masonry arches are used to support two main types of loads: selfweight and live load. *Figure 1.5 (a)* shows a thrust line in the arch under its selfweight. In the figure that situation is shown when the thickness is just small enough to produce five contacts between the thrust line and the arch, developing five hinges shown in *Figure 1.5 (b)*

(five instead of four, because of the symmetry). The structure cannot find an equilibrium for smaller thickness and collapses. The thickness *t* belonging to this state is the minimum thickness of stable arches of the span *2R*. This problem to determine the minimally thickness to carry selfweight is called "Couplet-Heyman problem", which will be introduced later.

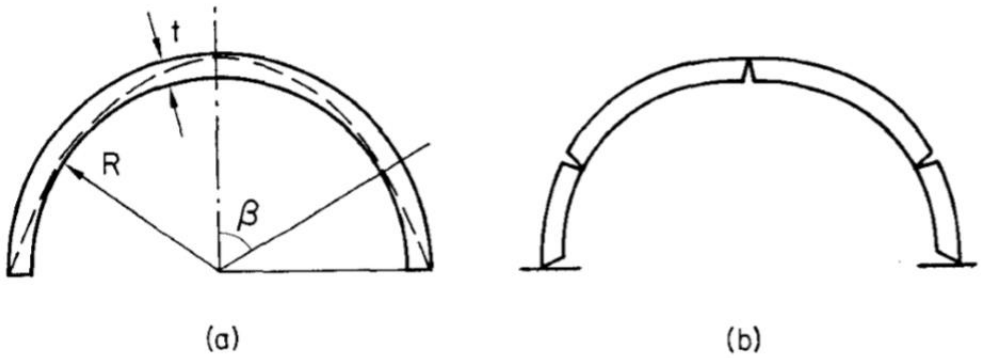


**Figure 1.5 Semicircular arch of least thickness (Heyman, 1968)**

Adding an additional live load, an arch could collapse due to a similar loss of stability. *Figure 1.6* shows an example. The sufficiently large non-symmetrical live load makes the thrust line out of the arch and four hinges are generated in the alternating intrados and extrados.

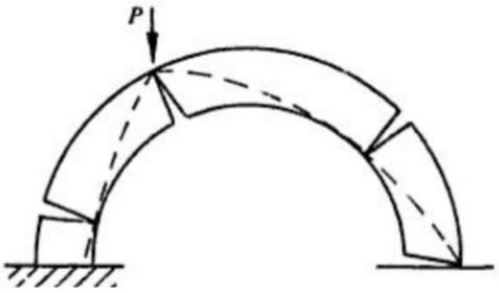


**Figure 1.6 Live load generating the fourth hinge (Lucio, 2014)**

### *1.1.2 Kinematic Theorem*

Kooharian (1952) formulated this theorem in the following way: "*collapse will occur (or will have occurred previously) if a kinematically admissible collapse state can be found*" (the meaning of the term "kinematically admissible collapse state" is explained a few rows below).

The kinematic theorem, also named unsafe theorem, leads to the conclusion that the arch will become a mechanism when suitably located four hinges are formed in the structure. Thus, we can assume the sufficient number of hinges in the structure and apply a "virtual displacement". Then calculate the work done by external forces and the work done by internal forces and satisfy. Taking only live load (with live load multiplier $\lambda_u$) into consideration:

$$\lambda_u \int_{Sq} q_{i0} v_i^u \, dS \geq \int_V \sigma_{ij}^u \dot{\varepsilon}_{ij}^u \, dV$$

where $\lambda_u$ refers to the kinematically admissible unstable load multipliers, i.e. such a load multiplier for which the structure collapses.

For rigid blocks as assumed in Heyman's theory, the internal work is always and automatically zero, as the stone blocks have infinite stiffness.

$$\int_V \sigma_{ij}^u \dot{\varepsilon}_{ij}^u \, dV = 0$$

$$\lambda_u \int_{Sq} q_{i0} v_i^u \, dS \geq 0$$

Solving the equation $\lambda_u \int_S q_{i0} v_i^k \, dS = 0$, a load multiplier can be calculated. Different positions of hinges on an arch can be set, and different mechanisms can be found, respectively. These mechanisms, i.e. those situations when a positive work is done by the loads, are called kinematically admissible collapse states. As a result, the kinematic theorem gives several solutions. The lowest load multiplier is to be found, which represents an upper bound value of failure loading for a structure. The corresponding mechanism is the one which makes the arch collapse.

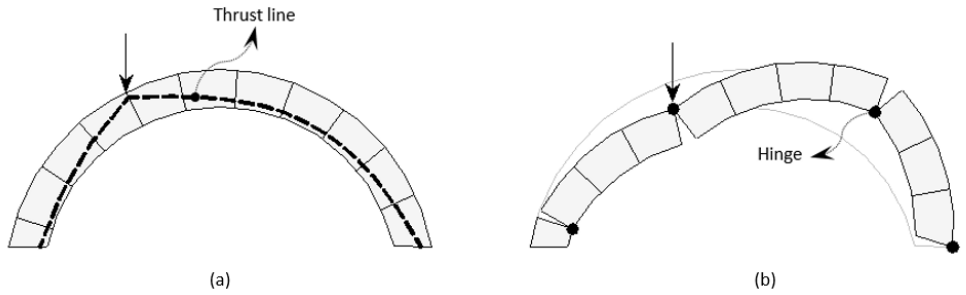


**Figure 1.7 Limit analysis to a masonry arch: (a) Static theorem; (b) Kinematic theorem (Nuno Mendes, 2015)**

In summary, by applying the static theorem, equilibrium conditions should be satisfied, and the load multiplier is less than or equal to the failure load. Then a lower bound value of loading for the structure is determined. Conversely, in kinematic theorem, a mechanism condition is found, and the load multiplier is larger than or equal to the failure load. So, an upper bound value of failure loading can be determined.

## *1.2 Failure of circular arches*

### *1.2.1 Under selfweight*

As what is mentioned above, arches may fail due to the insufficient of the ring thickness, when tensile stresses occur in the cross section. So, a minimally necessary thickness for equilibrium of a circular arch should be determined. The is the Couplet-Heyman problem.

Some assumptions were made in the Couplet-Heyman problem:

(i) Circular arch with uniform thickness is analyzed;
(ii) Infinitely dense radial contacts;
(iii) Arch can only fail by hinging; sliding and material crushing are excluded.

The failure mode is shown in *Figure 1.8* below, where $\beta$ refers to the angles from hinge A to B, and $\alpha$ refers to that from hinge A and C.

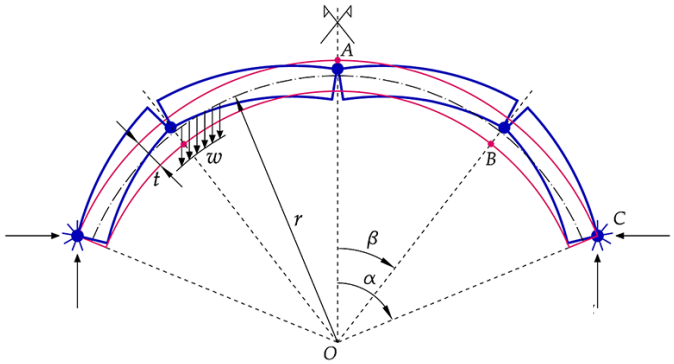


**Figure 1.8 Stretch of a symmetric circular arch subjected only to its own weight, with a symmetric five-hinge rotational collapse mechanism (Cocchetti et al, 2011)**

Several solutions for semicircular arch are given by different people with different methods. Couplet (1730) assumed that the hinge B would appear at a position $\beta = 45°$ and used elementary statics method to calculate a just failing arch. The minimum thickness he got is approximately 0,101 times the radius of middle axis ($r$ in *Figure 2.7*). Milutin Milankovitch (Foce, 2007) treated the thrust line theory from both a mechanical and mathematical point of view. He implicitly and instinctively applied the statical theorem (still not known at that time), and calculated the hinge position and minimally necessary thickness for selfweight. The results are:

$$\beta(90°) \approx 54{,}5°, t_{min}(90°) \approx 0{,}1075 \cdot r$$

Heyman(1967) found unique equilibrium force system while minimizing the ring thickness. The solution given by Heyman is:

$$\beta(90°) \approx 58{,}8°, t_{min}(90°) \approx 0{,}106 \cdot r$$

Cochetti at al gave a corrected analytical solution avoiding two mistakes Heyman had committed, and simulated the problem with the discrete element code DDA (Discontinuous Deformation Analysis, which will be introduced in section 2.1.2) models in 2011. They received the analytical solution and confirmed with the simulations:

$$\beta(90°) \approx 54{,}5°, t_{min}(90°) \approx 0{,}1074 \cdot r$$

### *1.2.2 Under live load*

Applying a live load, the arch collapses when a mechanism is formed. Failure of an arch may occur due to hinging, sliding, material crushing and cracking.

Boothby et al made a conclusion for possible failure in single-ring arch without material crushing (*Figure 1.9*). Sarhosis et al considered the possible crushing and cracking, which is shown in *Figure 1.10*. The failure mode depends on so many effects (like the exact position of the arch, material characteristics, exact geometry and stereotomy etc.) that each case has to be analyzed individually, with any of those methods that will be summarized in the next section.

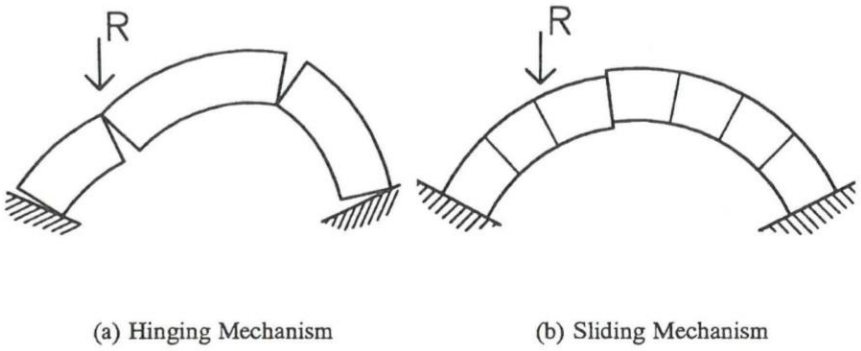


**Figure 1.9 Collapse mechanisms of a masonry arch with rigid abutments (Nuno Mendes, 2016)**

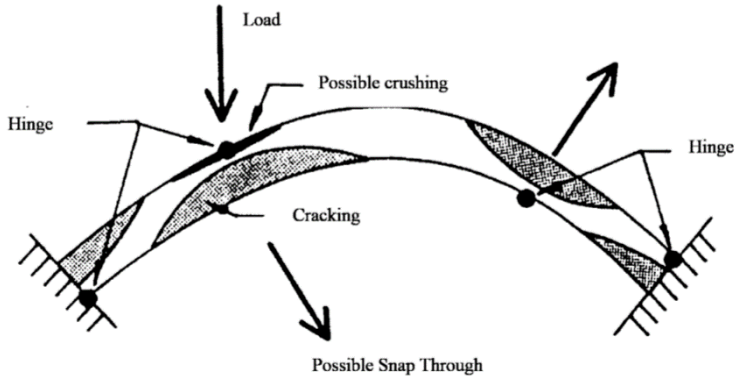


**Figure 1.10 Failure modes in masonry arch bridges (Sarhosis et al, 2016)**

# 2 Computational Methods

As far as my thesis project is concerned, the recent computational methods of stability analysis for arches can be roughly classified into five categories: graphic static method, empirical methods (such as MEXE), finite element method (FEM), discrete element method (DEM) and limit state analysis (LSA), based on both static theorem and kinematic theorem.

Graphic static method, assuming the structure is rigid and no change in form when subjected to the action of forces, looks forward to a solution of static equilibrium problems by means of accurately constructed geometrical figures. The magnitude, direction and line of action of a force are represented by the length, inclination and position of a straight line. The unknown quantities required are obtained directly from the figures by scaling lines and angles. An example is shown in *Figure 2.1*. In (a) weights of different blocks and the thrust line are indicated on the random arched structure. In (b) the internal forces of one block are shown and closed in a force polygon in (c). The total force polygon for all the blocks is shown in (d).

The MEXE (Military Engineering Experimental Establishment) method is a traditional technique which uses empiric calculations to assess the load carrying capacity of masonry arch bridges. It is still widely used in the practice for relatively simple bridges. In the last twenty years, FEM developed quickly, and was applied to the analysis of masonry arch bridges. The discrete nature of the masonry collection cannot be reflected in FEM and it is difficult to simulate the contact separation and sliding. What's more, with the deformations of masonry structures, changes in geometry will occur, but new contacts cannot be taken into consideration in FEM.

In this chapter, DEM and LSA are introduced in detail, with a particular emphasis on three commercial software – 3DEC, Archie-M and RING, which are widely used in the modern analysis of masonry arch bridges. They will be used in my later simulations and calculations.

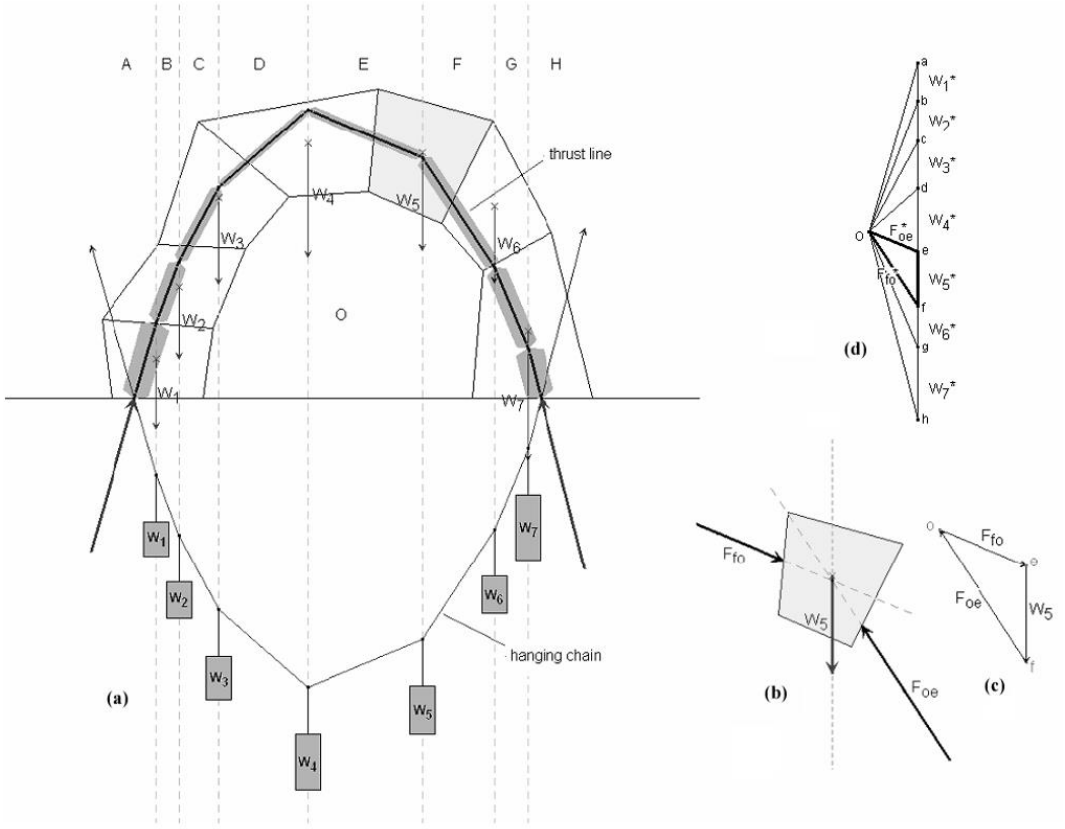


**Figure 2.1 Thrust line in a random arched structure (Block, DeJong et al, 2006)**

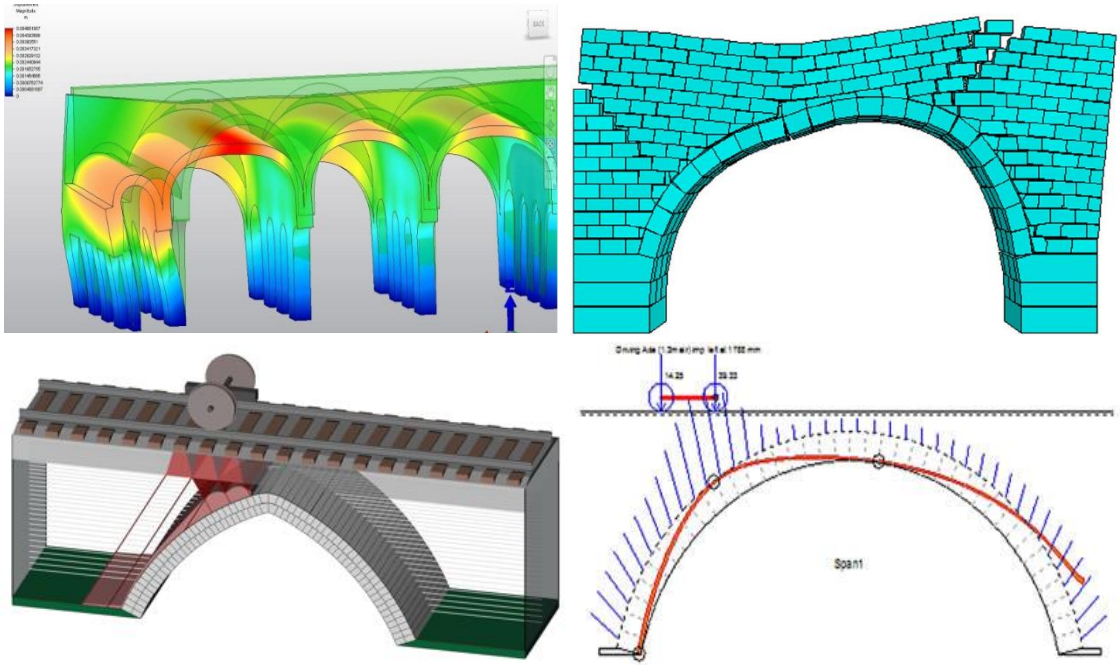

**Figure 2.2 Several arch models in computational methods: Finite element method model (*i*); Discrete element method model (*ii*); Limit state analysis - RING model (*iii*); Limit state analysis - Archie-M model(*iv*) (http://www.portusproject.org/methods/computer-graphics/structural-analysis/; Lemos 1998; http://www.limitstate.com/news/limitstate-ring-3-preview; http://www.obvis.com/archie-theory/)**

## 2.1 Discrete Element Method

Discrete element method was first presented by Peter A. Cundall in his thesis titled "The measurement and analysis of accelerations in rock slops" in 1971.

A numerical technique is said to be a discrete element model if:

*- it consists of separate, finite-sized bodies, so-called discrete elements, each of them being able to displace independently from each other, so the elements have independent degrees of freedom;*

*- the displacements of the elements can be large;*

*- the elements can come into contact with each other and loose contact, and these changes of topology are automatically detected during the calculations. (Bagi, 2012)*

As we can see, the main advantage of DEM over FEM is that it can be applied for discontinuous model. Structures can be assumed as a collection of finite-sized individual elements, such as bricks and granules. The elements are connected with joints. So, the discrete element method can simulate masonry structure and particulate matter better than FEM.

Every DEM model can be seen as the collection of separate elements and their contacts. The elements can be rigid or deformable and shapes of the elements vary: convex or concave, smooth or nonsmoothed, polyhedral, spherical, elliptical and so on. When two elements are in contact, contact forces are formed and can be transmitted from one to the other. The constitutive relations can be specified.

When the initial geometry and properties of elements and contacts are defined, boundary conditions, external load and/or prescribed displacements should be set by the users. Based on these data, the displacement increments are determined. The state of the system is history dependent, new contacts may be formed and calculations will be performed a lot of times. Two main kinds of time integration methods can be applied: explicit or implicit time integration. The main difference between them is that the explicit methods do not check whether the calculated equations of motion are satisfied at the end state in a time interval, but the implicit methods check it. As a result, explicit methods are less time-consuming and implicit methods are more numerically stable.

In the following part, the most widely used codes in DEM (3DEC, DDA, CD) are introduced.

### 2.1.1 3DEC

3DEC (Three-Dimensional Distinct Element Code) is a commercial program which is an extension of the 2-dimensional code UDEC of P.A. Cundall. They are both developed by Itasca and widely applied in the engineering practice for masonry structures and for rock mechanics problems.

3DEC can simulate both quasi-static and dynamic response to loading. It has the following main features:

- blocks can be rigid or deformable,
- suitable contacts behaviors can be defined by parameters like joint normal and shear stiffness properties etc.,
- an explicit time integration procedure is applied to find the solutions.

### *The elements*

The shape of the elements in 3DEC is polyhedral. The elements may be convex or concave. The elements can behave in a perfectly rigid way or as deformable blocks. For rigid blocks the elements have six degrees of freedom (three translational and three rotational). Deformable elements are divided into simplexes (tetrahedral) by bisecting planes. The vertices of the simplexes are nodes and 3D domains (Voronoi-cells around the nodes) are assigned to these nodes. Each node of the blocks has three translational DOFs, which means the deformable elements have 3*n* DOFs, where *n* represents the number of nodes.

Usually, for simulating masonry structures, especially rock or brick structures, the geometry of the model should be prepared in detail as individual blocks must be set detailed to model the whole structure.

### *The contacts*

In order to recognize the contacts between discrete elements, the software should check all the possible pairs at first, where a method called Cell Mapping and Searching is used in 3DEC. *Figure 2.3* illustrates the logic for Cell Mapping and Searching in 3DEC. First map all the blocks in block envelop into a cell space with identification numbers and entries. By mapping them, the neighboring elements can be found much easier. Note that the searching space is increased in all directions by a tolerance, so that all blocks within the given tolerance can be found.

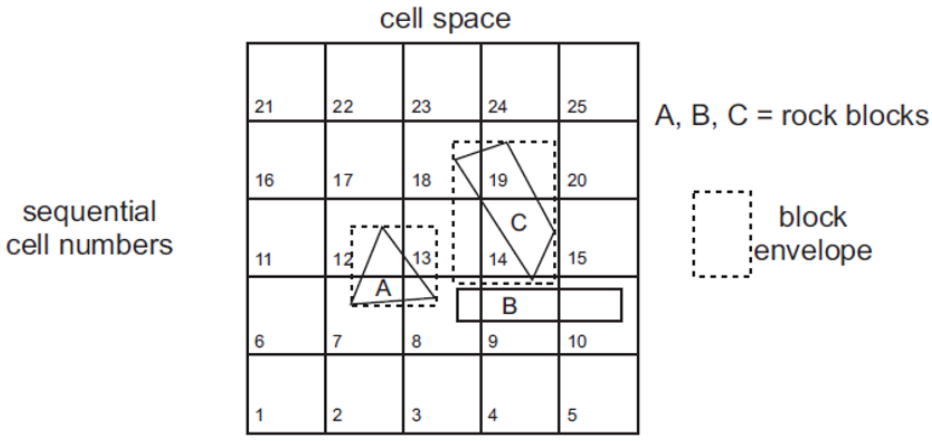


**Figure 2.3 Block mapping to cell space (Itasca Consulting Group, 2003)**

As the simulating process is history dependent, new contacts may form repeatedly. Moreover, the number of the elements is usually large. This step can be really time-consuming.

After finding the neighboring elements in pairs, we can determine the type of contacts (see explanation below). The analysis consists of two parts, determining a "common-plane" and testing both blocks separately for contact with the common-plane. The common-plane is, by definition, that plane which minimizes the overlap and maximizes the gap between two discrete elements, so that, in some sense, it bisects the space between the two blocks.

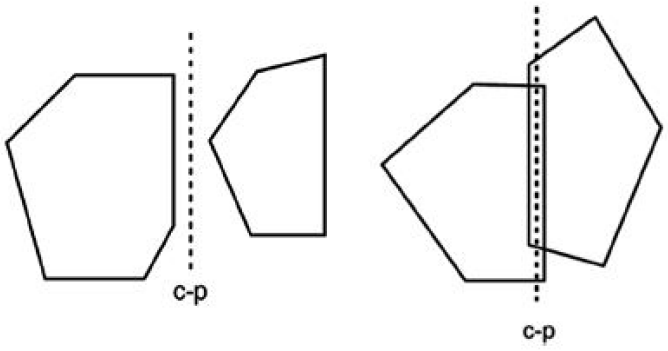


**Figure 2.4 Common-plane in 2D (Itasca Consulting Group, 2007)**

A contact is formed when two elements overlap each other. In two dimensions, which is not the topic of my thesis, topologically three types of contacts exist, (i) edge-to-edge contact, (ii) corner-to-edge contact, and (iii) corner-to-corner as shown in *Figure 2.5*.

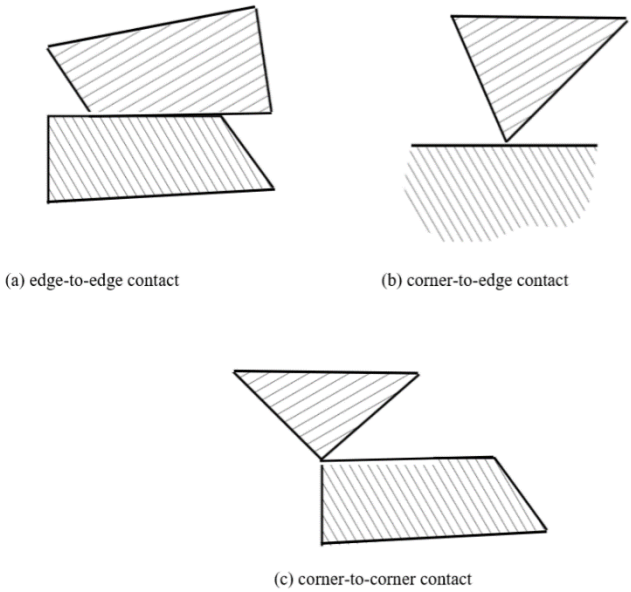


**Figure 2.5 Three types of contacts in 2D (Mohammad, 2010)**

When it comes to 3DEC (three dimensions), the contact types are extended to 7 types: face-to-face, edge-to-face, corner-to-face, edge-to-edge (intersecting), edge-to-edge (along each other), corner-to-edge and corner-to-corner.

For the convenience of calculation, sub-contacts are made by discretizing the common-plane. Block faces are discretized into triangles containing surface nodes. For rigid blocks, these sub-contacts are generally created at the vertices of the block face. For deformable blocks, there are a number of surface nodes in the triangular faces. Each node has three independent degrees of freedom. There are two types of sub-contacts: vertex-to-face and edge-to-edge.

In the *k*-th contact, the deformation increment of a sub-contact during $\Delta t$ is calculated using the node deformation increment minus the deformation of the coincident point on the opposing face. The deformation increment is decomposed into a normal and a tangential deformation, $\Delta u_n^k$ and $\Delta u_s^k$.

As for the constitutive law of the contacts, Coulomb-type frictional model is the most widely used one which constrains friction forces on every contact, depending on the magnitude of the applied normal force. The surface-distributed force transmitted through the sub-contact is decomposed into a normal and a tangential component, denoted by $\sigma_n^k$ and $\sigma_s^k$, respectively. The increment of normal and tangential distributed forces can be determined by the formula below:

$$\Delta\sigma_n^k = k_n^k \Delta u_n^k$$

$$\Delta\sigma_s^k = k_s^k \Delta u_s^k$$

where $\Delta u_n^k$ and $\Delta u_s^k$ are the increment of the normal and tangential relative translations in contact *k*; $k_n^k$ and $k_s^k$ are the normal and shear stiffnesses of the contact *k*.

### *The equations of motion*

In 3DEC, elements are made deformable by subdivision into finite elements, which is in some sense similar to finite element methods. All calculations are performed on Voronoi-cell which is shown in *Figure 2.6* (two-dimensional). Masses denote the mass of the Voronoi-cell of the node (blue zone) and forces are the resultant of the distributed forces acting on the Voronoi-cell of the node.

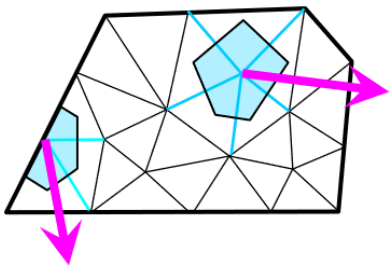

**Figure 2.6 Polyhedral element subdivided into simplexes and Voronoi-cell (Bagi, 2012)**

The kinematics of deformable discrete elements of 3DEC can be described by the translations of the nodes of its simplexes and are based on Newton's second law. Suppose there are *N* nodes in all elements, and the *p*-th node belongs to the whole block. The equations of motion for the *p*-th node can be written in the form

$m^p(t)\boldsymbol{a}^p(t) = \mathbf{f}^p\big(t, \mathbf{u}(t), \mathbf{v}(t)\big)$.

The complete system of the equations of motion is:

$\mathbf{M} \cdot \mathbf{a}(t) = \mathbf{f}\big(t, \mathbf{u}(t), \mathbf{v}(t)\big)$.

For rigid blocks, the equations of motion can be written in two parts, the translational and rotational motion. The two equations of motion for the *i*-th block can be written in the form

$$m_i(a_i + \alpha v_i - g_i) = f_i$$

$$I(\dot{\omega}_i + \alpha\omega_i) = M_i$$

where
- $a_i$ the acceleration of the centroid of the block
- $v_i$ the velocity of the centroid of the block
- $\alpha$ the viscous (mass-proportional) damping constant (will be explained later)
- $f_i$ the forces action on the block (contact forces, external forces and gravitational forces)
- $m_i$ the mass of the block
- $g_i$ the gravity acceleration vector
- $\dot{\omega}_i$ the angular acceleration about the principal axes
- $\omega_i$ the angular velocity about the principal axes
- $M_i$ total torque
- $I$ approximate moment of inertia

### *Time integration*

The program uses an explicit solution scheme. When considering a time interval, the end displacement and velocity values are determined by the starting values. When the end values are obtained, this technique does not check whether the equations of motion are satisfied at the endpoint of the actual interval. The calculated values are just used as the following time interval at the start point.

3DEC uses the method of central differences, in which the discrete approximation of a specific equation of motion of *p*-th node in the ($t_i$, $t_{i+1}$) time interval is:

$$m^p \frac{\mathbf{v}^p_{i+1/2} - \mathbf{v}^p_{i-1/2}}{\Delta t} = \mathbf{f}^p_i.$$

The state at time $t=t_i$ is known, and the state at $t_{i+1}$ can be calculated

$$\mathbf{v}^p_{i+1/2} = \mathbf{v}^p_{i-1/2} + \Delta t \cdot \frac{1}{m^p}\mathbf{f}^p_i,$$

$$\mathbf{u}_{i+1}^{p} = \mathbf{u}_{i}^{p} + \Delta t \cdot \mathbf{v}_{i+1/2}^{p},$$

where $\mathbf{v}_{i-1/2}^{p}$ and $\mathbf{v}_{i+1/2}^{p}$ is the approximation of the function $\mathbf{v}(t)$ of $p$-th node in the middle point of the interval $(t_{i-1}, t_i)$ and $(t_i, t_{i+1})$.

For there is no checking for the predicted values, numerical instabilities may occur. So, the time step should be adequately small to ensure the numerical stability.

### *Damping*

In physics, damping is the effect which reduces the amplitude of vibrations by dissipating kinetic energy. Damping used in computation process has the effect to reduce the dynamic vibration of the system and the unrealistic numerical oscillations around the exact solution. The applied damping methods help to increase the numerical stability of the engineering problems.

Two kinds of damping models are used in 3DEC: adaptive global damping and local damping. Adaptive global damping is proportional to the magnitude of velocity. The value of it should be modified constantly with coefficients to ensure that the calculated change of kinetic energy in a timestep is cut according to the user-requested ratio. If a system tends to be equilibrated so that the velocities do not change significantly any more, the adaptive global damping gradually decreases. When an equilibrium state is found, the damping becomes zero.

In local damping a force is added to the unbalanced force vector (i.e. the load vector acting on the nodes or on the rigid elements) in the equations of motion, and will be considered to reduce the unbalanced forces to help the solution to get convergence. It helps to decrease accelerating motions, while steady-state solutions are not affected.

During my work, adaptive global damping was used with a default value of damping coefficient ($\alpha$=0,5) in 3DEC. It means that the kinetic energy will be cut back by 50% if the node is not equilibrated. The kinetic energy dissipation is simulated and a solution will be found in less time than that of simulation without damping.

### *Applications*

3DEC is particularly well suited to simulate blocky structures, such as stone masonry arches. There are several important assessment experiments in the 1990s, which indicated the importance of the development of DEM, and in the meanwhile, did some efforts to study masonry structures and rock mechanics.

Till today, 3DEC has become the most widely used discrete element method code in the engineering practice of masonry structures and rock fracture mechanics.

### 2.1.2 The DDA Model

The discontinuous deformation analysis (DDA) method was first presented as an idea to determine the deformed configuration of a block from a series of measured displacements and deformations (Goodman and Shi, 1985). Then the method was extended to analyse the deformation of a discontinuous block system (Shi, 1988), with uniform polygonal elements, having undeformable contacts that transmitted forces between the elements.

#### The elements

The DDA method is somewhat quite similar to 3DEC at first sight. The shape of elements is also polyhedral, but in addition to the translation and rotation as a rigid body (6 degrees of freedom), a uniform deformation field also belongs to the element. All together there are 12 DOFs in a DDA element. Similarly, a uniform stress field should be considered when it comes to reduced force vector of an element.

$$u^p = \begin{bmatrix} u_x{}^p \\ u_y{}^p \\ u_z{}^p \\ \varphi_x{}^p \\ \varphi_y{}^p \\ \varphi_z{}^p \\ \varepsilon_x{}^p \\ \varepsilon_y{}^p \\ \varepsilon_z{}^p \\ \gamma_x{}^p \\ \gamma_y{}^p \\ \gamma_z{}^p \end{bmatrix} \qquad f^p = \begin{bmatrix} f_x{}^p \\ f_y{}^p \\ f_z{}^p \\ m_x{}^p \\ m_y{}^p \\ m_z{}^p \\ V^p\sigma_x{}^p \\ V^p\sigma_y{}^p \\ V^p\sigma_z{}^p \\ V^p\tau_x{}^p \\ V^p\tau_y{}^p \\ V^p\tau_z{}^p \end{bmatrix}$$

where $u^p$ is the generalized displacement vector of element $p$ and $f^p$ is the generalized reduced force vector of element $p$.

#### The contacts

In DDA, the contacts are assumed to be rigid due to a penalty-constraint approach. In the penalty method, contact springs constrain the overlapping of two elements, as Coulomb-friction gives a limit to the tangential force magnitude. As a result, no overlapping or interpenetration of blocks is allowed.

The Mohr-Coulomb joint failure criterion is used in DDA method. Three types of contact states exist:

(i) Free contact if the normal reduced force is positive, in this case the values of forces will be modified to zero.

(ii) The normal component of the contact force is compressive and the friction (the tangential reduced force) is constrained and when it reaches the biggest

magnitude, the blocks will slide. The sliding force is rearranged from the known normal contact force.

(iii) The normal component of the contact force is compressive and the tangential component of the contact force doesn't reach the biggest value. In this case, no sliding between the two elements and the reduced forces is calculated according to the Mohr-Coulomb criterion.

### *The equations of motion*

The equations of motion in DDA are derived by the principle of minimization of Hu-Washizu functional, in which kinetic energy is taken into account. Note that don't neglect the potential energy of the contacts.

$$\mathbf{M} \cdot \mathbf{a}(t) + \mathbf{C} \cdot \mathbf{v}(t) + \mathbf{K} \cdot \mathbf{u}(t) = \mathbf{f}^{ext}(t, \mathbf{v}(t), \mathbf{u}(t))$$

### *Time integration*

When solving the equations of motion, DDA uses an implicit time marching scheme, the Newmark-β method, which is totally different from 3DEC. Implicit methods are generally numerically stable and larger time-step size can be used. But the problem is that it may be more time-assuming than explicit calculations. In addition, when there are extensive topological changes (like in case of a sliding soil slope), a phenomenon called "open-close iterations" may occur, which leads to very time consuming simulations, see Bagi (2012) for details.

### *Comparison of DDA and 3DEC*

The differences between DDA and 3DEC are presented in the preceding sections. Now I summarize them:

- For DDA model, each element considers uniform stress and strain vectors while for 3DEC model, the deformations are either zero (rigid elements), or vary from tetrahedron to tetrahedron inside the element that is made deformable by being subdivided into simplexes.
- Deformable contact can be used in 3DEC and DDA while penalty-constraint (no overlapping) approach existed in early versions of DDA (in recent DDA versions the contacts are deformable).
- Explicit time integration is used in 3DEC while DDA uses an implicit method.
- Artificial damping is necessary in 3DEC to ensure numerical stability, but in DDA this is not necessary. If the user wants to simulate physical damping in DDA, damping can be included in the stiffness matrix.
- The equations of motion in 3DEC are based on Newton's second law while in DDA principle of minimization of Hu-Washizu functional.

### 2.1.3 The CD Method

The contact dynamics (CD) method, also called nonsmooth contact dynamics (NSCD), was presented by M. Jean and J. J. Moreau at the end of the 1980s. This method was first applied for the analysis of granular materials, and it showed a faster and more efficient approach than 3DEC to simulate the granular mechanics with a relatively large particle scale and implicit time integration. Also, in some dynamic problems such as earthquake analysis and sound waves testing, the CD method is very helpful.

#### *The pair of two elements and the contacts*

The method of contact dynamics is very different from the methods above (3DEC and DDA). The basic unit in CD is the pair of two randomly chosen elements, not a single element alone. Also, the interactions between pairs are described by very simple contact laws instead of constitutive laws. The contact laws will be introduced later.

Since the individual deformations of the grains are usually negligible in real problems, the elements in CD are modelled as perfectly rigid. For rigid elements, I will only discuss spherical ones in this thesis for the case of simplicity. The polyhedral elements are also widely used in many problems in CD.

An arbitrarily chosen pair of two neighboring elements is shown in *Figure 2.7*. If the gap distance between the two elements equal to zero, we say the two elements have a point-like contact. Note that elements cannot overlap each other in CD method.

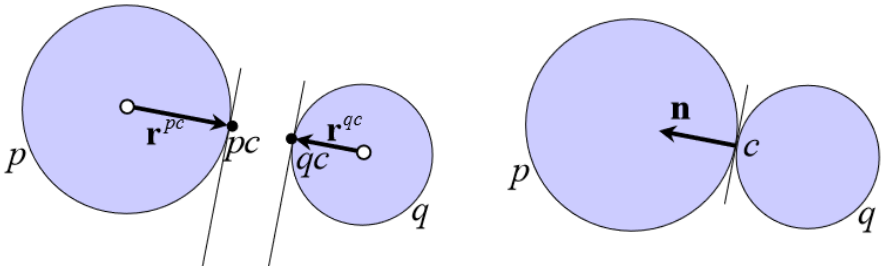


**Figure 2.7 The pair of two neighboring elements (Bagi, 2012)**

In addition to Cell Mapping and Searching introduced earlier, for a lot of elements, the potential contacts can be identified as the edges in a Delaunay triangulation where the vertices coincide with the particle centers (*Figure 2.8*). This method is usually conservative and time-consuming. The number of potential contacts may be larger than the real number of contacts. What's more, if the potential contact of the two colliding

particles is not recorded, particle penetration may occur. But the error is usually minor and can be reduced by decreasing the time step.

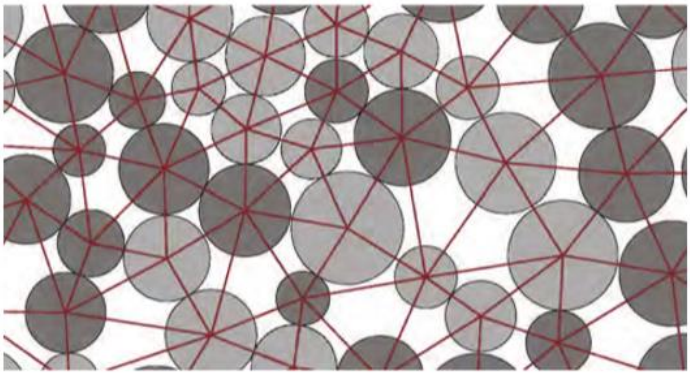

**Figure 2.8 Potential contacts as given by Delaunay triangulation (Krabbenhoft et al, 2012)**

### *Nonsmooth contact laws*

If there is a gap between the two elements, no force is activated and the normal force $f_n$ is identically zero (*Figure 2.9*). If the gap is closed, the normal force is a compression which can have any value which is necessary to satisfy the equations of motion.

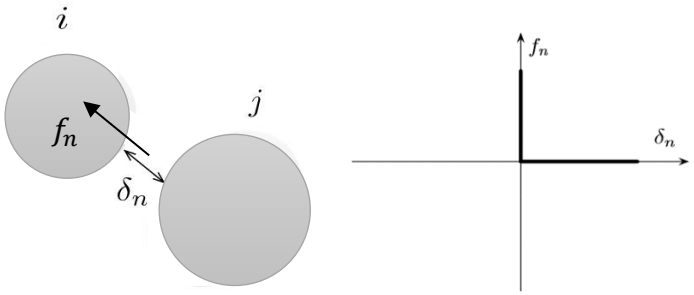


**Figure 2.9 A potential contact and Characteristics of Signorini's complementarity relation**

These conditions define a complementary relation, named Signorini's conditions, which can be shown in formula below:

$$\begin{cases} \delta_n > 0 \Rightarrow f_n = 0 \\ \delta_n = 0 \Rightarrow f_n \geq 0 \end{cases}$$

Notice that the normal force $f_n$ could only be negative i.e. compressional.

A contact is persistent if both $\delta_n = 0$ and $v_n = \dot{\delta}_n = 0$. Hence, Signorini's complementarity relation can be developed as follows:

$$\begin{cases} \delta_n > 0 \Rightarrow f_n = 0 \\ \delta_n = 0 \begin{cases} v_n > 0 \Rightarrow f_n = 0 \\ v_n = 0 \Rightarrow f_n \geq 0 \end{cases} \end{cases}$$

The friction also influences the model importantly. Coulomb's friction law is considered in the CD method, which determines the relationship between friction force $f_t$ and the sliding velocity $u_t$ at a contact point between two elements for dry friction (see *Figure 2.10*).

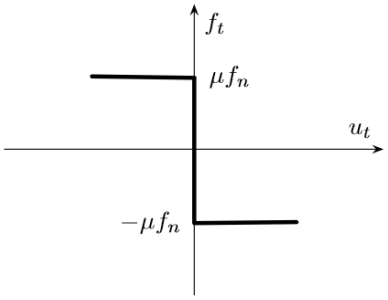


**Figure 2.10 Coulomb's friction law (Radjai and Richefeu, 2010)**

$$\begin{cases} u_t > 0 \Rightarrow f_t = -\mu f_n \\ u_t = 0 \Rightarrow -\mu f_n \le f_t \le \mu f_n \\ u_t < 0 \Rightarrow f_t = \mu f_n \end{cases}$$

Here we can see that the number of the unknown contact forces and their values in the model depend on the velocity (both normal and tangential component) of the contacts, just as the name "Contact Dynamics" literally suggests.

### *The equations of motion and the time integration*

In CD, the fundamental kinematical unknowns are time-dependent, just like in 3DEC or DDA. The velocities, positions and reduced forces vectors of the *p* and *q* pair are calculated by applying the implicit version of the Euler method, which can be written as:

$$\begin{bmatrix} \mathbf{v}_{i+1}^p \\ \mathbf{v}_{i+1}^q \end{bmatrix} := \begin{bmatrix} \mathbf{v}_i^p \\ \mathbf{v}_i^q \end{bmatrix} + \Delta t \cdot \begin{bmatrix} (\mathbf{M}^p)^{-1} & \\ & (\mathbf{M}^q)^{-1} \end{bmatrix} \cdot \begin{bmatrix} \mathbf{f}_{i+1}^p \\ \mathbf{f}_{i+1}^q \end{bmatrix}$$

$$\begin{bmatrix} \mathbf{u}_{i+1}^p \\ \mathbf{u}_{i+1}^q \end{bmatrix} := \begin{bmatrix} \mathbf{u}_i^p \\ \mathbf{u}_i^q \end{bmatrix} + \Delta t \cdot \begin{bmatrix} \mathbf{v}_{i+1}^p \\ \mathbf{v}_{i+1}^q \end{bmatrix} .$$

$$\begin{bmatrix} \mathbf{f}_{i+1}^p \\ \mathbf{f}_{i+1}^q \end{bmatrix} := \begin{bmatrix} \mathbf{f}_{i+1}^{p,ext} + \sum_{(pk)} \mathbf{B}^{pk} \cdot \mathbf{f}_{i+1}^{pk} \\ \mathbf{f}_{i+1}^{q,ext} + \sum_{(qk)} \mathbf{B}^{qk} \cdot \mathbf{f}_{i+1}^{qk} \end{bmatrix}$$

where $v_i^p$ and $v_i^q$ are the velocities of *p* and *q* at $t=t_i$;

$u_i^p$ and $u_i^q$ are the positions of *p* and *q* at $t=t_i$;

$f_{i+1}^p$ and $f_{i+1}^q$ are resultants of the external and all contact forces acting on *p* and *q*;

$f_{i+1}^{pk}$ and $f_{i+1}^{qk}$ are resultants of the external and all contact forces acting on $p$ by $q$ and on $q$ by $p$, respectively;

$B_i^{pk}$ and $B_i^{qk}$ are the transition matrices;

$M^p$ and $M^q$ are the matrices where the mass and rotational inertia of the elements are collected.

Because the state of system at $t_i$ is known, thus, what we should do is to find the state of the system at $t_{i+1}$.

To find the state of system at time $t_{i+1}$, the contact dynamics method introduced the concept of "iterative solver", which is used to find the contact forces at $t_{i+1}$. The iterative solver will sweep along all pairs in the system one by one in a random order. Note that Cell Mapping and Searching scheme is used here.

When analysis the $p$ and $q$ pair, first assume that there is no contact force between them (no contact in $p$ and $q$ pair) and compile the reduced forces $f_{i+1}^{p}$ and $f_{i+1}^{q}$. Assume constant acceleration during the time interval, calculate the predicted position of $p$ and $q$. If the pair is indeed not in contact, the analysis of the pair is ended. If not, determine the contact force in the pair based on the equations of motion (and truncate the tangential force component if the friction limit is exceeded). The iterative solver has to be performed over and over again until the change in the forces becomes negligibly small and the forces belonging to $t_{i+1}$ are received.

By using an implicit time discretization, large time steps are allowed, which speed up significantly the time to find a result. The results derived are more reliable, and show better numerical stability than explicit time integration.

## *2.2 LSA: Archie-M*

Archie-M is a Windows software which helps with the analysis of masonry bridges and viaducts. It is developed by Obvis. The first version of Archie was built in 1984 by Bill Harvey and till now it has been developing in a long way. While there are so many unknows and intangibles in masonry structures and it is impossible to fully analyze masonry bridges in all details, the Obvis team tends to achieve a level of confidence that the structure is sound. Archie-M helps to explore possibilities rather than results.

Archie-M is based on Heyman's static theorem (hence it completely ignores the possibility of frictional sliding between the blocks), and does a thrust line analysis with the help of powerful calculators in computer, instead of tedious hand calculation. The possibility of material crushing is included by using a finite-width "thrust zone" instead of a zero-width thrust line. Archie-M carries out a form of equilibrium analysis. The aim of Archie-M is to simulate whether a specific load can be supported by the bridge,

and to estimate the collapse load, but it cannot be used to consider how the bridge will deform.

In the following part, the theory and model of Archie-M will be introduced.

### *2.2.1 Equilibrium*

*The basis of equilibrium analysis is set out by Heyman (The Masonry Arch, J Heyman, Ellis Horwood, 1980). It is based on the plastic theorems which were probably first developed in Hungary, but which were brought to Britain by Baker. (http://www.obvis.com/archie-theory/)* The details of plastic theorems can be seen in the preceeding section 2.1.

Based on the upper bound plastic theorems, Heyman set some equilibrium conditions to prevent the appearance of mechanism and used a large safety factor to simplify his solution. Archie-M follows some of Heyman's simplifications to do equilibrium analysis but not mechanism analysis.

*Figure 2.11* shows two hinging arrangements of an arch as built and as collapse. Three hinges appear when the arch is under selfweight but still safe, usually at the intrados at the crown and at the extrados near the springings (symmetrically). The whole system can be seen as a three-bar linkage (one bar is the ground). Applying a live load, the shape of thrust line changes. As the load increases and the load position changes, the arch may collapse, when the mechanism becomes a four-bar one with a new crack appearing. At collapse, the arch sways to one side.

The main difference between multi-span and single span bridges lies in piers. The movement of the pier which dues to a load applies to one span, can result in a reaction to the adjacent span.

Further to the resistance to the applied overturning forces by piers, the fill, backing and the spandrel walls above the arch will stiffen the arch.

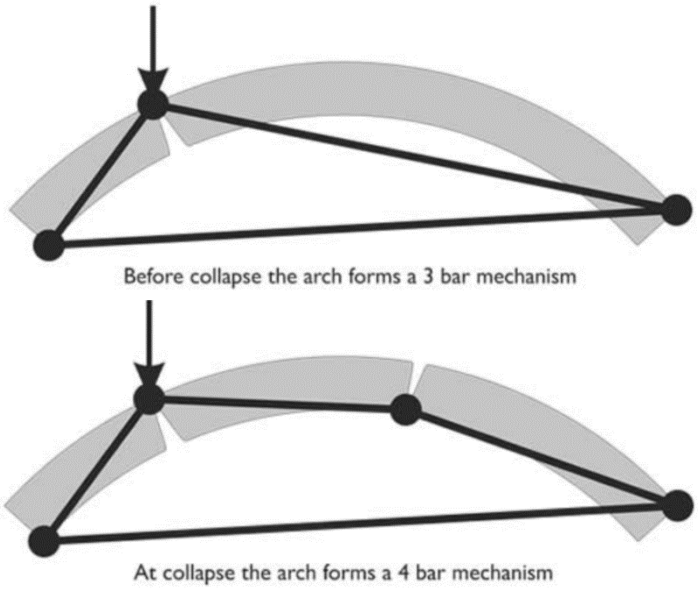


**Figure 2.11 Arch mechanisms (http://www.obvis.com/archie-theory/)**

### *2.2.2 The Thrust line analysis*

Based on Heyman's safe theorem (1966), a thrust line shows one possible statically admissible state of the arch bridge under load. When the thrust line touches the boundary of the arch, the arch collapses.

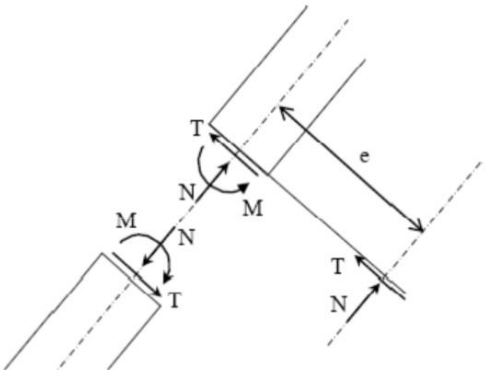


**Figure 2.12 Determination of thrust line (Nobile, 2014)**

Equilibrium analysis is applied to determine a thrust line in the structure, and to check whether the thrust line is inside the cross section. To determine a point of the thrust line, eccentricity (*e*) of force resultant and the relation between normal force and shear force are important. With these two parameters, position and slope of the thrust line in one cross section can be defined. As arch is a statically indeterminate structure, the solution is not unique. The thrust line analysis defined the load carrying capacity by limiting the zone where the resultant force can be positioned.

Heyman then proposed the concept of a geometric factor of safety (G.F.O.S.), which *gives an indication of how much larger the arch under consideration is in comparison to one that is just stable under the given loading pattern* (Gilbert, 2007). Harvey (1988)

extended the trust line to thrust zone, combining the safe theorem and geometric factor of safety. The physical meaning of thrust zone is a collection of effective cross-sections, which carry the load.

Archie-M uses thrust zone instead of thrust line. The thrust zone is based on consideration of the actual material crushing strength. As a result, material crushing is included as a possible failure mode of an arch.

### *2.2.3 Frictional Sliding*

Archie-M is based on Heyman's theory of masonry structures. One of the assumptions he made is that sliding between masonry units cannot occur.

Arch models in Archie-M is considered to be rigid and no sliding exists. Structures fail only by hinging mechanism or material crushing. Concerning the hinging mechanism, the arch fails because of the openness of contacts. Bagi (2014) summarized the Heymanian and Non-Heymanian contact displacements.

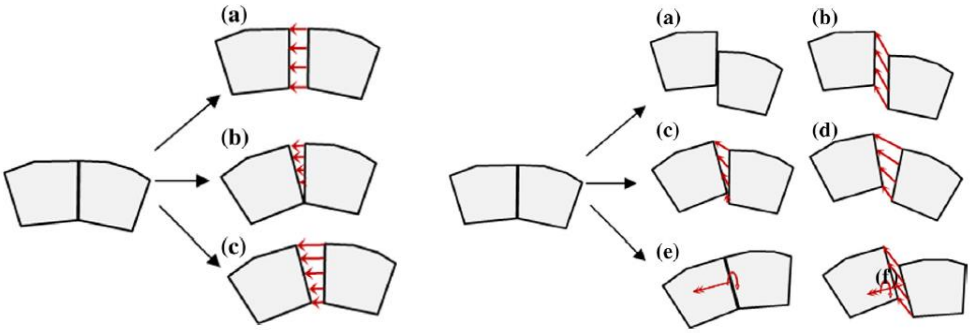


**Figure 2.13 Contact displacements: (i) Heymanian contact displacement; (ii) Non-Heymanian contact displacement (Bagi, 2014)**

### *2.2.4 Conservatism*

Archie-M is a conservative program following some of the simplifications of Heyman which uses a large safety factor. Partial factors can be reset by users, with default conservative values from BD 21/97.

***It (Archie-M) is of paramount importance, that any analytical approach can be demonstrated to be conservative****. This statement flies in the face of the suggestion from BA16 annex E that for assessment purposes, analytical results should lie in a band +- 20% from the true collapse load established by testing. (http://www.obvis.com/archie-theory/)*

### 2.2.5 Bridge Model of Archie-M

Single and multi-span bridges can be modeled in Archie-M, an object-oriented program. Users should determine the geometry, material properties and load conditions carefully when simulating a real bridge.

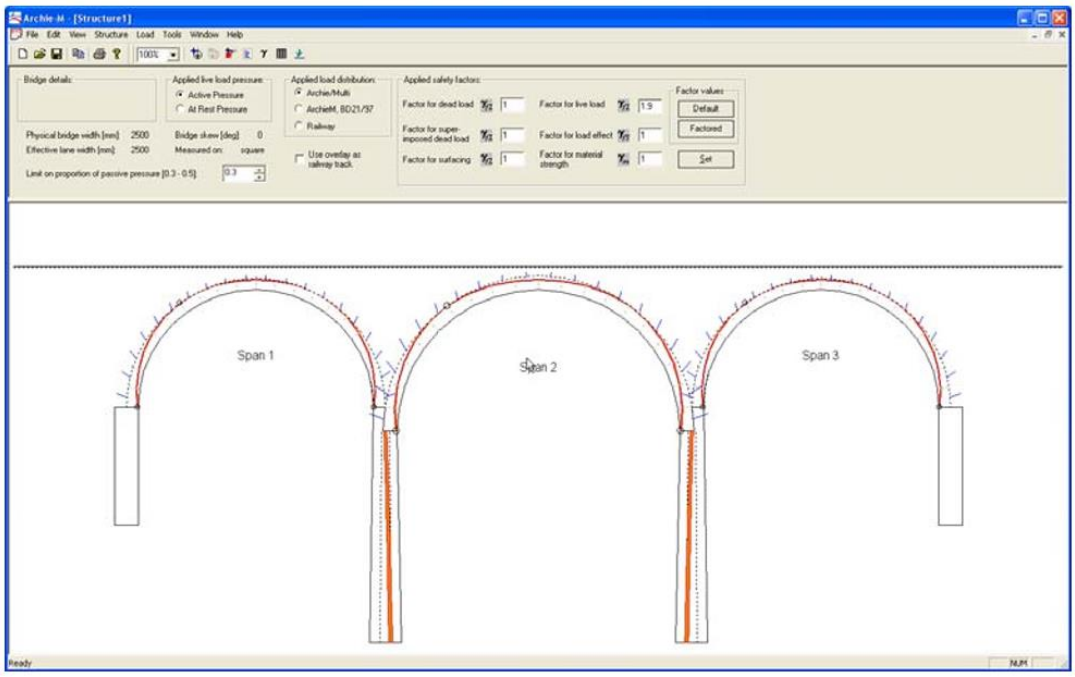


**Figure 2.14 A complex multi-span masonry bridge model in Archie-M (Obvis Ltd (2007))**

Several arch shapes are supported in Archie-M: circular, elliptical, three-centred, pointed, flat and true-shape which can be set by users by specifying some coordinates of the bridge.

The abutments are not obligatory to create, and the software will assume the necessary reactive forces, while the piers are necessary to be specified as the trust line will be shown in the pier model.

Archie-M model is an arch model with backfill and road on the arch. Similar to the arch shape, the road shape can be defined by different shapes or just use some points to define a fit curve. Two types of backing, flat-top and tangential ones, can be supported in Archie-M. Note that only the vertical component of the backing force is assessed by the software.

In summary, Archie-M can approximately take into account the geometry of the arch and the properties of arch, fill and backing, i.e. masonry strength, masonry unit weight, mortar loss (which is used in the analysis of old bridges) and the angle of friction ($\varphi$) of the fill unit. With or without extra live load, the program can calculate the thrust line and visualize it in the arch. If the trust zone does not excess the extra boundaries of the arch, the bridge is in a safe condition. In this way, we can determine the collapse load of the arch easily.

## 2.3 LSA: RING

RING is commercial software developed by the University of Sheffield spin-off company, LimitState Ltd. RING helps to analyze rigid-plastic arches, using a mechanism method in two-dimension. Different from Archie-M, RING would directly identify the collapse state, giving a result of minimum adequacy load factor and collapse mode (hinging, sliding or material crushing). In addition, the failure mode together with a thrust line would be represented on the screen. The program employs an efficient linear programming (LP) method, using mathematical optimization to find the minimum solution of virtual works equations.

The realism of computational model in RING was developed, considering the effect of sliding, soil-structure interaction and material crushing. Multi-span and multi-ring masonry arch bridges can be analyzed in this program, built of arch barrels, supports and backfill, while Archie-M cannot analyze multi-ring arches.

### 2.3.1 LP Limit Analysis method

Livesley (1978) proposed a discrete limit analysis model for masonry structures. In RING, an arch is assumed to be a collection of rigid blocks connected by joints. The mechanism method combines the upper bond and the lower bond theorems and is solved by linear programming efficiently. RING considers only associated friction, which means the contact dilation angle is equal to the friction angle in the contacts. As a result, the upper and lower bound solutions for finding the failure load multiplier are equal, which is presented graphically in *Figure 2.15*. In this way, a unique solution can be found. However, it is important to emphasize that in reality the friction angle of a contact between masonry blocks (typically about 35-45°) is not equal to the dilation angle (around 0-10°), so the application of associative contact failure model is not really realistic.

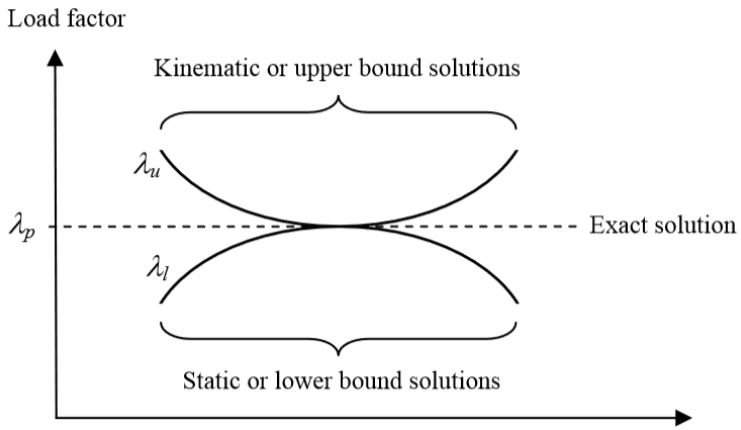


**Figure 2.15 The relationship between upper and lower bound solutions in RING (Gilbert, 2014)**

A joint equilibrium formulation, which is used to find the adequacy factor, can be solved by LP algorithms. The formulation is shown below.

Assuming there are *b* blocks and *c* contact surfaces in an arch, contact and block forces are shown in *Figure 2.16*. The problem to find a collapse load factor is to find the maximum value of load factor based on static theorem, i.e.:

$$\text{Max } \lambda$$

Equilibrium constraints:

$$\mathbf{Bq} - \lambda \mathbf{f}_L = \mathbf{f}_D$$

where B is an equilibrium matrix (3b × 3c) containing the direction cosines; $\mathbf{f}$ is the block forces vector, $\mathbf{f} = \mathbf{f}_D + \mathbf{f}_L$, where $\mathbf{f}_D$ and $\mathbf{f}_L$ are vectors of dead and live loads applied at the centroid of blocks, respectively; $\mathbf{q}$ is the contact forces vector,

$$\mathbf{q}^T = \{n_1, s_1, m_1, n_2, s_2, m_2, \ldots n_c, n_c, n_c\}$$

No-tension ('rocking') yield constraints:

$$\left.\begin{matrix} m_i \leq 0{,}5 n_i t_i \\ m_i \geq -0{,}5 n_i t_i \end{matrix}\right\} \text{for each contact, } i = 1, \ldots, c$$

And the sliding yield constraints:

$$\left.\begin{matrix} s_i \leq \mu_i n_i \\ s_i \geq -\mu_i n_i \end{matrix}\right\} \text{for each contact, } i = 1, \ldots, c$$

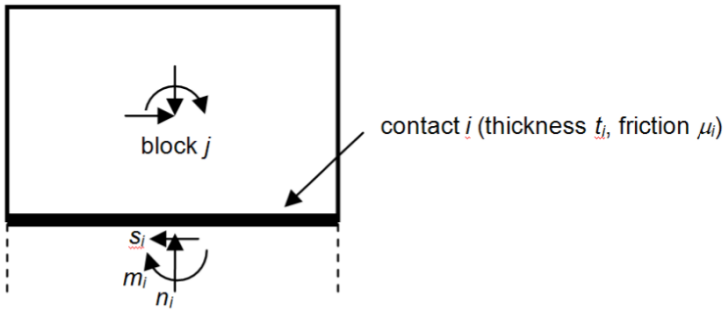


**Figure 2.16 Block and contact forces (LimitState Ltd, 2016)**

Using this formulation the LP problem variables are the contact forces and the unknown load factor λ.

### *2.3.2 Masonry crushing*

RING considers the fact that no material can bear infinite compressive stresses. It is assumed that the compressive stress is carried by a rectangular stress block in the vicinity of hinges (*Figure 2.17*). It is obvious that the envelope is non-linear.

To achieve linear programming, a LP solver for moment is still to be used to obtain a solution to the global program (the third equation in *section 2.3.1*), then these constraints need to be approximated as a series of linear constraints. In other words, the true non-linear moment yield surface is found by a piece-wise linear representation.

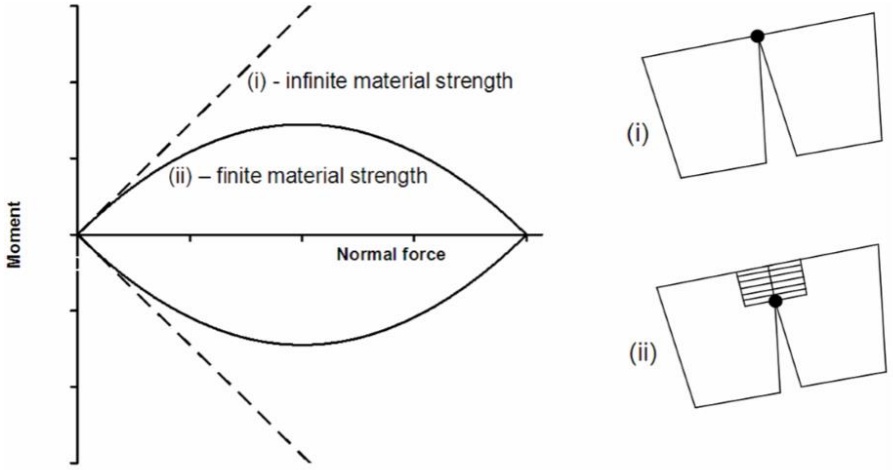


**Figure 2.17 Contact surface moment vs. normal force failure envelopes for: (i) infinite; (ii) finite masonry crushing strengths (LimitState Ltd, 2016)**

### *2.3.3 Frictional Sliding*

As mentioned earlier, an "associative friction (saw tooth)" model is used in RING to analyze the effect of sliding. It is not quite realistic for masonry structures where the contact dilation angle is much smaller than the friction angle. But this kind of friction model saves the linear character of the problem. *Figure 2.18* shows the idealized sliding models and real behavior of masonry joints.

Whilst it can be shown that *use of a "raw tooth" model for friction can lead to non-conservative adequacy factors being obtained if sliding is involved in the critical failure mode* (Drucker 1954), *when previously applied to multi-ring brickwork arch bridges reasonably good agreement between experimental and numerical results were obtained* (RING manual).

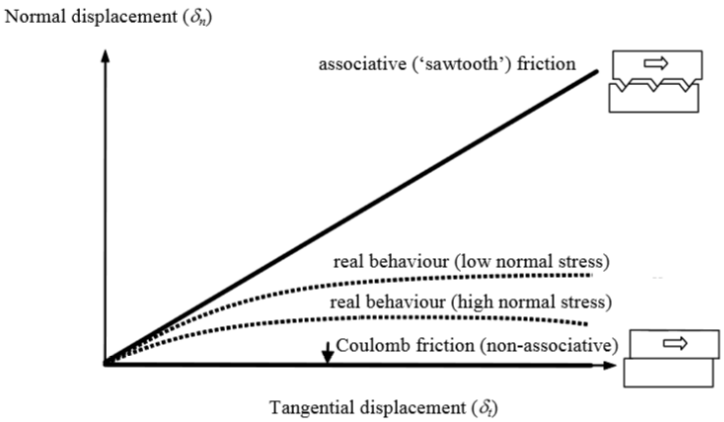


**Figure 2.18 Idealized sliding models and real behavior of masonry joints (Gilbert et al. 2006)**

# 3 Numerical Modeling – 3DEC

In this part, 5 arch models were built with the help of 3DEC, making two groups of arrangements.

Group 1: three arches with the same number of blocks (51 blocks). The angles of embrace of the arches are 180°, 120° and 60°, respectively.

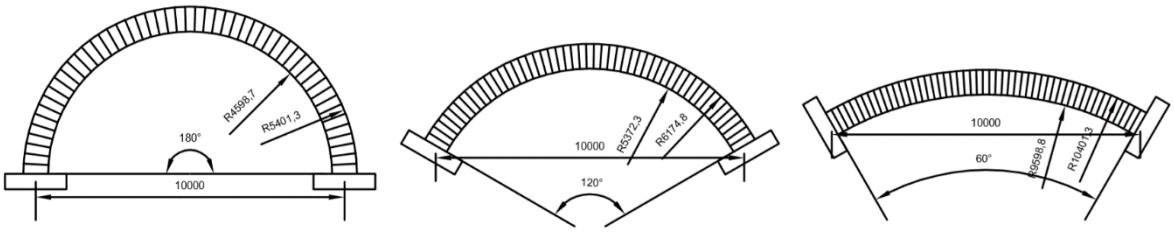


**Figure 3.1 The AutoCAD models of the arches in Group 1 [mm]**

Group 2: three arches with the same size (middle arc line) of blocks (≈0.205 m). The angles of embrace of the arches are 180°, 120° and 60°, respectively.

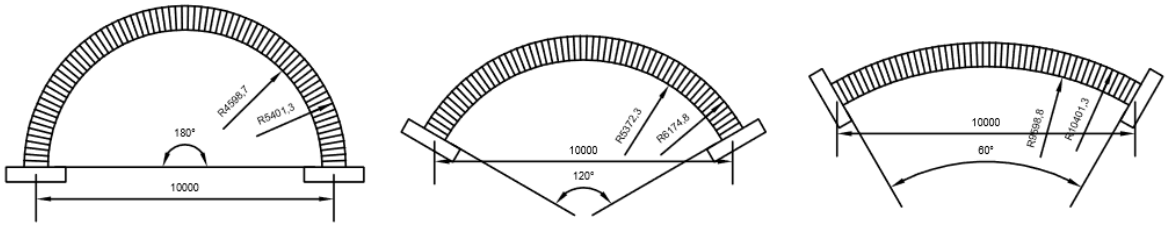


**Figure 3.2 The AutoCAD models of the arches in Group 2 [mm]**

As I determined the size of blocks in group 2 using the arch in group 1 with 60° embrace angle, the total number of arches is five.

The thickness *t* is invariant, whose value is 1,5 times the minimally necessary thickness for selfweight for the semicircular arch, which is 0,107 times the radius of middle line (Cocchetti et al). Also, for each group of the arches, different frictional angles are set to evaluate the sliding effect of arches. In my work, 30°, 40° and 45° are analyzed.

The solution strategy of 3DEC models:

1. Define the geometries with the help of MATLAB and AutoCAD.
2. Set material properties of the elements and contacts.
3. Fixed boundary conditions are given and the structures are equilibrated under selfweight.
4. Live load is applied dynamically; the complete load with its full magnitude is dropped on the structure. This is repeated using different positions of the arches to find the failure loads (which makes the structure fail) and corresponding failure modes that belong to the different positions.

5. Compare the results. The smallest failure load in one arch is defined as critical load. Critical loads and critical positions in several arches can be found. Register the types of failure modes.
6. Apply quasi-static load around the critical positions of arches, and compare the values of dynamic critical loads and quasi-static loads. The aim is to check whether there is a considerable difference between dynamically applied and quasi-statically increased loads.
7. Check whether the failure load can safely travel starting from outside along the arch until its critical position.

An example of code to determine coordinates of arches with the help of MATLAB can be seen in *Appendix A*. *Appendix B* and *C* are codes in 3DEC finding failure dynamics load and quasi-static load applied to a certain load position to an arch, respectively. *Appendix D* checks the travelling load along the arch with 51 blocks, 60-degree embrace angle and 40-degree friction angle.

## *3.1 The models of the arches in 3DEC*

The units in 3DEC code are all in the international system of units (SI), with length in meter (*m*), mass in kilogram (*kg*) and time in second (*s*).

### *3.1.1 Geometry of the models of the arches in 3DEC*

All the arches have the same middle span of 10 m, and the same uniform thickness (*t*) of 0,8025 m and the same width (*d*) of 0,8025 m. The value of the length is set to be equal to the value of thickness, which is 1,5 times the minimally necessary thickness for selfweight for the semicircular arch, i.e. 0,8025 m. This value was chosen in the following way:

Literally, the minimally necessary thickness for selfweight refers to the critical thickness for which an equilibrium force system can be found when the arch carries its own weight. If the thickness is smaller than this value, the arch will not be equilibrated. As mentioned above, the minimally necessary thickness for a semicircular arch is about 0,107 times the middle line radius (Cocchetti et al), which means:

$$t = 1{,}5 \times 0{,}107 \times R = 1{,}5 \times 0{,}107 \times 5 = 0{,}8025\ m$$

$$d = t = 0{,}8025\ m$$

For the models of Group 1, every arch consists of 51 trapezoidal blocks, while the same size of blocks is set for the models of Group 2.

To calculate the number of blocks of the models in Group 2, first I set the block size of 60° segmental circular arch as the reference. Since the blocks are slightly trapezoidal, I used the middle arc line (red line in *Figure 3.3*) to measure the size of the blocks.

The length of the middle arc for 60 ° segmental circular arch is:

$$R = \frac{L/2}{sin30^\circ} = 10\ m$$

$$L_{curve} = \frac{60}{180} \cdot \pi R = 10{,}47\ m$$

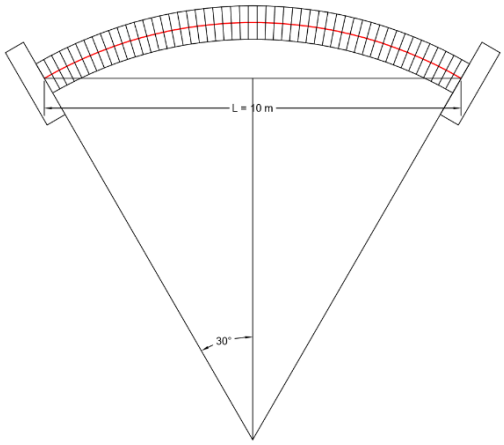


**Figure 3.3 Determination of the size of blocks**

The size of the blocks:

$$l = \frac{L_{curve}}{n} = \frac{10{,}47}{51} = 0{,}205\ m$$

Determine the number of blocks for semicircular arch:

$$R = L/2 = 5\ m$$

$$L_{curve} = \pi R = 15{,}7\ m$$

$$n = \frac{L_{curve}}{l} = \frac{15{,}7}{0{,}205} = 77$$

Determine the number of blocks for 120° segmental circular arch:

$$R = \frac{L/2}{sin60^\circ} = 5{,}77\ m$$

$$L_{curve} = \frac{120}{180} \cdot \pi R = 12{,}09\ m$$

$$n = \frac{L_{curve}}{l} = \frac{12{,}09}{0{,}205} = 59$$

As a result, the semicircular arch consists of 77 blocks, the segmental arch with 120° of 59 blocks and the segmental arch with 60° of 51 blocks.

For every arch, I created two blocks to serve as support blocks. The size of the support blocks is 2 m × 0,8025m × 0,50 m. The support blocks perfectly touch the two outer blocks without gaps or overlaps before adding the selfweight.

Two groups of models built in 3DEC are shown in *Figure 3.4* and *Figure 3.5*, respectively.

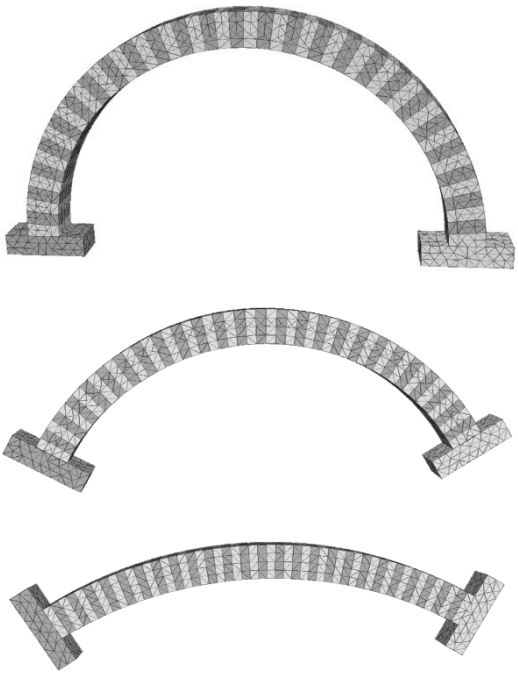

**Figure 3.4 The 3DEC models of Group 1**

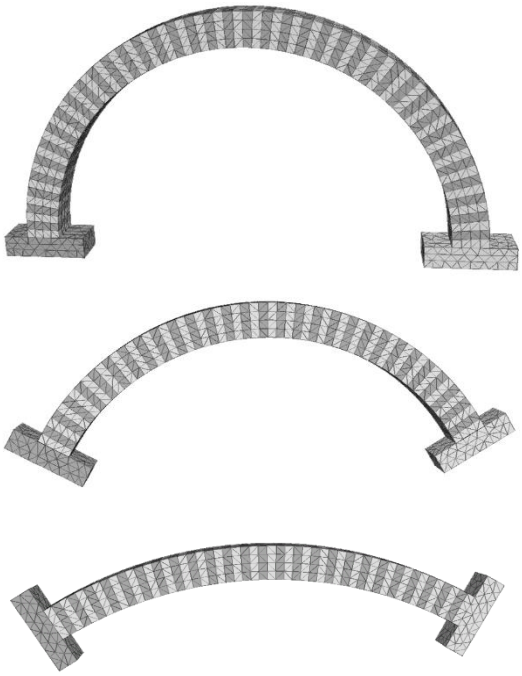

**Figure 3.5 The 3DEC models of Group 2**

In order to produce live load, a loading block should be put on the arch before the structure is equilibrated under selfweight with a practically zero initial density. (This is necessary because of the requirement in 3DEC that every block has to exist already from the beginning of the simulation procedure; after cycling, blocks cannot be added.) An example is shown in the figure below.

### *3.1.2 Material of the models of the arches in 3DEC*

In the project, the DEM code 3DEC should be used as virtual reality, to produce computer-simulated experimental results. Deformable limestone voussoirs and dry contacts are applied in models.

Limestone is widely distributed over the world and has rather uniform lithology. It is easy to be quarried and used for the base material of building bricks, so it is the most common material for masonry structures. I refer to the geostatistics results from the University of Texas at Austin, Jackson School of Geosciences (*https://www.jsg.utexas.edu/tyzhu/files/Some-Useful-Numbers.pdf*) to set the material properties in my thesis work.

| **Density (ρ)** | **Young's Modulus (E)** | **Poisson's ratio (ν)** |
|---|---|---|
| 2700 kg/m$^3$ | 15-55 GPa | 0.18-0.33 |

**Table 3.1: Some Useful Numbers on the Engineering Properties of Limestone (GEOL 615)**

The density of blocks is set to 2700 $kg/m^3$, the Young's modulus is 35 *GPa* and the Poisson's ratio is 0,25. The material properties of supporting blocks are the same as those of the arches. As for loading blocks, I chose a very small density value (100 $kg/m^3$) at the initial stage, so that the additional blocks could not noticeably influence selfweight equilibrium of the structures.

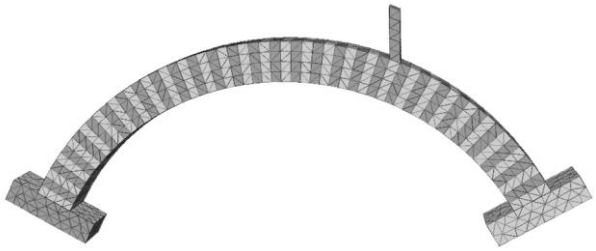

**Figure 3.6 The 3DEC models with a loading block**

The joints are represented by face-to-face contacts of blocks. Coulomb frictional contacts are used in my project: cohesionless contacts with friction, but with zero dilation angle. The shear stiffness (ks) and normal stiffness (kn) are $10^{11}$ $N/m^2$, according to the recommendation of "3DEC 5.0 Manual – Problem Solving 3.8.2". To analyze the sliding mode in arches, different friction angles were set and simulations were repeated for all of them. Considering that models in RING cannot set a friction angle larger than 45 degrees, the largest value of friction angle is 45° in 3DEC too. So, the friction angles I used are 30°, 40° and 45°.

- **Blocks**
- Density: $\rho$=2700 $kg/m^3$
- Young's modulus: E=35×$10^{11}$ *Pa*
- Poisson's ratio: $\nu$=0,25

- **Joints**
- Normal stiffness: $k_n=10^{11}$ $N/m^2$
- Shear stiffness: $k_s=10^{11}$ $N/m^2$
- Friction angle: $\varphi$=30°, 40° or 45°

### *3.1.3 Boundary conditions and equilibrium of selfweight in 3DEC*

The two supporting blocks of the arch are fixed, which means that these blocks cannot move and the velocities of their nodes are zero. Nodes mean the vertices of the tetrahedral subdivision of the deformable blocks; the whole structure is meshed due to the deformable property.

As a load, I applied the gravity to the structure (9,81 $m/s^2$ in the vertical, i.e. in the *y*-direction) and cycles a certain time to find the equilibrium state of all structures under selfweight. When the unbalanced force is relatively small, we can say that the structure is equilibrated.

Take one model for example. After 70000 cycles of calculation, the unbalanced force of the semicircular arch in Group 1 is $5.782 \times 10^{-7}$ *N* as we can see in *Figure 3.7*.

*Figure 3.8* shows the displacement vectors under selfweight in the structure, with a maximum value 0,25 *mm*.

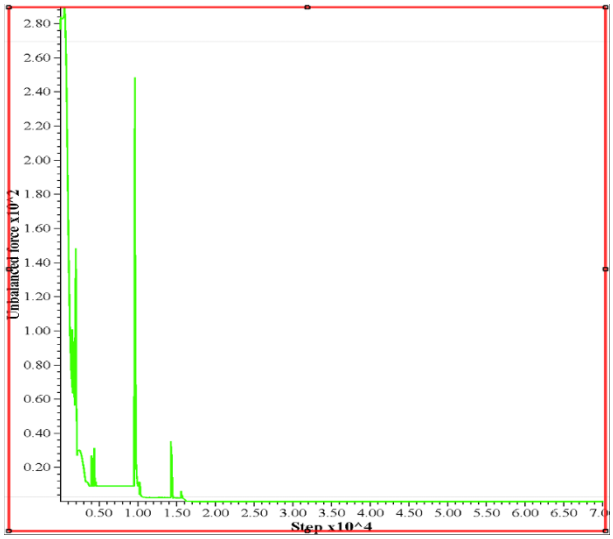


**Figure 3.7 Unbalanced force – semicircular in Group 1**

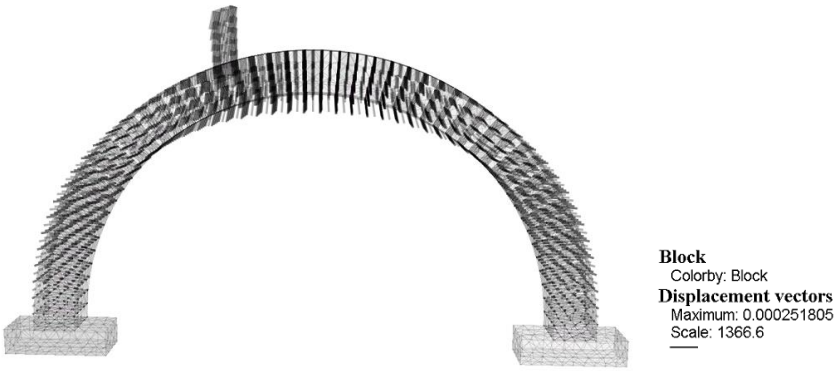


**Figure 3.8 Displacement vectors under selfweight – semicircular in Group 1**

Compare unbalanced forces of all the models:

| | **Model 1** | **Model 2** | **Model 3** | **Model 4** | **Model 5** |
|---|---|---|---|---|---|
| Unbalanced force [*N*] | $5.782 \times 10^{-7}$ | $1.211 \times 10^{-8}$ | $3.352 \times 10^{-9}$ | $1.600 \times 10^{-7}$ | $5.055 \times 10^{-9}$ |
| Weight of the structure [*N*] | $3.104 \times 10^{5}$ | $2.490 \times 10^{5}$ | $2.208 \times 10^{5}$ | $3.104 \times 10^{5}$ | $2.490 \times 10^{5}$ |
| Error | $1.863 \times 10^{-12}$ | $4.863 \times 10^{-12}$ | $1.518 \times 10^{-14}$ | $5.155 \times 10^{-11}$ | $2.030 \times 10^{-14}$ |

Note: Model 1 refers to the semicircular arch in Group 1; Model 2 – 120-degree segmental arch in Group 1; Model 3 – 60-degree segmental arch; Model 4 – semicircular arch in Group 2; Model 5 – 120-degree segmental arch in Group 2.

**Table 3.2: Comparison of the unbalanced force**

Error in the table is the value of the maximum unbalanced force magnitude in the system divided with the total applied forces in the model. According to *Table 3.2*, we can observe that the unbalanced forces are very small in comparison to the whole weight of the structures. So, we can say that the arches are equilibrated under selfweight. And without live load, the displacements are small in all the cases (fractions of a mm, as shown in *Figure 3.8*).

### *3.1.4 Live loads in 3DEC*

After equilibrating the arches under self-weight, live loads can be applied with the help of loading blocks. In discrete element modeling, giving the blocks prescribed velocities is rather complicated; so instead, I increased the density of the additional loading block until the structures could not find an equilibrium state, in other words, collapsed. The volume of the loading block ($V$) can be read out from 3DEC. With a known density ($\rho$) which makes the structure fail, the failure load can be calculated by the formula:

$$F = \rho V g$$

Using the units set in 3DEC code, the failure loads received are in Newton ($N$). However, in the following text, the results are shown in $kN$.

## *3.2 The results in 3DEC*

Different comparisons of failure modes and failure loads are performed in this part – different angles of embrace, different groups and different friction angles. In this thesis work, the origin point of the coordinate system is set to the middle of the arch at the springing, which can be seen in *Figure 3.9* (this was done in order to have the same coordinate system in 3DEC, RING and Archie-M). The loading position refers to the horizontal distance of the point where the live load is applied, from the origin, i.e., $d$ in the figure, which will be presented into $n*L$ in the same time ($L$ is the middle span). For example, when load is applied at the crown of the arch, the load position is 0.5L.

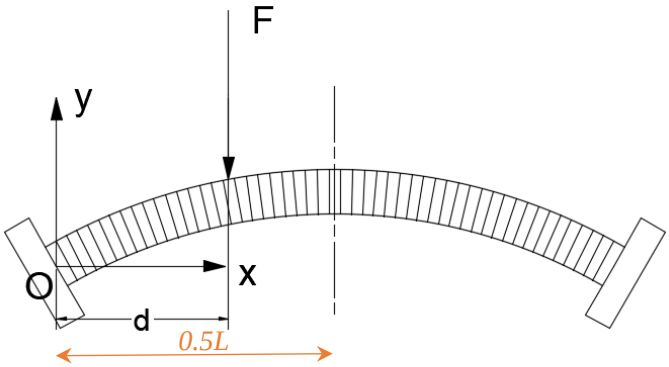


**Figure 3.9 Description of origin and position**

The detailed results can be seen in *Appendix F*.

### 3.2.1 The same number of blocks vs the same size of the block

Wondering if the number of blocks influences the results significantly, I compared the failure loads and critical load for the two groups (remember that 180° and 120° arches in Group 1 had a smaller number of voussoirs than those in Group 2). The friction angle in these tests was 30°. *Figure 3.10* illustrates the curves of failure loads depending on loading positions, from where we can see the differences are small for the two groups. *Figure 3.11* shows the failure modes. It is obvious that all the failure modes are hinging mechanisms.

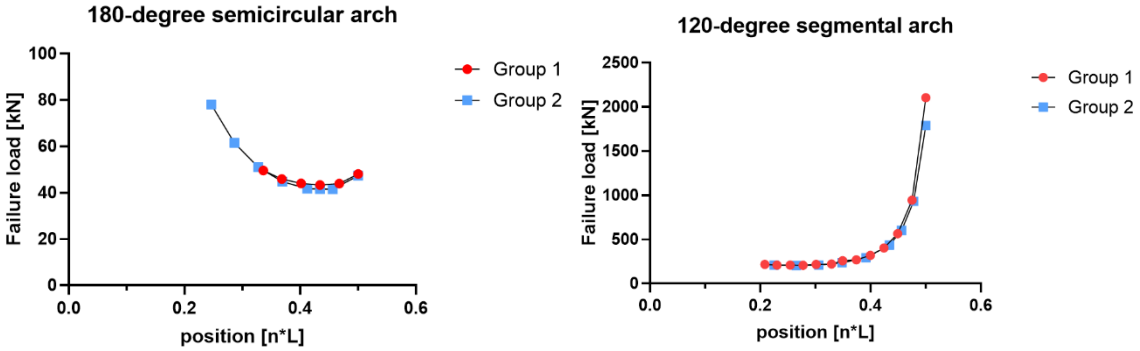


**Figure 3.10 Failure load – position curve with different groups**

| Embrace angle | Group | Critical position | Difference | Critical load [kN] | Difference |
|---|---|---|---|---|---|
| 180° | 51 blocks | 0.434L | 5.07% | 43.399 | 4.34% |
| | 77 blocks | 0.456L | | 41.515 | |
| 120° | 51 blocks | 0.277L | 4.33% | 207.589 | 1.37% |
| | 59 blocks | 0.265L | | 204.736 | |

**Table 3.3: Comparison of the critical positions and critical loads of different groups**

Compare the critical loads and critical positions for the two groups. For the critical position, the difference between the two groups is approximately equal to 5% (see the explanation below). Considering that the observed positions are not continuous, due to the transverse finite size of the blocks (200~300 *mm*), I think there is only negligible difference in the critical positions. Arches with different numbers of blocks give similar results.

Concerning the critical load, arches in Group 2 having more blocks than those in Group 1, are proved to get smaller values of failure loads. This may be explained in this way: applying a certain load in the block, bending moment can occur in the block, which makes the bottom of the block in tension; if the size of the block gets smaller, let us make it the half size of the original one (*Figure 3.12*), the tension cannot be resisted and the contact opens up.

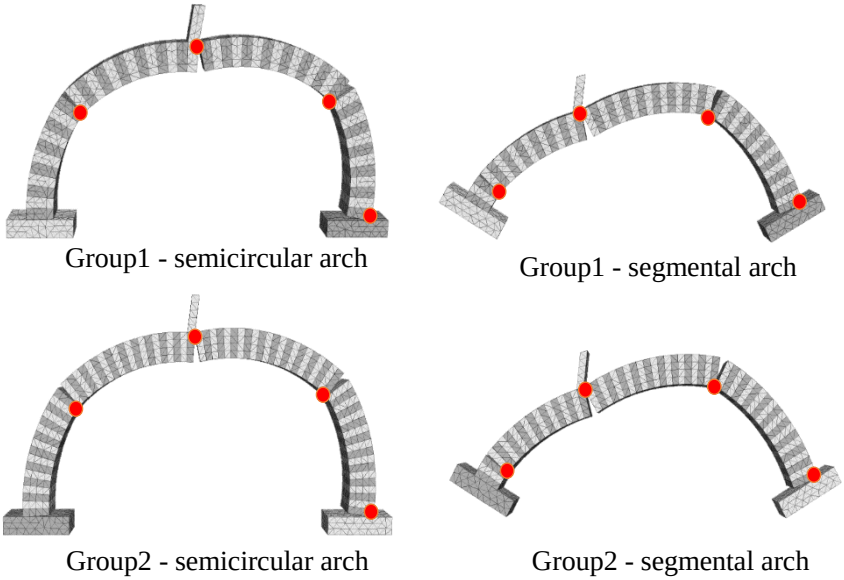


**Figure 3.11: Comparison of the failure modes in critical positions of different groups**

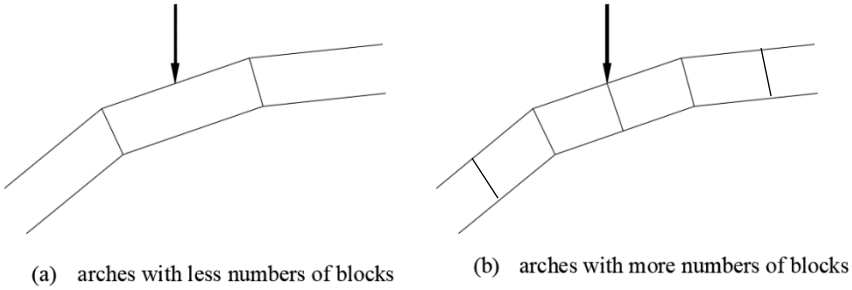


**Figure 3.12: The effect of numbers of blocks on failure load**

### *3.2.2 Effect of the angle of embrace*

In this part, I compared the arches with different angles of embrace, while the joints are in the same friction angle - 30 degrees. Remember that the arches have the same thickness, i.e. 1,5 times the mininally necessary thickness for selfweight for the semicircular arch. It is significantly above what is minimally needed for the segmental arches to keep their selfweight equilibrated. So, the segmental arches would have a rather large margin for live load. The failure load – position curves in *Fugure 3.13* illustrate the results. It is obvious to see that the smaller the angle of embrace is, the larger the load bearing capacity is. And the effect is especially huge in the arches with 60-degree angle of embrace, which may be associated with flat arch (Heyman, 1982). More discussion on the flat arch will be given in *Chapter 6*.

Concerning the critical positions, the semicircular arch has its critical position near half span, while as the angle of embrace decreases, the critical position get close to the arch springing. The results are shown in *Table 3.4*.

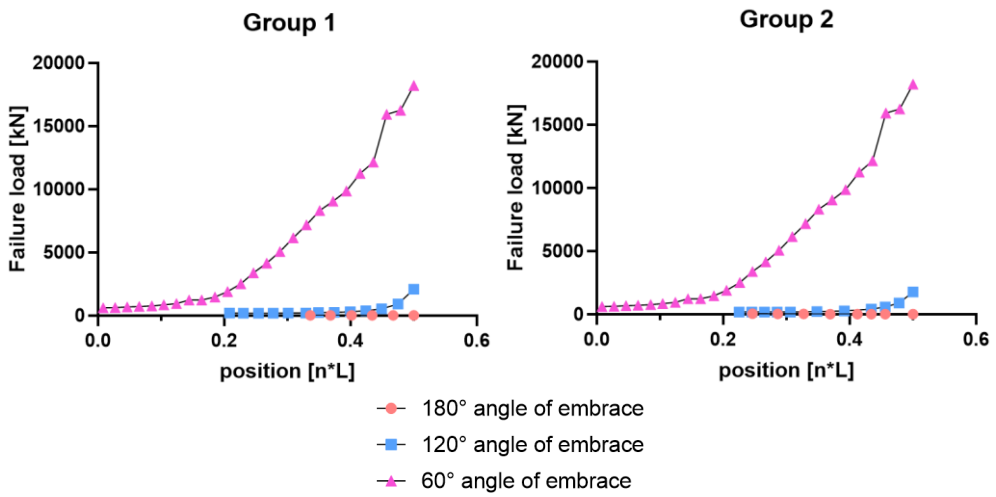


**Figure 3.13: Failure load – Position curves with different angles of embrace**

| Group | Embrace angle | Critical position | Critical load [kN] |
|---|---|---|---|
| 1 | 180° | 0.434L | 43.399 |
| | 120° | 0.277L | 207.589 |
| | 60° | 0.008L | 644.489 |
| 2 | 180° | 0.456L | 41.515 |
| | 120° | 0.265L | 204.736 |
| | 60° | 0.008L | 644.489 |

**Table 3.4: Comparison of the critical positions and critical loads of different angles of embrace**

As for the failure modes (*Figure 3.14*) of the arches, the 180-degree and 120-degree angles of embrace arches belong to pure hinge mechanism. The arch with 60-degree embrace angle has different failure modes. Near the arch springing (0.008L ~ 0.124L), a combined shear-hinge mechanism is shown. If loaded near the crown (0.457L ~ 0.500L), individual block slides down and the structure fails under a pure shear mechanism. When the load is applied at 0.144L ~ 0.226L, four hinges are formed and the arch collapses. There is also a combined shear-hinge mode when load is applied between 0.246L and 0.436L.

The failure modes that occur in the arch with the smallest angle of embrace will be described in detail.

### Combined shear-hinge mechanism (c1 & c3)

The voussoir under the loading block slides down when live load is added. During iteration, the arch deforms more and more, and the joint between the voussoir under the loading block and its neighbor voussoir opens up. Finally, a buckling-type of loss of stability may occur.

It should be mentioned that the sliding in (c1) is significant while in (c3) is small. *Figure 3.15* shows a pre-buckled shape when load is applied away from the springing, where

we can see the sliding is small. And the arch would collapse in the shape of what (c3) shows in *Figure 3.14*.

### Hinging (c2)

During the load process, four hinges are generated in the intrados and extrados of the arch. The arch sways to one side.

### Sliding (c4)

Firstly, when a dynamic load is applied, the individual block under the loading block slides abruptly. The fast sliding would not last for long and the individual block directly acted upon by the loading block will slide slowly due to the frictional resistance. During this process, the middle part of the arch deforms slowly to a straight line-like shape (*Figure 3.16*). Finally, the individual block slides down and the arch collapses.

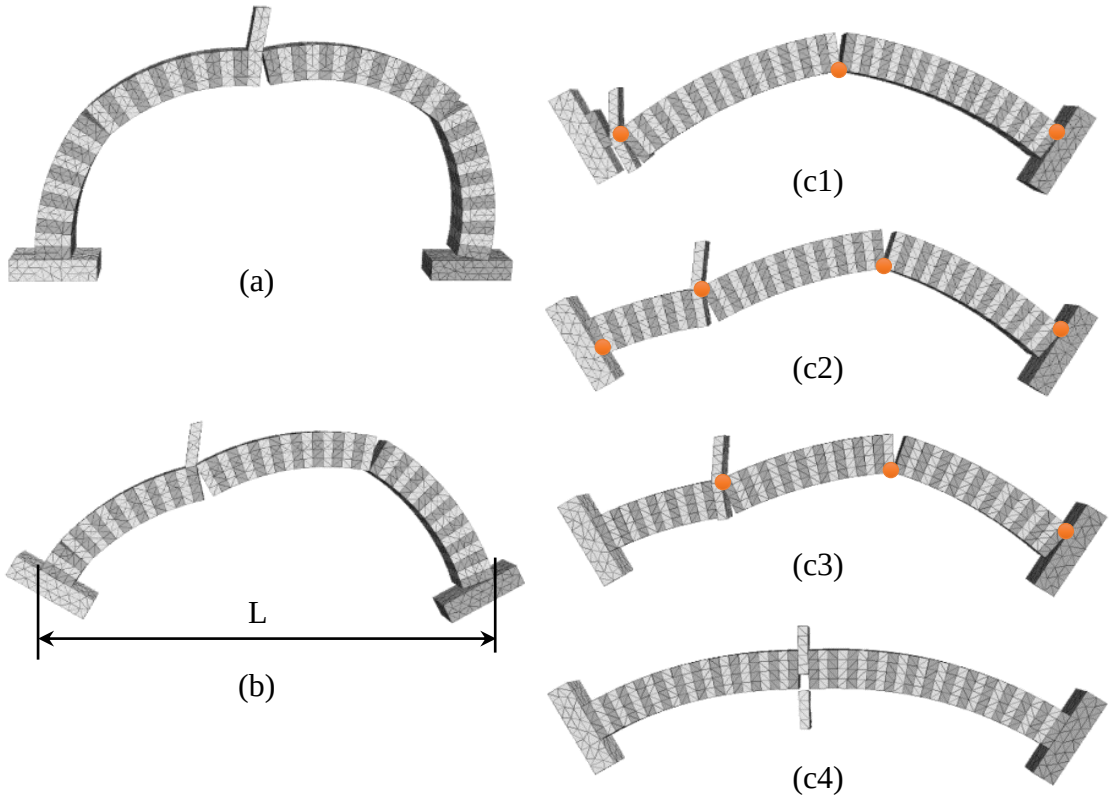


**Figure 3.14: Comparison of the failure modes of different angles of embrace: (a) semicircular arch – hinge mechanism; (b) 120-degree of embrace arch – hinge mechanism; (c) 60-degree of embrace arch: 1. Combined shear-hinge mechanism, 2. Hinge mechanism, 3. Combined shear-hinge mechanism, 4. Sliding**

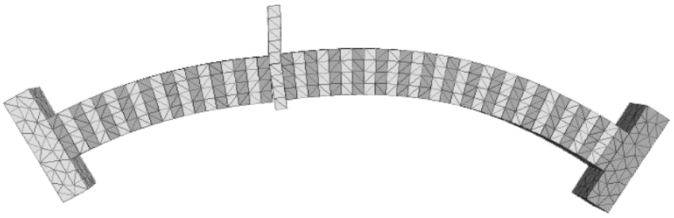

**Figure 3.15: Pre-buckling state**

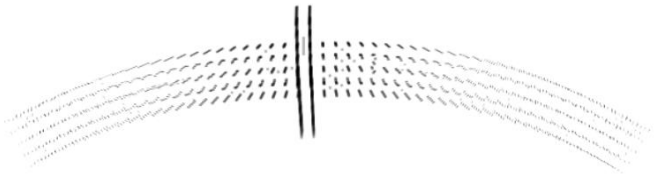

**Figure 3.16: Displacement vectors when the load is applied to the middle span**

### *3.2.3 Effect of friction angle*

I list the comparison of different friction angles in Group 1, while the results of arches in Group 2 can be found in *Appendix F*.

*1) Semicircular arch*

| Position | Failure load [kN] | | |
|---|---|---|---|
| | 30° friction angle | 40° friction angle | 45° friction angle |
| 0.500L | 48.149 | 48.149 | 48.149 |
| 0.467L | 43.972 | 43.972 | 43.972 |
| 0.434L | 43.399 | 43.399 | 43.399 |
| 0.401L | 44.021 | 44.021 | 44.021 |
| 0.368L | 45.968 | 45.968 | 45.968 |
| 0.336L | 49.662 | 49.662 | 49.662 |

**Table 3.5: Failure loads of semicircular arch**

With different friction angles, the failure loads in the same position of the semicircular arch are the same. Critical position and critical load remain the same. As a result, friction angle has no effect on the failure loads. The results shown in *Table 3.5* illustrate that the failure mode of semicircular arch is a perfect hinging mechanism as there is no difference for different friction angles, which means that no frictional sliding exists.

*2) 120-degree angle of embrace segmental circular arch*

| Position | Failure load [kN] | | |
|---|---|---|---|
| | 30° friction angle | 40° friction angle | 45° friction angle |
| 0.500L | 2105.879 | 2535.919 | 2634.944 |
| 0.475L | 945.408 | 998.651 | 1013.806 |
| 0.449L | 566.18 | 575.928 | 577.917 |
| 0.424L | 402.088 | 403.672 | 404.266 |
| 0.399L | 319.359 | 319.949 | 320.146 |
| 0.374L | 270.428 | 270.428 | 270.428 |
| 0.349L | 258.668 | 259.083 | 259.083 |
| 0.329L | 222.476 | 222.476 | 222.476 |
| 0.301L | 217.847 | 217.654 | 217.654 |

| | | | |
|---|---|---|---|
| 0.277L | 207.589 | 206.651 | 206.651 |
| 0.254L | 209.576 | 209.576 | 209.576 |
| 0.230L | 208.663 | 208.663 | 208.663 |
| 0.208L | 217.202 | 217.906 | 217.906 |

Note: The blue numbers refer to the positions where failure loads change with different friction angle; the red numbers refer to the critical position and critical loads.

**Table 3.6: Failure loads of 120-degree angle of embrace segmental arch**

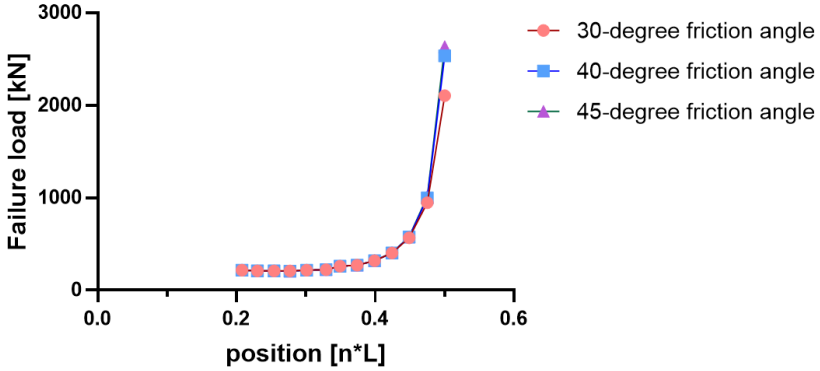


**Figure 3.17: Failure load – Position curves with different friction angles**

From *Table 3.6* and *Figure 3.17*, we can see that for the most positions, the magnitude of friction angle doesn't influence the failure loads. But if the live load is applied in the middle part of the span, i.e. 0,424 L~0,500 L, sliding will make a little change in failure load. With larger friction angle, the failure loads are slightly larger too. This may be explained with the sliding of individual blocks in the middle of the arch when a dynamic (large) load is suddenly applied on the arch (see *Figure 3.18*). Dynamic loading and quasi-static loading will be compared in *Section 4.2.4*.

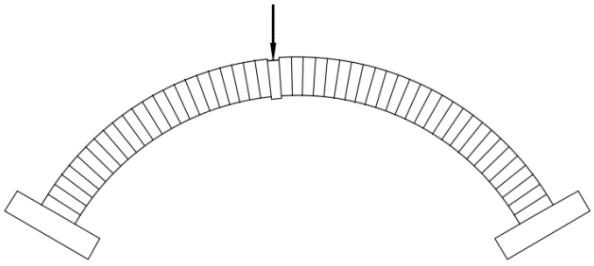

**Figure 3.18: Slightly sliding of individual blocks**

*3) 60-degree angle of embrace segmental circular arch*

| **Position** | **Failure load [kN]** | | |
|---|---|---|---|
| | **30° friction angle** | **40° friction angle** | **45° friction angle** |
| 0.185L | 1489.915 | 1597.733 | 1621.604 |
| 0.164L | 1253.101 | 1279.671 | 1287.467 |
| 0.144L | 1256.903 | 1118.967 | 1121.811 |
| 0.124L | 977.286 | 1045.782 | 1047.193 |
| 0.104L | 869.924 | 1040.643 | 1043.287 |
| 0.085L | 793.071 | 1121.244 | 1122.939 |
| 0.065L | 740.42 | 1147.743 | 1346.594 |

| | | | |
|---|---|---|---|
| 0.046L | 701.265 | 1105.952 | 1454.234 |
| 0.027L | 657.638 | 1054.137 | 1410.208 |
| 0.008L | 644.489 | 1052.581 | 1450.582 |

Note: The red numbers refer to the critical position and critical loads; failure modes for the circled positions in the chart are hinge mechanism, while for the rest of places, failure modes are combined shear-hinge mechanism.

**Table 3.7: Failure loads of 60-degree angle of embrace segmental arch (part of data)**

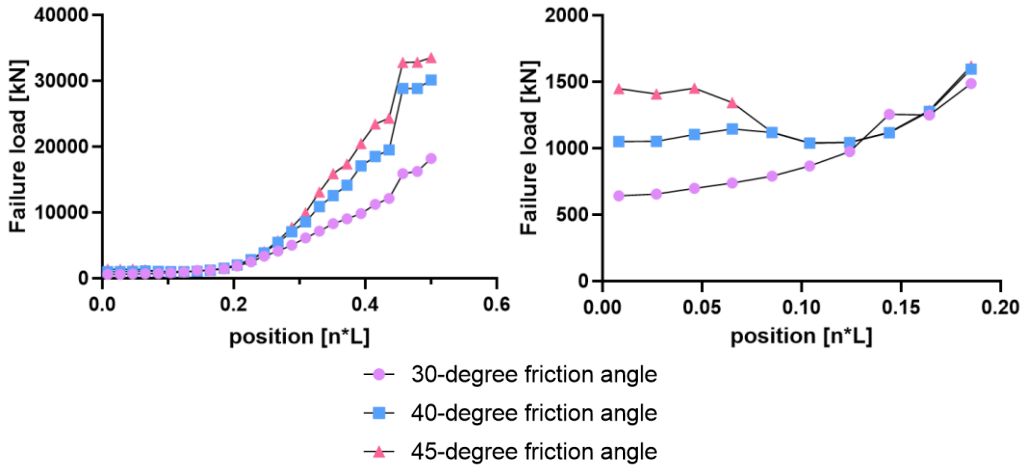


**Figure 3.19: Failure load – Position curves with different friction angles**

| Friction angle | Critical position | Critical load [kN] |
|---|---|---|
| 30° | 0.008L | 644.489 |
| 40° | 0.104L | 1040.643 |
| 45° | 0.104L | 1043.287 |

**Table 3.8: Comparison of the critical positions and critical loads of different friction angles**

The results illustrate that frictional sliding has a significant effect on the behavior of the small embrace angle arch. Usually, as the friction angle becomes larger, the collapse load applied to the same position also becomes larger.

Have known that there are three possible kinds of failure mode in the arch: sliding, hinge mechanism and combined shear-hinge mechanism. The ranges of load positions for three modes are determined in the *Table 3.9*.

| Failure mode | Position rang | | |
|---|---|---|---|
| | 30° | 40° | 45° |
| Sliding (c4) | 0.457L~0.500L | 0.457L~0.500L | 0.457L~0.500L |
| Combined shear-hinge mechanism (c3&c1) | 0.246L~0.436L, 0.008L~0.124L | 0.246L~0.436L, 0.008L~0.065L | 0.246L~0.436L, 0.008L~0.046L |
| Hinge mechanism (c2) | 0.144L~0.226L | 0.085L~0.226L | 0.065L~0.226L |

**Table 3.9: Position range for different failure modes**

Arches with smaller friction angle have more assess to slide, as the frictional resistance is smaller. As a result, frictional sliding takes the biggest role in the arch with 30-degree friction angle. This explains why the failure load – position curve for the arch 30-degree friction angle has a different shape from the others (*Figure 3.19* & *Table 3,8*). It is sliding that influences collapse load and collapse load is lower than that in hinge mechanism. The positions that sliding occurs in the other two arches are smaller than 700 mm, where a minimum value of collapse load occur due to pure hinge mechanism. So, failure loads fluctuate as the right graph in *Figure 3.19*.

Checking the failure loads in different ranges for different failure modes, we can see that the differences of failure loads are small in cases when the arch fails due to pure hinge mechanism, and differ about 7% maximum for this case study. For other failure modes (those when sliding is involved), friction coefficient does take an important role.

### *3.2.4 Dynamic loading VS quasi-static loading*

The results above are dynamic failure loads, which means that a large enough value of load is applied on the arch directly and make the arch collapse. The minimum value of it is the failure load I found. Considering that the dynamic load may cause the sudden failure of the arch, or make the arch deform a lot in the beginning, I simulated a quasi-static load to check for the critical positions and the neighboring positions of them. Quasi-static load is applied using a slowly increasing density of the loading block. The two kinds of loads can be recognized through the plots of unbalanced force during time, see *Figure 3.20* and *Figure 3.21*.

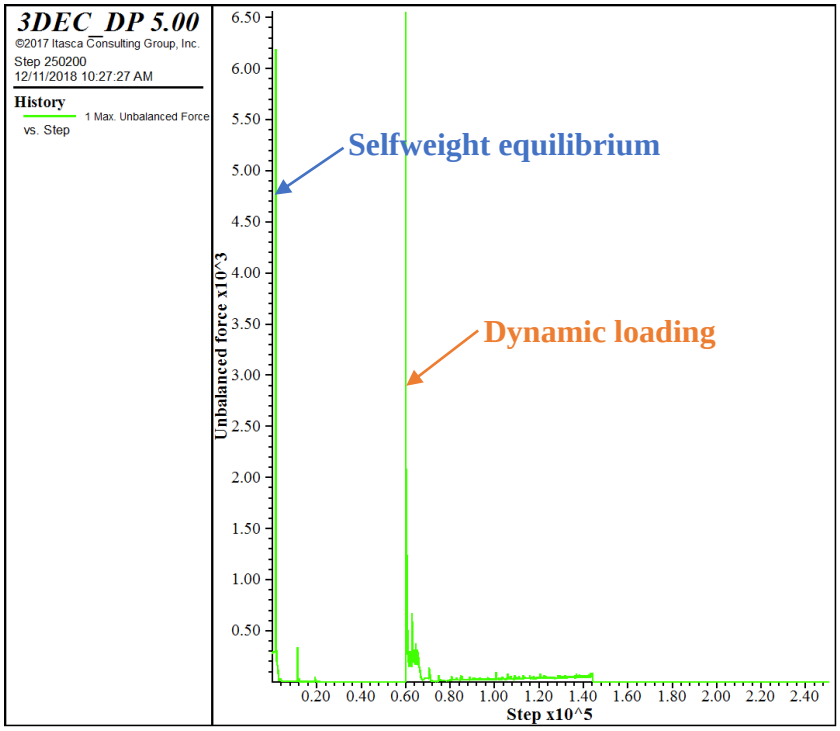


**Figure 3.20: Dynamic loading**

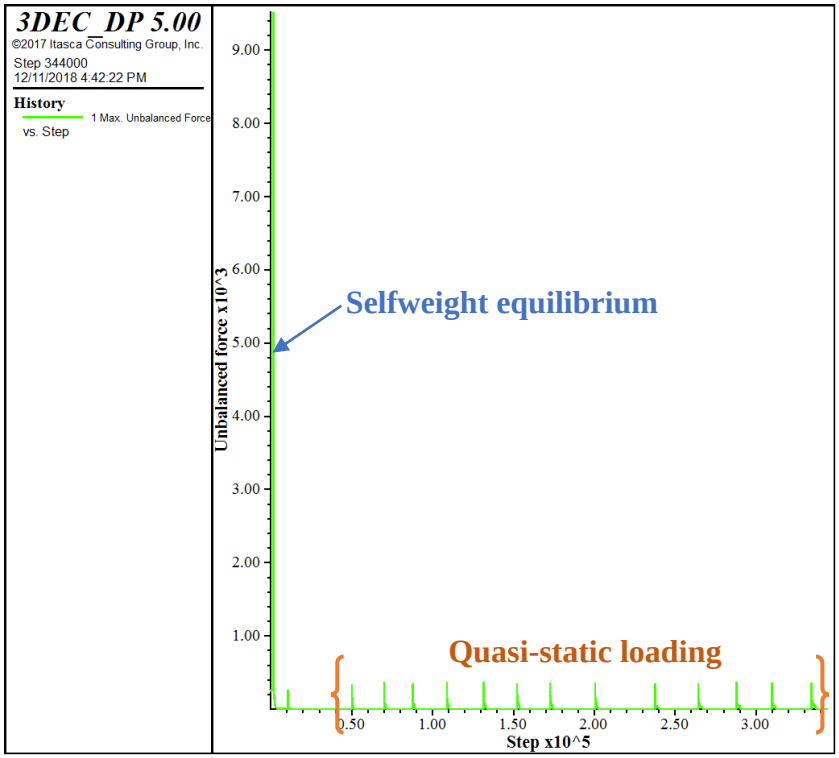


**Figure 3.21: Quasi-static loading**

| angle of embrace | position | friction angle = 30° | | |
|---|---|---|---|---|
| | | dynamic load [kN] | static load [kN] | difference |
| 180° | 0.467L | 43.972 | 43.972 | 0.00% |
| | 0.434L | 43.399 | 43.399 | 0.00% |
| | 0.401L | 44.021 | 44.021 | 0.00% |
| 120° | 0.301L | 217.847 | 217.654 | 0.09% |
| | 0.277L | 207.589 | 207.964 | -0.18% |
| | 0.254L | 209.576 | 209.759 | -0.09% |
| 60° | 0.027L | 657.638 | 660.333 | -0.41% |
| | 0.008L | 644.489 | 644.934 | -0.07% |
| **angle of embrace** | **position** | **friction angle = 40°** | | |
| | | **dynamic load [kN]** | **static load [kN]** | **difference** |
| 180° | 0.467L | 43.972 | 43.972 | 0.00% |
| | 0.434L | 43.399 | 43.399 | 0.00% |
| | 0.401L | 44.021 | 44.021 | 0.00% |
| 120° | 0.301L | 217.654 | 218.040 | -0.18% |
| | 0.277L | 207.589 | 207.776 | -0.09% |
| | 0.254L | 209.576 | 209.759 | -0.09% |
| 60° | 0.124L | 1045.782 | 1051.425 | -0.54% |
| | 0.104L | 1040.643 | 1045.463 | -0.46% |
| | 0.085L | 1121.244 | 1124.327 | -0.27% |

| angle of embrace | position | friction angle = 45° | | |
|---|---|---|---|---|
| | | dynamic load [kN] | static load [kN] | difference |
| 180° | 0.467L | 43.972 | 43.972 | 0.00% |
| | 0.434L | 43.399 | 43.399 | 0.00% |
| | 0.401L | 44.021 | 44.021 | 0.00% |
| 120° | 0.301L | 217.654 | 217.654 | 0.00% |
| | 0.277L | 207.776 | 207.776 | 0.00% |
| | 0.254L | 209.576 | 209.759 | -0.09% |
| 60° | 0.124L | 1047.193 | 1052.366 | -0.49% |
| | 644 | 1043.287 | 1045.308 | -0.19% |
| | 0.104L | 1122.939 | 1124.172 | -0.11% |

**Table 3.10: Comparison of dynamic loading and quasi-static loading**

The negative values in difference (*Table 3.10*) mean that the dynamic failure loads are smaller than the static loads, which corresponds to what is generally expected from a discrete element model using explicit time integration like 3DEC. However, the differences are really small and we can give the conclusion that at the critical positions and also near the critical positions, the values of quasi-static failure loads are approximately equal to those of dynamic failure loads. What's even more, we can see that the critical positions remain unchanged in the three models. So, the critical loads and critical positions received from dynamic loading are reliable approximations of the magnitude of a gradually increasing quasi-static load. This is an important outcome for practical engineering applications for the following reason. Based on this result, the loading history in 3DEC simulations can significantly be simplified: when checking in practice whether a given load magnitude remains under the failure load belonging to a certain position, the time-consuming procedure of gradually increasing the load until failure can be replaced by putting just single load with the required magnitude on the structure.

### *3.2.5 Check travelling loadings*

In reality, load usually comes from one end of the arch and gradually deforms the arch, perhaps causing partial slides and cracks, which could, in principle, lead to the situation that the arch already becomes unable to carry the load before it arrives to the critical position.

The strategy to check whether the failure load can safely travel starting from outside along the arch until its critical position is:

1. Create several adjacent loading blocks as shown in *Figure 3.22* below. While for some positions, the slope of the arch is big enough that the loading blocks may slide down along the arch. So, for arches with 120-degree and 180-degree of embrace the

loading blocks are set from a certain position where sliding of the loading block will not occur.

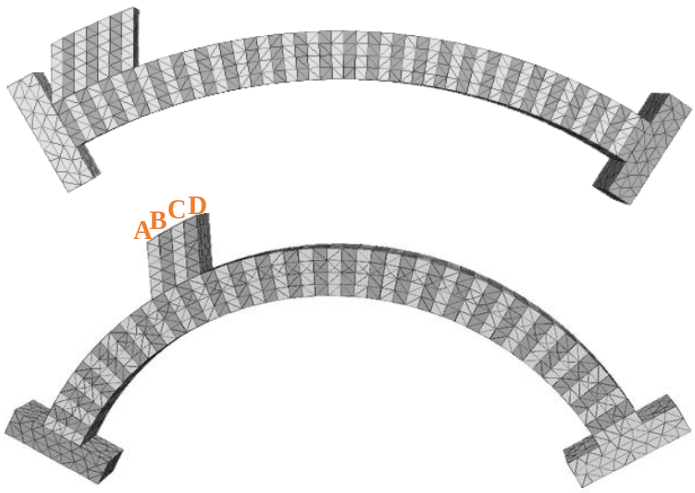


**Figure 3.22 Travelling load blocks in two arches**

2. Change the density of the adjacent blocks to fulfill the condition that the self-weight of the blocks equals to the critical load (quasi-static load) in the according structure. First, block A (*Figure 3.22*) offers the whole critical load and the other blocks have a density of 10 kg/m$^3$ (density of block cannot be zero in 3DEC).
3. Gradually increase the density of B and at the same time decrease that of A. Finally, block A gets a density of 10 kg/m$^3$ (which is the applied approximation of "zero" in the model) and B offers the whole critical failure load.
4. Check whether the structure is safe. If it is, repeat the 2$^{nd}$ and 3$^{rd}$ steps to the next following neighbored blocks, for example, block B and C.
5. If in this process the structures can always be equilibrated, we can say that the failure load can safely travel starting from outside along the arch until its critical position.

The travelling load test considers the effect of accumulated deformations. As load travels, arch deforms more and more. The next load is applied to the deformed arch. *Figure 3.23* shows the process of checking the arch with 120-degree embrace angle and 30-degree friction angle.

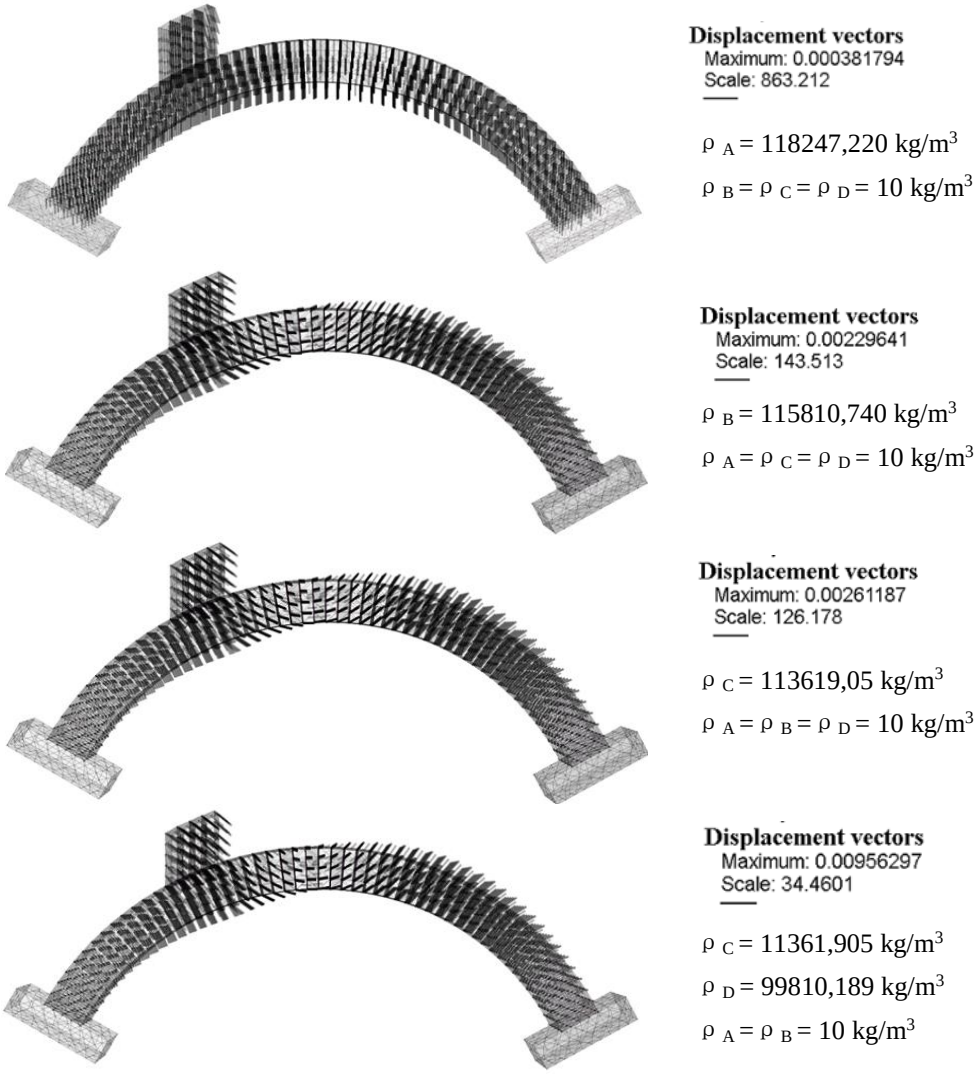


**Figure 3.23 Process of travelling load test**

The next step when the block D support the whole load, the arch collapses. This verified that for the arch with 120-degree embrace angle, the failure load can safely travel starting from outside along the arch until its critical position.

The main idea to determine densities of blocks is that the gravity of these blocks should be equal to the critical quasi-static failure load, i.e. $\sum \rho_i V_i = F$. The densities of each step in my test can be found in *Appendix E*.

After running all of the models, the results I got are shown in *Table 3.11*.

| Angle of embrace | Friction angle | | |
|---|---|---|---|
| | **30°** | **40°** | **45°** |
| 180° | × | × | × |
| 120° | √ | √ | √ |
| 60° | √ | × | √ |

**Table 3.11: Results of travelling load test**

Obviously, when a load travels starting from outside along the arch, the arch may fail before the failure load reaches its critical position. This can be explained to deformation of the arch. For arches with 60-degree of embrace, a special case is that the arch with 30-degree friction angle didn’t fail. This is because the critical position of it is close to the arch springing.

# 4 Numerical Modeling – Archie-M

In this part, the models set in Archie-M should be as close to those in 3DEC as possible. Three models with the same numbers of blocks (40) are built, as the number of segments cannot be modified in a demo version. With the opinion in the previous chapter, I think the failure loads received in this part should be a little larger than those in higher numbers of blocks, such as 51 blocks in the previous section.

## *4.1 The models of the arches in Archie-M*

### *4.1.1 Arches in Archie-M*

The following properties have to be specified: span, rise, ring thickness at crown, ring thickness at springing and position of left-hand springing. If the arch is in segmental circular arch shape, quarter rise parameter is not needed to specify. These are illustrated in *Figure 4.1*. The default LHS coordinates are (0,0) and I just used the default value.

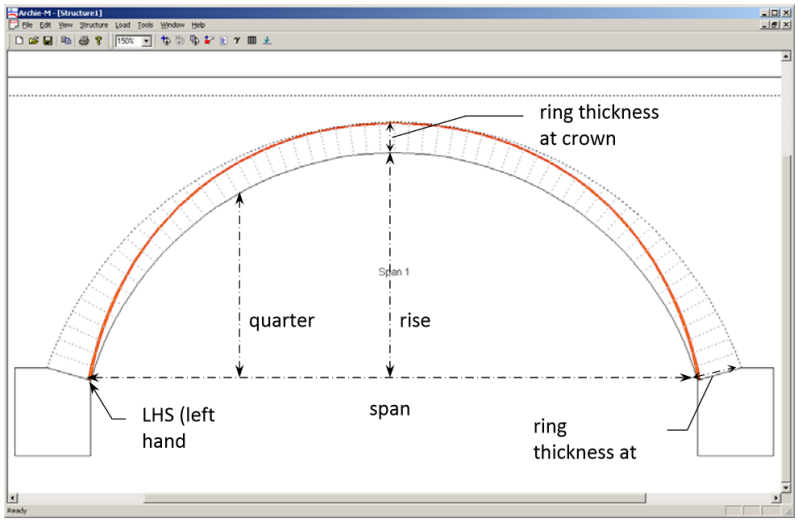


**Figure 4.1 Geometric properties of the predefined arches in Archie-M (Manual)**

With the help of AutoCAD, the geometric properties are set (middle span is 10 m for each arch):

| Arch | Shape | Span [mm] | Rise [mm] | Ring thickness at crown [mm] | Ring thickness at springing [mm] |
|---|---|---|---|---|---|
| 180° embrace angle | Circular | 9197 | 4598 | 802 | 802 |
| 120° embrace angle | Circular | 9305 | 2684 | 802 | 802 |
| 60° embrace angle | Circular | 9598 | 1286 | 802 | 802 |

**Table 4.1: Geometric properties of the arches in Archie-M**

Masonry crushing strength and masonry unit weight have to be specified.

Masonry crushing strength refers to compressive strength of masonry representative units, which shows the capacity of masonry to withstand the compressive force. Note that the masonry crushing strength does not consider the individual voussoir or mortar, but the complex masonry. The value of this strength can be influenced by lots of factors, such as mortar conditions and porosity, grain size, clay content and saturation of blocks. Amaryllis Audenaert and Johan Bake (2010) modelled an arch with backfill in Archie-M and RING, and compared the relationship of masonry strength and collapse load. The results illustrated that the crushing strength had little influence on the collapse loads (differs about 5% maximum from 5N/mm$^2$ and 8N/mm$^2$), which is shown in *Figure 4.2*. Looking through several examples of arch analysis in Archie-M and RING, the masonry strength is about 5 to 8 MPa. In my work, I set two groups of masonry strength and compare the results of them, one is 5 MPa, and the other is 10 MPa.

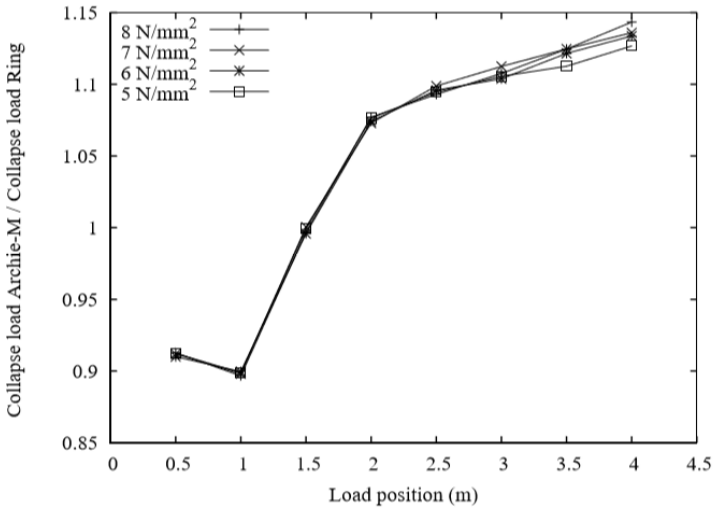


**Figure 4.2 Collapse load ratio for different positions and masonry strength (Amaryllis and Johan, 2010)**

The thickness of mortar in 3DEC is infinitely small and the gravity of the structure depends on limestone blocks. So, the masonry unit weight in Archie-M is calculated with the density of limestone.

$$\gamma = \rho g = 2700 \times 9{,}81\, N/m^2 = 26{,}5\, kN/m^2$$

### *4.1.2 Abutments and fill in Archie-M*

Abutments were not created in my models, as a result, the underlying calculation would assume the necessary reactive forces.

Uniform fill can be supported by Archie-M. While there is no fill in my models, I set the unit weight of fill to zero.

### 4.1.3 Road in Archie-M

Archie-M is designed to analyze masonry bridges and road is an important part to be predefined. But my work is to analyze single arches. To simulate the models that I built in 3DEC, I defined the shape of road in a three-point mode, which makes the road shape is a circular segment. The road is just lying directly on the arch, with a depth of surfacing 1 mm, which is negligible. The width of the bridge is set to be 802 mm.

The models are shown in *Figure 4.3*. The blue line on each segment represents the load applied to it, for both selfweight and live load.

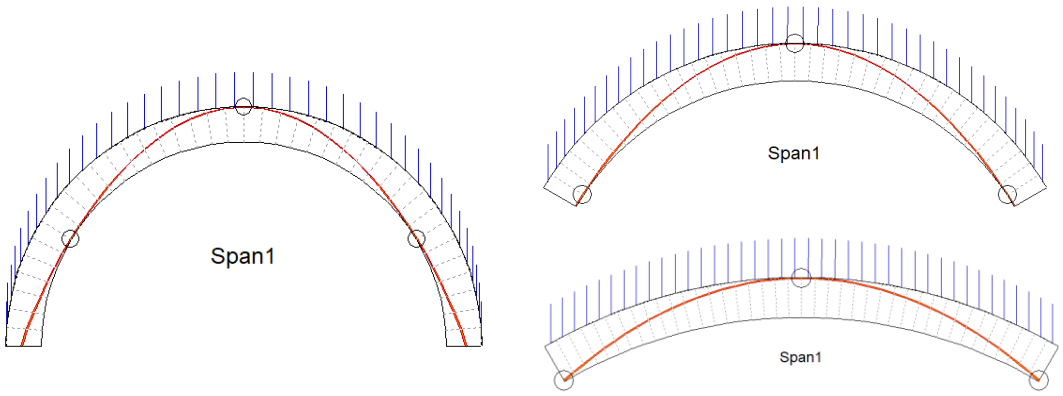


**Figure 4.3 The Archie-M models of the arches**

- **Arches**
- Masonry strength: 5 MPa or 10 MPa
- Masonry unit weight: 26,5 kN/m$^3$
- Mortar loss: 0

- **Fill**
- Unit weight: 0
- Angle of friction: 30°

- **Road**
- Depth of surfacing: 1 mm (minimum value, negligible)
- Depth of overlay: 0
- Surfacing unit weight: 15 kN/m$^3$ (minimum value)
- Overlay unit weight: 1 kN/m$^3$ (minimum value)
- Bridge width: 802 mm

### 4.1.4 Load in Archie-M

Apply an axel load with unit weight to the arch, which means that the value of the load is 9,81 kN. Change the factor for live load $\gamma$ until the thrust line is out of the cross-section and a sufficient number of hinges is formed.

## 4.2 The results in Archie-M

The program shows thrust line and positions of hinges, while it doesn't show how the structure deforms or fails. We can check internal forces and thrust zone position for each segment in Archie-M. The collapse load of the three arches for different load positions is calculated. And a similar comparison is done.

### 4.2.1 Effect of masonry strength

Compare the collapse loads for different masonry strengths in *Figure 4.4* and *Table 4.2*. *Figure 4.5* illustrates the failure load-position curves for 120-degree and 60-degree embrace angle arches. The results shown are different from what Amaryllis and Johan have found (*Figure 4.2*), as the angle of embrace differs. The conclusion is that masonry strength has an important effect on the collapse load, especially for arches with rather smaller embrace angle. In this case study, the collapse load differs about 50% maximum for the arch with 60-degree angle of embrace, while 30% maximum for the arch with 120-degree angle of embrace, and 7,5% maximum for the semicircular arch.

As the effect of masonry strength is not negligible, two sets of masonry strengths will be considered in the later comparison.

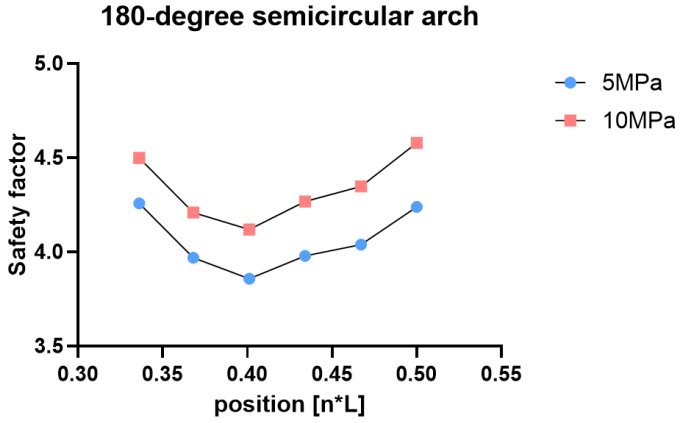


**Figure 4.4: Failure load – Position curves with different masonry strengths (semicircular arch)**

| position | Failure load [kN] | | Difference |
|---|---|---|---|
| | Masonry strength 5MPa | Masonry strength 10MPa | |
| 0.500L | 4.24 | 4.58 | 7.42% |
| 0.467L | 4.04 | 4.35 | 7.13% |
| 0.434L | 3.98 | 4.27 | 6.79% |
| 0.401L | 3.86 | 4.12 | 6.31% |
| 0.368L | 3.97 | 4.21 | 5.70% |
| 0.336L | 4.26 | 4.5 | 5.33% |

**Table 4.2: Comparison of failure loads for different masonry strengths (semicircular arch)**

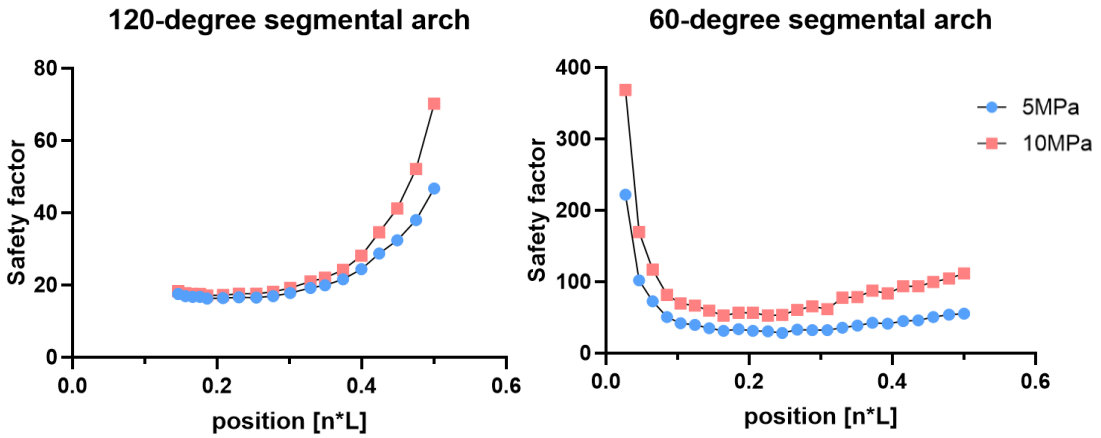


**Figure 4.5: Failure load – Position curves with different masonry strengths**

### *4.2.2 Effect of angle of embrace*

As shown in *Figure 4.6*, the collapse load differs significantly for arches with different embrace angles. The error bar shows values of failure loads in two masonry strengths – the higher one for 10 MPa and the lower one for 5 MPa. The curves show the trends for mean values. It is obvious that with the same ring thickness, bearing capacity of semicircular arch is the lowest, and that of arch with 60-degree angle of embrace is the highest.

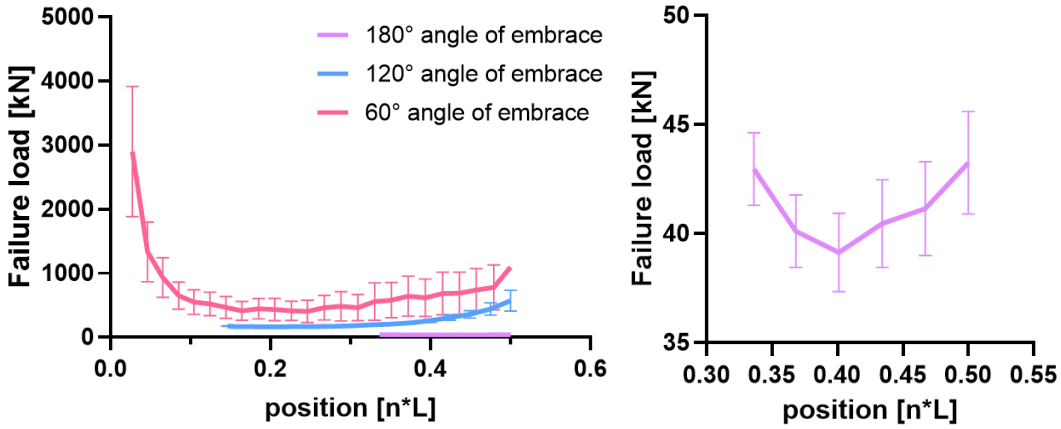


**Figure 4.6: Failure load – Position curves with different angles of embrace in Archie-M**

A summary of critical positions and critical loads of arches in Archie-M is shown in *Table 4.3*.

| Angle of embrace | Masonry strength | Critical position | Difference | Critical load [kN] | Difference |
|---|---|---|---|---|---|
| 180° | 5 Mpa | 0.401L | 0 | 37.867 | 6.31% |
| | 10 Mpa | 0.401L | | 40.417 | |
| 120° | 5 Mpa | 0.186L | 0 | 160.884 | 4.71% |
| | 10 Mpa | 0.186L | | 168.830 | |

| | | | | | |
|---|---|---|---|---|---|
| 60° | 5 Mpa | 0.164L | 0 | 311.958 | 40.00% |
| | 10 Mpa | 0.164L | | 519.930 | |

**Table 4.3: Comparison of critical positions and critical loads in Archie-M**

Arch with smaller angle of embrace has smaller critical position (closer to the springing) and larger critical load. The difference of critical load in arch with 60-degree of embrace is much larger than those in arches with 180-degree or 120-degree embrace angles.

Positions of hinges could be shown in Archie-M. As *Figure 4.7* shows, hinge mechanism forms when four hinges appear in the arches with 180-degree and 120-degree embrace angles. While for arch with 60-degree embrace angle, something interesting happens. The arch would not fail or collapse due to four-hinge mechanism, but the voussoir would be crushed at the position where the load is applied to. This explains why arches with stronger masonry strength could bear larger load. Note that frictional sliding is not taken into consideration in Archie-M program so the failure can be due to hinging, or to the crushing of the material.

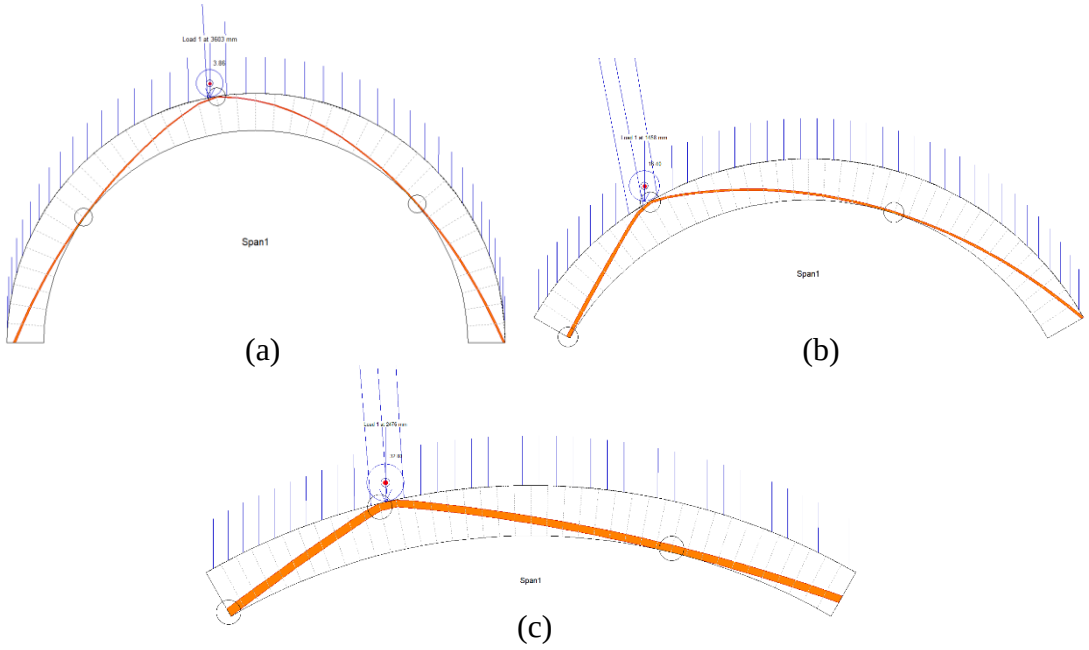


**Figure 4.7: Failure modes: (a) semicircular arch: hinge mechanism; (b) 120° embrace angle arch: hinge mechanism; (c) 60° embrace angle: masonry crush**

From the left graph in *Figure 4.6* we can see that failure loads near the springing are extremely large for the arch with 60° embrace angle. *Figure 4.8* shows the failure when a load is applied to a certain position. Archie-M considers that the abutment under the arch could withstand the compressive stresses and only consider the crush on the

extrados. So, the values are not realistic and in the following comparisons, collapse loads at the abutments will not be considered.

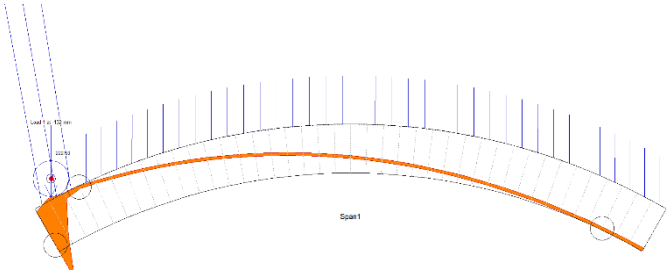


**Figure 4.8: Failure modes at the abutments**

# 5 Numerical Modeling – RING

In this part, five models simulating those in 3DEC are built.

## *5.1 The models of the arches in RING*

### *5.1.1 Geometry of arches in RING*

A span with stone voussoir and in segmental shape has to be specified with span (*l*), midspan rise (*h*), ring thickness (*t*) and numbers of units. A backfill whose top cannot be lower than the arch rings should be set. So, I set the height to surface (*y*) is equal to the highest point of the arch. The surface fill depth (*d*) is zero. *Figure 5.1* shows the geometric properties of the predefined in RING. The final geometric properties are shown in *Table 5.1* and the final models can be seen in *Figure 5.2*.

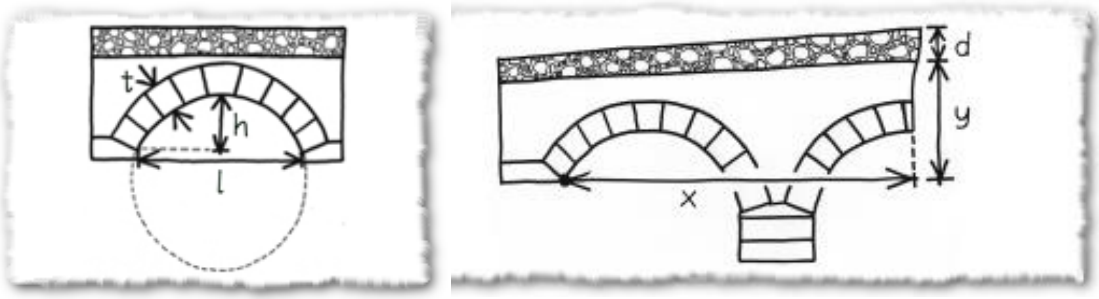


**Figure 5.1 Geometric properties of the predefined arches in RING (Program)**

| Model | Span [mm] | Midspan rise [mm] | No. of units | Ring thickness [mm] | Hight to surfaces depth [mm] |
|---|---|---|---|---|---|
| Arch1 | 9197.4 | 4598.68 | 51 | 802.5 | 5401.25 |
| Arch2 | 9305.2 | 2684.9 | 51 | 802.5 | 3488.6 |
| Arch3 | 9598.8 | 1286 | 51 | 802.5 | 2088.5 |
| Arch4 | 9197.4 | 4598.68 | 77 | 802.5 | 5401.25 |
| Arch5 | 9305.2 | 2684.9 | 59 | 802.5 | 3488.6 |

**Table 5.1: Geometric properties of the arches in RING**

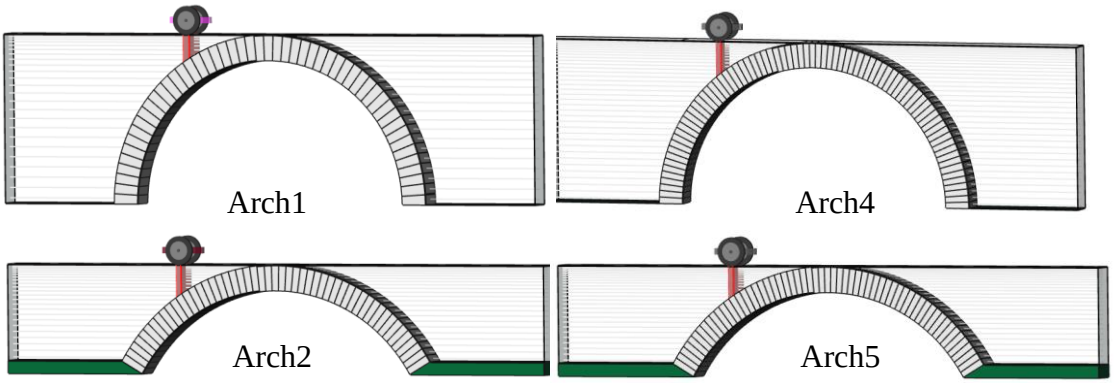

Arch3

**Figure 5.2 The RING models of the arches**

### *5.1.2 Materials of arches in RING*

For the masonry, the unit weight is 26,5 kN/m$^3$. Crushing properties are not considered which means that the model will not be able to fail by masonry crushing. Sliding properties with the usual friction coefficient of the contacts are taken into consideration. The three friction angles, 30°, 40° and 45° are analyzed. So, the friction coefficients are 0,577, 0,839 and 1,000, respectively.

For the backfill, soil unit weight is set to be zero, so that there is no additional load applied on the arch. It does not consider the soil effects such as model dispersion of live load and model horizontal passive pressures.

- **Masonry**
- Masonry unit weight: 26,5 kN/m$^3$
- Mortar sliding:
  Standard friction coefficient: 0,577, 0,839 or 1,000
- **Backfill**
- Soil unit weight: 0
- Soil effects: not considered

### *5.1.3 Load in RING*

Apply a unit force (1 kN) with 802,5 mm width to the arch. Loaded length can be modified to find a best value to simulate the block loads in 3DEC. For example, an appropriate value for the loaded length in Arch 1 is 170 mm, while 130 mm goes well in Arch 4 (*Figure 5.3*).

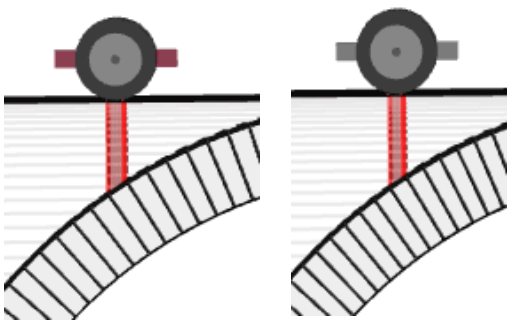

**Figure 5.3 Modifications of loaded length in RING**

## 5.2 The results in RING

### 5.2.1 Effect of fill depth

Considering there is backfill in the models, which is different to the initial conditions, I analyzed arches with different fill depths to see whether the backfill has an influence on the failure modes and failure loads on the condition that the soil effects are not taken into consideration in the program.

*Table 5.2* shows the failure loads for different positions in semicircular arches.

| **position** | | **0.500L** | **0.467L** | **0.434L** | **0.401L** | **0.368L** | **0.336L** |
|---|---|---|---|---|---|---|---|
| Failure load [kN] | depth 0 | 49.5 | 46 | 44.6 | 45 | 46.9 | 50.5 |
| | depth 500 | 49.5 | 46 | 44.6 | 45 | 46.9 | 50.5 |
| | depth 1000 | 49.5 | 46 | 44.6 | 45 | 46.9 | 50.5 |

Note: "depth *x*", *x* here means the height from the crown to the backfill surface

**Table 5.2: Failure loads with different fill depths for Arch 1 with 30-degree friction angle**

| **position** | | **0.50 L** | **0.45 L** | **0.40 L** | **0.35 L** | **0.30 L** | **0.28 L** | **0.25 L** | **0.23 L** | **0.20 L** |
|---|---|---|---|---|---|---|---|---|---|---|
| Failure load [kN] | depth 0 | 3950 | 544 | 324 | 253 | 225 | 220 | 219 | 222 | 238 |
| | depth 500 | 3950 | 544 | 324 | 253 | 225 | 220 | 219 | 222 | 238 |
| | depth 1000 | 3950 | 544 | 324 | 253 | 225 | 220 | 219 | 222 | 238 |

**Table 5.3: Failure loads with different fill depths for Arch 2 with 45-degree friction angle**

The two tables above show only a part of the results, while the complete set of the detailed results can be found in *Appendix E*. Failure modes in two positions for Arch 2 are shown in *Figure 5.4*.

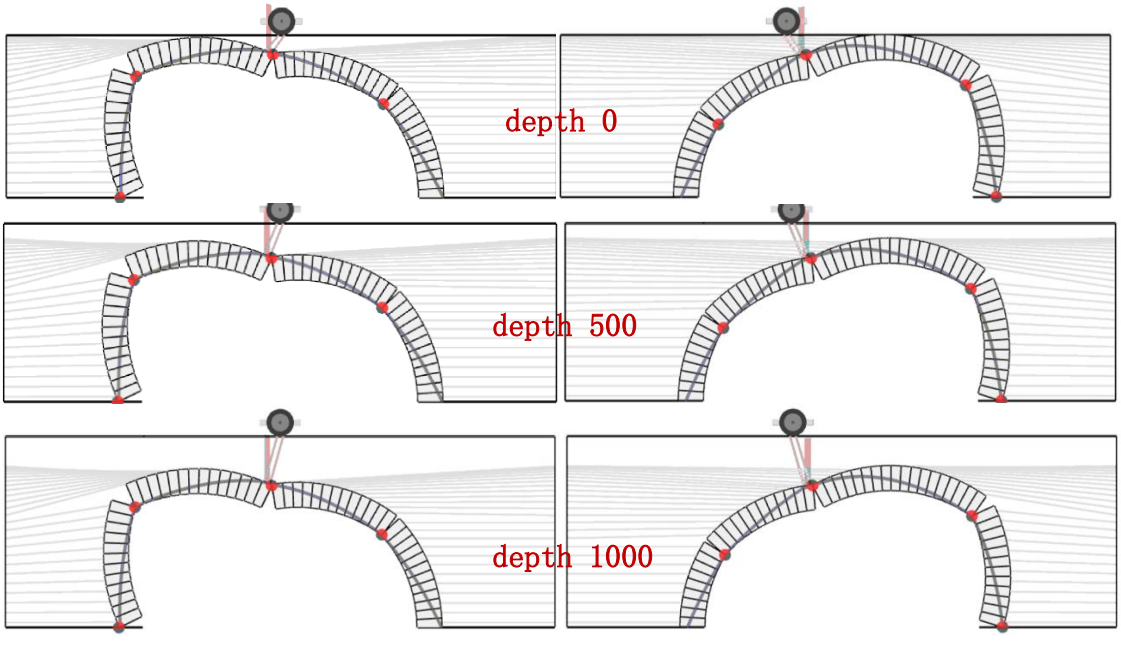


**Figure 5.4 Failure modes for arches with different backfill depth**

It is clear that the depth of backfill has no effect on the results, neither on failure load nor on failure mode. Even the hinge positions do not show any difference. It provides the conclusion that the models I built can be considered as a "concentrated load" applied to the arch without backfill, which is important for later comparisons.

### 5.2.2 Effect of number of blocks

In this case, arches with 30-degree friction angle are analyzed. Similar to the results in 3DEC modelling, number of blocks has small influences in the failure loads for different positions. As shown in *Figure 5.5* and *Table 5.4*, for arches with larger blocks (smaller the number of blocks), collapse loads are slightly smaller. The critical load differs about 1,5%, which is absolutely negligible. The critical position differs about 5% for this case study.

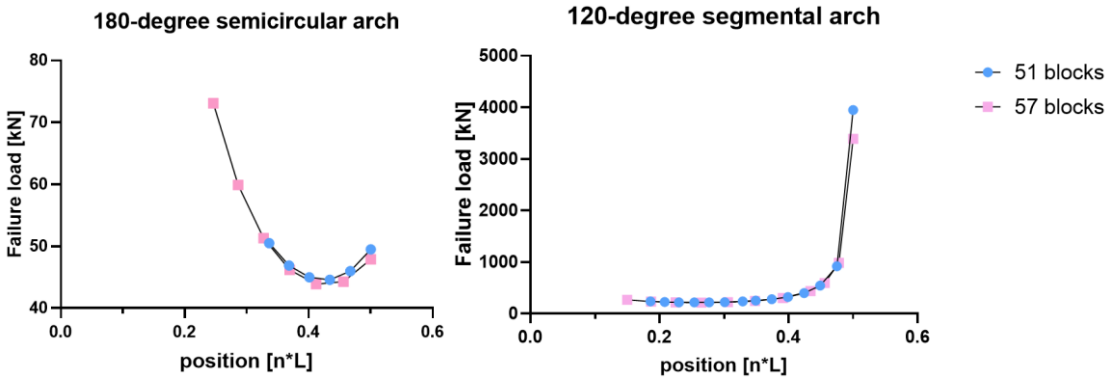


**Figure 5.5 Failure load – position curve with different numbers of blocks**

| Embrace angle | Group | Critical position | Difference | Critical load [kN] | Difference |
|---|---|---|---|---|---|
| 180° | 51 blocks | 0.434L | 5.07% | 44.6 | 1.57% |
| | 77 blocks | 0.412L | | 43.9 | |
| 120° | 51 blocks | 0.254L | -4.33% | 219 | 1.37% |
| | 59 blocks | 0.265L | | 216 | |

**Table 5.4: Comparison of the critical positions and critical loads of different block numbers**

### 5.2.3 Effect of angle of embrace

The angle of embrace has a significant effect on the failure load and failure mode. The case study analyzes the three arches with angle of embrace 180°, 120° and 60°, having 51 segments. The friction angle is 30°.

Similar to the conclusions of the 3DEC modelling and Archie-M modelling, arch with smaller angle of embrace has larger bearing capacity. Critical positions will be close to the arch springing, if embrace of angle decreases.

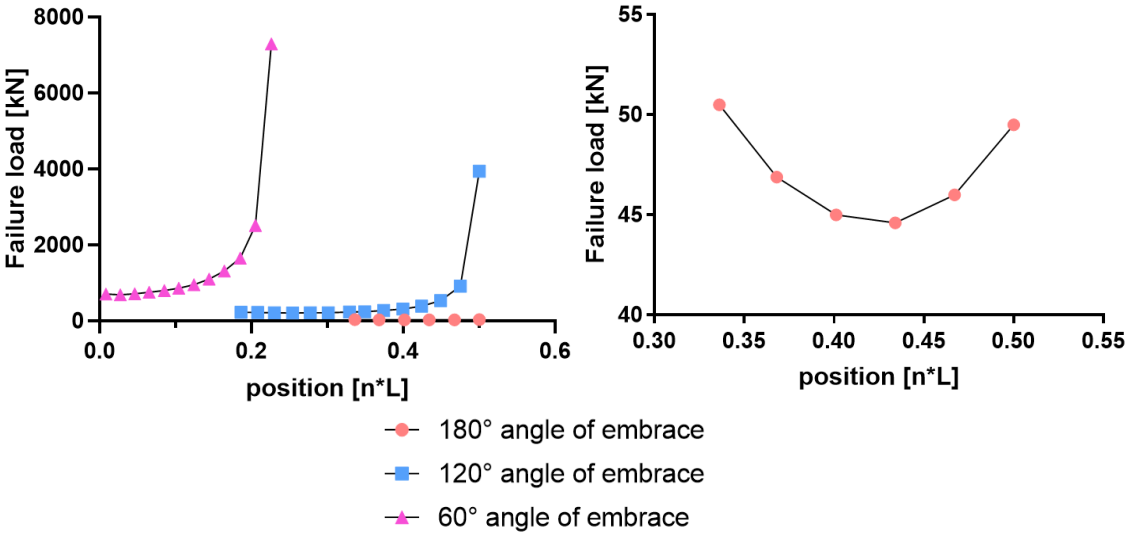


**Figure 5.6: Failure load – Position curves with different angles of embrace**

| Group | Embrace angle | Critical position | Critical load [kN] |
|---|---|---|---|
| 1 | 180° | 0.434L | 44.6 |
| | 120° | 0.254L | 219 |
| | 60° | 0.027L | 696 |

**Table 5.5: Comparison of the critical positions and critical loads of different angles of embrace**

Concerning the failure modes in *Figure 5.8*, we can see that the arches with 180-degree and 120-degree embrace collapse with a pure hinge mechanism.

For the arch with 60-degree of embrace, there are several cases calculating collapse load from the arch springing to the crown. At the position from 0,008L to 0,144L, the arch fails on account of frictional sliding near the load position and three hinges. A hinge mechanism will be formed from 0,144L to 0,226L. A special phenomenon is found when the load travels from 0,226L to 0,500L (half span), that a "geometrically locked" situation appears (*Figure 5.8* (c)).

It is an idea that the geometry could be locked in the case, if the arch could bear infinitely large forces or loads. As the blocks used in RING are rigid, the geometry of the arch is not deformable. What's more, crushing is not taken into account in the model, so, the reaction forces could be arbitrarily large. The situation can be explained by a graphical static analysis, which is shown in *Figure 5.7*. As the blue line shows, the three lines of action intersect, which means no matter how much the applied force is, the system can find an equilibrium. Note that the selfweight of the arch is neglected, when the applied force is considered to be infinitely large.

A position range for infinitely large bearing capacity can be determined by the orange line in *Figure 5.7*. Draw a straight line from one side of arch springing, which is always within the cross section of the arch. B is the tangent point of the line and intrados. Extend AB to the extrados and the intersect point is denoted by C. Then C is the critical

position we are looking for. With the help of AutoCAD, the *x* coordinate of C is 0.228L. In the simulation in RING, the critical position is 0.246L. The graphical static predictions are in agreement with the RING results.

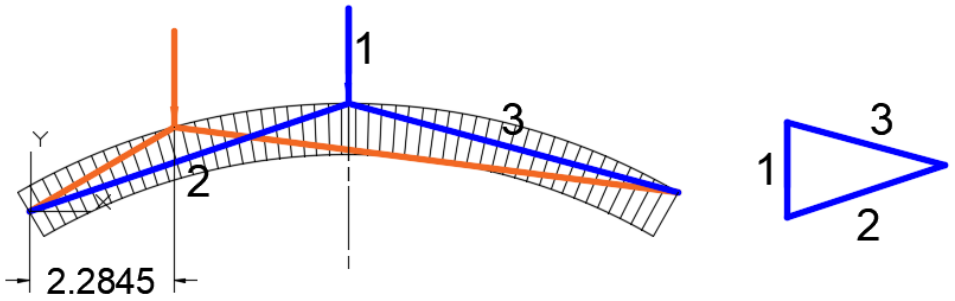


**Figure 5.7: Graphical static analysis to find the position range for geometrically locked situation**

If an arch can bear any downwards load applied to any arbitrary positions on the arch, i.e. a statically admissible force system can always be found, then the arch can be called a "flat arch". This concept is proposed by Heyman in 1982. This kind of arches cannot fail with any Heymanian collapse modes (which means that only hinging mechanism exists). Failure in flat arches can happen due to material crushing or contact sliding.

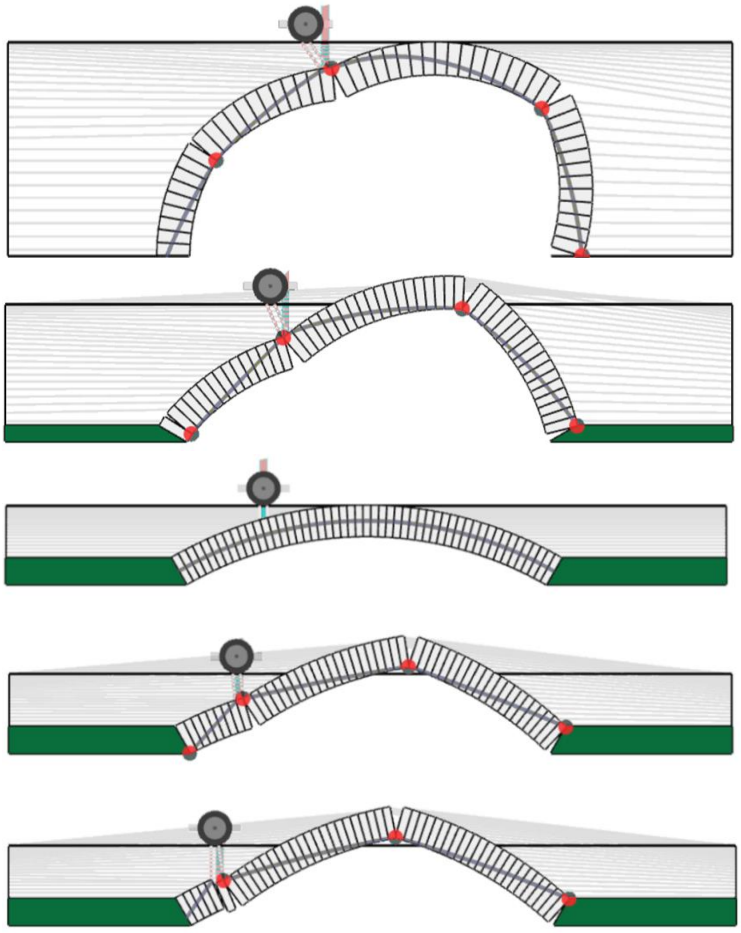

Angle of embrace: 180°
Hinge mechanism

Angle of embrace: 120°
Hinge mechanism

Angle of embrace: 60°
No failure
0,226 L ~ 0,500 L

Hinge mechanism
0,144 L ~ 0,266 L

Combined shear-hinge mechanism

**Figure 5.8: Failure modes of arches with different angles of embrace (friction angle = 30°)**

### 5.2.4 *Effect of friction angle*

The detailed results of load positions and corresponding collapse loads can be found in *Appendix F*.

*1) Semicircular arch & 120-degree embrace angle segmental arch*

Everything remains the same though frictional angle changes from 30° to 45°:

- Same value of failure load in the same load position;
- Same failure mode – Hinge mechanism;
- Same critical position and same critical load.

I tried to set a friction angle of 20° to see what would happen, though the value is not realistic for masonry structures. *Figure 5.9* and *Table 5.6* show the result.

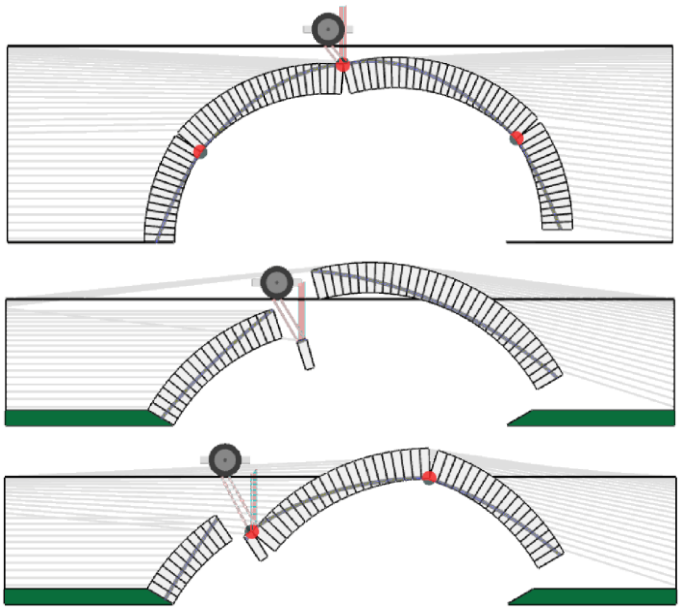

**Figure 5.9: Failure modes of arches with different angles of embrace (friction angle = 20°)**

Angle of embrace: 180°

| Position | Failure load [kN] | | Difference |
|---|---|---|---|
| | 20° | 30°/40°/45° | |
| 0.500L | 6.42 | 49.5 | 671% |
| 0.467L | 6.4 | 46 | 619% |
| 0.434L | 6.94 | 44.6 | 543% |
| 0.401L | 7.74 | 45 | 481% |
| 0.368L | 8.72 | 46.9 | 438% |
| 0.336L | 9.95 | 50.5 | 408% |

Angle of embrace: 120°

| Position [mm] | Failure load [kN] | | Difference |
|---|---|---|---|
| | 20° | 30°/40°/45° | |
| 0.500L | 176 | 3950 | 2144% |

| | | | |
|---|---|---|---|
| 0.449L | 159 | 544 | 242% |
| 0.424L | 154 | 399 | 159% |
| 0.349L | 149 | 253 | 70% |
| 0.301L | 150 | 225 | 50% |
| 0.277L | 150 | 220 | 47% |
| 0.230L | 154 | 222 | 44% |
| 0.186L | 165 | 238 | 44% |

**Table 5.6: Comparison of the critical positions and critical loads of different friction angles**

Sliding between blocks and abutments can occur due to weak connections. For semicircular arch, three hinges and one slide may be formed. For an arch with 120-degree angle of embrace, two conditions can occur: sliding at the abutment and at the load position; two hinges and two slides. What's more, the difference of failure loads for 20- and 30-degree friction angle is really huge, which also confirms that frictional sliding occurs at failure.

*2) 60-degree embrace angle segmental arch*

Frictional sliding is taken into account in RING.

| **position** | **Failure load [kN]** | | |
|---|---|---|---|
| | **30° friction angle** | **40° friction angle** | **45° friction angle** |
| 0.246L | - | - | - |
| 0.226L | 7300 | 7300 | 7300 |
| 0.205L | 2520 | 2520 | 2520 |
| 0.185L | 1660 | 1660 | 1660 |
| 0.164L | 1320 | 1320 | 1320 |
| 0.144L | 1110 | 1180 | 1180 |
| **0.124L** | 965 | **1140** | **1140** |
| 0.104L | 873 | 1210 | 1210 |
| 0.085L | 812 | 1250 | 1450 |
| 0.065L | 761 | 1210 | 1590 |
| 0.046L | 722 | 1170 | 1590 |
| **0.027L** | **696** | 1150 | 1600 |
| 0.008L | 719 | 1200 | 1660 |

Note: The red numbers refer to the critical position and critical loads; failure modes for the circled positions in the table are hinge mechanism, while for the rest of places, failure modes are combined shear-hinge mechanism; "-" means no solution is found due to geometrically locked force system.

**Table 5.7: Failure loads of 60-degree angle of embrace segmental arch (part of data)**

It is clear that friction angle does not influence the failure loads when a pure hinge mechanism is found in the arch. But in the case that sliding takes part in the failure of arches, friction angle would have a significant effect on the results. The smaller the

friction angle is, the smaller the failure load is. *Figure 5.10* shows the failure load – position curve with different friction angles.

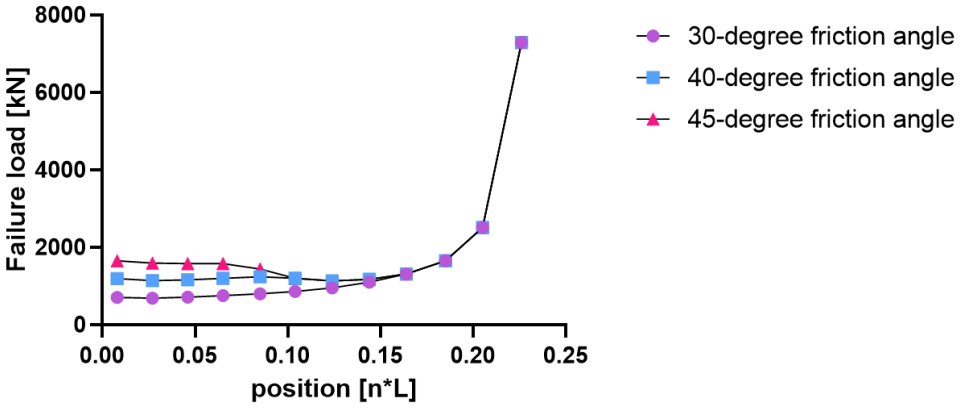


**Figure 5.10: Failure load – Position curves with different friction angles for the 60-degree arch**

# 6 Comparisons of the three methods

In this chapter, failure load and failure mode obtained from the three programs are compared and a brief summary of the thesis is made.

## *6.1 Semicircular arch*

Friction does not participate in the four models with 180-degree embrace angle. With different friction angles, the results are the same. *Figure 6.1* and *Table 6.1* illustrate that collapse load in Archie-M is smaller than that in 3DEC (no matter how large the masonry strength is), while collapse load in RING is larger than 3DEC. As for the critical position and critical load, the results in RING are closer to those in 3DEC, compared to Archie-M.

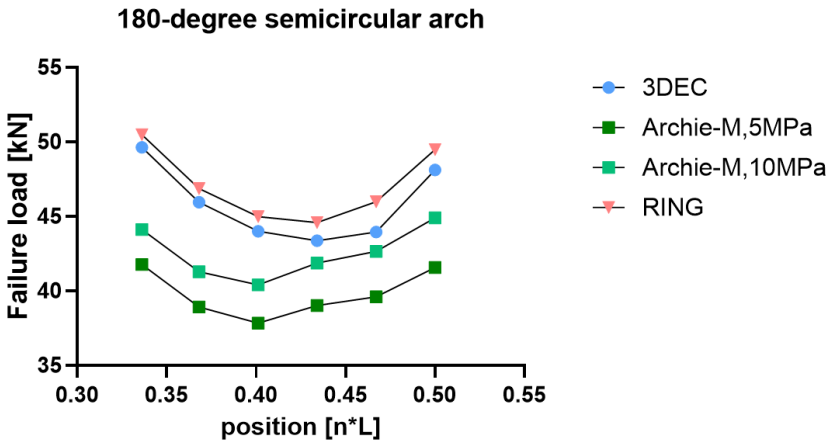


**Figure 6.1 Failure load – position curve with different programs (semicircular arch)**

| Model | Critical position | Difference | Critical load [kN] | Difference |
|---|---|---|---|---|
| 3DEC | 0.434L | - | 43.399 | - |
| Archie-M, 5MPa | 0.401L | 7.60% | 37.867 | 12.75% |
| Archie-M, 10MPa | 0.401L | 7.60% | 40.417 | 6.87% |
| RING | 0.434L | 0 | 44.6 | -2.77% |

Note: the difference in the table refers to the difference between the corresponding value and that of 3DEC

**Table 6.1: Critical position and critical load in different programs (semicircular arch)**

Arches would fail due to hinge mechanism in all of these models.

## *6.2 120-degree angle of embrace segmental arch*

A similar comparison is done for arches with 120-degree embrace angle. As shown in *Figure 6.2* and *Table 6.2*, the failure load differs about 6% maximum for RING and 3DEC, neglecting one value when load applied on the crown. At that load position, the

arch in 3DEC would deform a little and the voussoir under the loading block may slide a little, while the RING model is rigid and would not deform. This can also explain why in 3DEC model, friction angle would influence the values of failure load around the arch crown. Archie-M models produce a smaller result with a difference around 20% (compared to the result in 3DEC model).

The three models produce a similar trend for the failure load in different load position, while 3DEC model and RING model give a similar result for critical position and critical load. But the results in Archie-M are much safer.

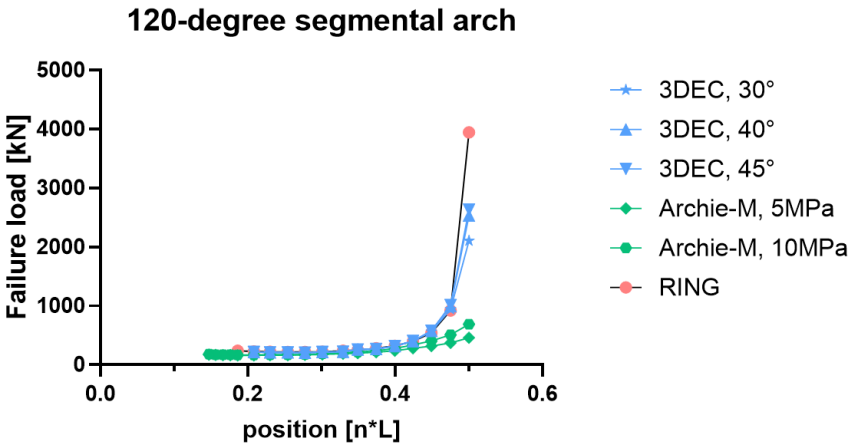


**Figure 6.2 Failure load – position curve with different programs (segmental arch – 120° embrace angle)**

| Model | Critical position | Difference | Critical load [kN] | Difference |
|---|---|---|---|---|
| 3DEC | 0.277L | - | 206.651 | - |
| Archie-M, 5MPa | 0.186L | 32.85% | 160.884 | -22.15% |
| Archie-M, 10MPa | 0.186L | 32.85% | 168.83 | -18.30% |
| RING | 0.254L | 8.30% | 219 | +5.98% |

**Table 6.2: Critical position and critical load in different programs (segmental arch – 120° embrace angle)**

The three models produce the same collapse mode, i.e. hinge mechanism, which can be seen in previous chapters.

## *6.3 60-degree angle of embrace segmental arch*

Situations in arches with a small angle of embrace are complicate as frictional sliding takes part in the failure mode and friction influences the value of collapse load. Firstly, failure modes in different models are compared, and the results are shown in *Table 6.3*.

Obviously, Archie-M couldn't consider the effect of frictional sliding. As a result, the arch fails because of material crushing, on which masonry strength has an important effect. RING cannot produce a failure load at position between 0.246L to 0.500L, while because of the deformability of the material and contacts, a failure can be found in 3DEC (this has been explained in section 3.2.2). But the failure modes at the position

range 0.008L ~ 0.226L are similar in RING and 3DEC. Note that RING can also consider the effect of material crushing, but since the aim of this project was to compare the possibly most similar situations in 3DEC and the other codes, the RING models in this thesis don't consider it. The compressive strength in 3DEC model is infinitely large, and structures in it can only fail by contact cracking up or sliding of blocks.

<table>
<tr><th rowspan="2">Position</th><th colspan="2">30° friction angle</th><th colspan="2">40° friction angle</th><th colspan="2">45° friction angle</th><th rowspan="2">Archie-M</th></tr>
<tr><th>3DEC</th><th>RING</th><th>3DEC</th><th>RING</th><th>3DEC</th><th>RING</th></tr>
<tr><td>0.500L</td><td rowspan="2">Sliding</td><td rowspan="4">-</td><td rowspan="2">Sliding</td><td rowspan="4">-</td><td rowspan="2">Sliding</td><td rowspan="4">-</td><td rowspan="15">Material Crushing</td></tr>
<tr><td>0.457L</td></tr>
<tr><td>0.436L</td><td rowspan="2">Combined</td><td rowspan="2">Combined</td><td rowspan="2">Combined</td></tr>
<tr><td>0.246L</td></tr>
<tr><td>0.226L</td><td rowspan="3">Hinging</td><td rowspan="2">Hinging</td><td rowspan="5">Hinging</td><td rowspan="5">Hinging</td><td rowspan="7">Hinging</td><td rowspan="5">Hinging</td></tr>
<tr><td>0.164L</td></tr>
<tr><td>0.144L</td><td rowspan="8">Combined</td></tr>
<tr><td>0.124L</td><td rowspan="7">Combined</td></tr>
<tr><td>0.104L</td><td rowspan="6">Combined</td></tr>
<tr><td>0.085L</td><td rowspan="5">Combined</td></tr>
<tr><td>0.065L</td><td rowspan="4">Combined</td><td rowspan="4">Combined</td></tr>
<tr><td>0.046L</td><td rowspan="3">Combined</td></tr>
<tr><td>0.027L</td></tr>
<tr><td>0.008L</td></tr>
</table>

**Table 6.3: Failure modes in different programs (segmental arch – 60° embrace angle)**

As shown in *Figure 6.3*, generally, failure load in Archie-M ⩽ failure load in 3DEC ⩽ failure load in RING. Magnification of the curve for certain positions can be shown in *Figure 6.4*, where we can see a similar result is provided by 3DEC and RING, while Archie-M gives a totally different one.

*Table 6.4* shows critical positions and critical loads in these models. The difference of failure loads between 3DEC and RING with the same friction angle is approximately 9%.

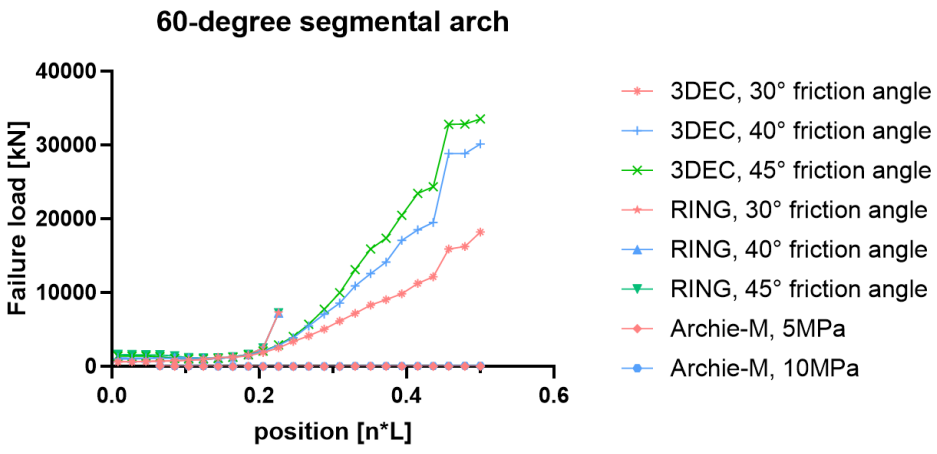


**Figure 6.3 Failure load – position curve with different programs (segmental arch – 60° embrace angle)**

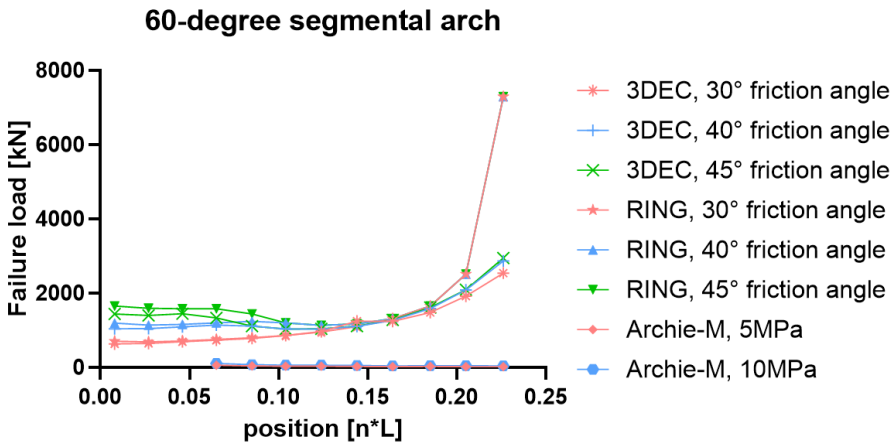


**Figure 6.4 Magnification failure load – position curve with different programs (segmental arch – 60° embrace angle)**

| Model | Friction angle/ Masonry strength | Critical position | Critical load [kN] | Difference |
|---|---|---|---|---|
| 3DEC | 30° | 0.008L | 644.489 | - |
| | 40° | 0.104L | 1040.643 | - |
| | 45° | 0.104L | 1043.287 | - |
| Archie-M | 5 MPa | 0.246L | 283.509 | - |
| | 10 MPa | 0.164L | 519.93 | - |
| RING | 30° | 0.027L | 696 | 7.99% |
| | 40° | 0.124L | 1140 | 9.55% |
| | 45° | 0.124L | 1140 | 9.27% |

**Table 6.4: Critical position and critical load in different programs (segmental arch – 60° embrace angle)**

## *6.4 Summary*

The summary will be in two parts, one for behaviors of arches, and the other for the comparison of the three methods (3DEC, Archie-M and RING).

### *6.4.1 Arch behaviors*

- For single-ring arches with the same ring thickness, the smaller angle of embrace causes larger load bearing capacity.
- Arches with smaller size of blocks have lower load bearing capacity. However, the difference was found small (4.34% maximum) in my thesis.
- Concerning the critical positions, semicircular arch has a critical position near half span of the arch, while as the angle of embrace decreases, the critical position shifts to the arch springing.

- Arches with 180- and 120-degree angles of embrace fail due to hinge mechanism. Arches with 60-degree angle of embrace may fail due to different reasons: combined sliding-hinging mechanism (large sliding) occurs when load is applied near abutments; pure hinge mechanism; combined sliding-hinging mechanism (small sliding) and pure frictional sliding mechanism is found when load is applied around the arch crown. In addition, material crushing should also be taken into account.
- Contact friction angle has an important effect on the arch with 60-degree angle of embrace. With smaller friction angle, failure load is smaller. But it has no effect on collapse load where hinge mechanism dominates the failure mode, i.e. where no frictional sliding exists.
- Dynamic failure load and quasi-static failure load are roughly equal around the critical position of the arch.
- When a load travels starting from outside to inside along the arch, the arch may fail before the failure load reaches its critical position. This can be explained by the deformation of the arch.

### *6.4.2 Comparisons of 3DEC, Archie-M and RING*

- The collapse load differs in the three programs. Generally, failure load in Archie-M $\leqslant$ failure load in 3DEC $\leqslant$ failure load in RING. This means Archie-M model is the safest one to apply among these three programs, if material crushing is an issue to consider.
- Compared to Archie-M, RING produce closer results to 3DEC modelling, not only for failure load, but also for failure mode.
- Archie-M model does not include the possibility of sliding failure, while RING does. In addition, RING can also consider material crushing in masonry bridges, which is the main failure mode in Archie-M for arches with small angle of embrace. 3DEC models cannot fail by material crushing, as compressive strength of material is infinitely large.
- RING may not accurately predict the failure load and failure mode of an arch which contains flat sections because the structure is considered undeformable in RING. In 3DEC, elastic deformations prior to collapse will significantly change the arch geometry.
- Archie-M does not give a solution on how the arch deforms after failure, while RING and 3DEC do give.
- 3DEC needs a long time to iterate (1 ~ 5 hours for a dynamic load simulation) while Archie-M and RING get results fast (immediately).

- Regarding theoretical fundaments, Archie-M checks whether the arch is safe by a trust line method (static theorem), while RING combines the kinematic and static theorems.

## References


Audenaert, A., Beke, J. (2010). *Applicability analysis of 2D-models for masonry arch bridge assessment: RING, Archie-M and the elasto-plastic model*, WSEAS Transactions on Applied and Theoretical Mechanics, Vol. 5 pp. 221-230

Bagi, K. (2012). *Fundaments of the discrete element method*, Lecture Notes, Budapest University of Technology and Economics

Bagi, K. (2014). *When Heyman's Safe Theorem of rigid block systems fails: Non-Heymanian collapse modes of masonry structures*, International Journal of Solids and Structures Vol. 51, Issue 14, pp. 2696 – 2705

Beatini, V., Royer-Carfagni, G. and Tasora, A. (2018). *Modeling the shear failure of segmental arches*, International Journal of Solids and Structures, doi: 10.1016/j.ijsolstr.2018.08.023.

Block, P., DeJong, M. and Ochsendorf, J. (2006). *As hangs the flexible line: equilibrium of masonry arches*, Nexus network journal 8(2), pp. 13-24

Boothby, T. E., Nelson, S. E., Scolforo, M. J. (1994). *A visual classification system for masonry arch failures.* In: Procs. 10th IB$^2$MaC, 5-7 July 1994, Calgary, Canada, pp. 349-358

Cocchetti, G., Colasantle, G., Rizzi, E. (2011). *On the analysis of minimum thickness in circular masonry arches*, Applied Mechanics Reviews, ASME, 64(5), 050802

Cundall, P. A. (1971). *The measurement and analysis of accelerations in rock slops*, PhD Thesis, University of London

Cundall, P. A. and Hart, R. D. (1992). *Numerical modelling of discontinua*, Engineering Computations, 9(2), 101-113, doi:10.1108/eb023851

Drucker, D. C. (1954). *Coulomb Friction, Plasticity and Limit Loads*, Journal of Applied Mechanics 21, pp. 71 – 74

Foce, F. (2007). *Milankovitch's Theorie der Druckkurven: Good mechanics for masonry architecture*, Nexus Network Journal 9(2), pp. 185–210

Gilbert, M. (2007). *Limit analysis applied to masonry arch bridges: State-of-art and recent developments*, Conference Paper: 5th International Arch Bridges Conference

Gilbert, M., Casapulla, C., Ahmed, H.M. (2006). *Limit analysis of masonry block structures with non-associative frictional joints using linear programming*. Computers and Structures 84, pp. 873-887.

Gilbert, M., Ahmed, H. M. (2004). *Developments to the RING masonry arch bridge analysis software*, 4th International Arch Bridges Conference

Heyman, J. (1966). *The Stone Skeleton*, International Journal of Solids and Structures Vol.2, pp. 249 – 279

*http://www.obvis.com/archie-theory/*

*https://www.jsg.utexas.edu/tyzhu/files/Some-Useful-Numbers.pdf*

Itasca consulting group (2003). *3DEC - 3 Dimensional Distinct Element Code - Online Manual*.

Itasca Consulting Group (2007). *3 Dimensional Distinct Element Code. Theory and Background.* Minneapolis, Minnesota, USA

Jing, L. (1998). *Formulation of discontinuous deformation analysis (DDA) – an implicit discrete element model for block systems*, Engineering Geology Vol. 49, Issue 3-4, pp. 371-381

Khan, M. S. (2010). *Investigation of Discontinuous Deformation Analysis for Application in Jointed Rock Masses*, Ph.D. Thesis, University of Toronto

Kooharian, A. (1952). *Limit Analysis of Voussoir (Segmental) and Concrete arches*, Journal of the American Concrete Institute 24, pp. 317 – 328

Krabbenhoft, K., Lyamin, A. V., Huang, J., Vicente da Silva, M. (2012). *Granular contact dynamics using mathematical programming methods*, Computers and Geotechnics 43(2012), pp. 165-176

Lemos, J. V. (2007). *Discrete Element Modeling of Masonry Structures*, International Journal of Architectural Heritage 1(2), pp. 190-213

LimitState Ltd (2016). *LimitState:RING Manual Version 3.2.b*

Manicka Selvam, V.K. (1993), *Fundamentals of Limit Analysis of Structures (A Course in Plastic Analysis of Structures),* ISBN-10: 9383182180

Mendes, N. (2015). *Masonry macro-block analysis*, Frequency-Magnitude Distribution of Seismicity in Volcanic Regions, pp. 1411-1419

Nobile, L., Bartolomeo, V. (2014). *Methods for the Assessment of Historical Masonry Arches*, Recent Advances in Civil Engineering and Mechanics, pp. 160-167, ISBN: 978-960-474-403-9

Nobile, L., Bartolomeo, V. (2017). *Comparison between available assessment methods of historical masonry arches*, International Journal of Mathematical Models and Methods in Applied Sciences, Vol. 11 pp. 61-67

Obvis Ltd (2007). *Archie-M, masonry arch bridge and viaduct assessment software*, Version 2.3.1

Radjai, F. and Richefeu, V. (2010). *Contact dynamics method*, Laboratoire de M´ecanique et G´enie Civil, CNRS - Universit´e Montpellier

Sarhosis, V., De Santis, S. and De Felice, G. (2016). *A review of experimental investigations and assessment methods for masonry arch bridges*, Structure and Infrastructure Engineering, 12(11), pp. 1439-1464

Tralli, A., Alessandri, C. and Milani, G. (2014). *Computational Methods for Masonry Vaults: A Review of Recent Results*, The Open Civil Engineering Journal 8, pp. 272-287

Unger, T. and Kertesz, J. (2003). *The Contact Dynamics Method for Granular Media*, AIP Conference Proceedings Vol.661

# Appendix A – MATLAB code of the segmental arch (120°) with 0.205 m blocks

```
clc;clear;close all

% generate a 59-element vector, divide a 120 degree segmental circle into 59 parts
angle = linspace(pi/6,5*pi/6,60);

% calculate the radius of the arch
r = 5/(sin(pi/3))
r20 = r+0.8025/2
r10 = r-0.8025/2

% create another vector with the value of the outer radius
r2 = linspace(r20,r20,60);

% calculate the coordinates of the points in the outer circle
x2 = r20*cos(angle)
y2 = r20*sin(angle)

% plot the circle and the chosen 52 points with little red circles(ro)
polar(angle,r2,'o')

% name the figure 'Single-ring arch'
title('semicircular arch')
hold on

% create another 59-element vector for the inner radius
r1 = linspace(r10,r10,60);

% calculate the coordinates of the points in the inner circle
x1 = r10*cos(angle)
y1 = r10*sin(angle)

% plot this circle and the chosen 59 points with little blue x-es(bx)
polar (angle, r1,'bx')

% mark the center of the circles with a black square(ks)
polar(0,0,'ks')
z1 = -0.401250;
z2 = 0.401250;

% print the command to build the arch blocks
for i = 1:59
      fprintf('polyhedron prism a %f,%f,%f %f,%f,%f %f,%f,%f %f,%f,%f
b %f,%f,%f %f,%f,%f %f,%f,%f %f,%f,%f\n',
```

```
x2(i),y2(i),z1,x1(i),y1(i),z1,x1(i+1),y1(i+1),z1,x2(i+1),y2(i+1),z1,x2(i),y2(i),z2,x1(i),
y1(i),z2,x1(i+1),y1(i+1),z2,x2(i+1),y2(i+1),z2)
end

% print the command to build the support blocks
fprintf(';Define the support blocks with the same command\n')
fprintf('polyhedron prism a -6.1161,2.9536,-0.401250 -5.8661,3.3866,-0.401250 -
4.1341,2.3866,-0.401250 -4.3841,1.9536,-0.401250 b -6.1161,2.9536,0.401250 -
5.8661,3.3866,0.401250 -4.1341,2.3866,0.401250 -4.3841,1.9536,0.401250\n')
fprintf('polyhedron prism a 6.1161,2.9536,-0.401250 5.8661,3.3866,-0.401250
4.1341,2.3866,-0.401250 4.3841,1.9536,-0.401250 b 6.1161,2.9536,0.401250
5.8661,3.3866,0.401250 4.1341,2.3866,0.401250 4.3841,1.9536,0.401250\n')

% print the command to build the loading blocks
for i=1:30
    fprintf(';Define the loading block %d with the same command\n',i)
    fprintf('polyhedron prism a %f,%f,%f %f,%f,%f %f,%f,%f %f,%f,%f
b %f,%f,%f %f,%f,%f %f,%f,%f %f,%f,%f\n',x2(32-i),y2(32-i),z1,x2(32-i),y2(32-
i)+1,z1,x2(31-i),y2(31-i)+1,z1,x2(31-i),y2(31-i),z1,x2(32-i),y2(32-i),z2,x2(32-
i),y2(32-i)+1,z2,x2(31-i),y2(31-i)+1,z2,x2(31-i),y2(31-i),z2)
end
```

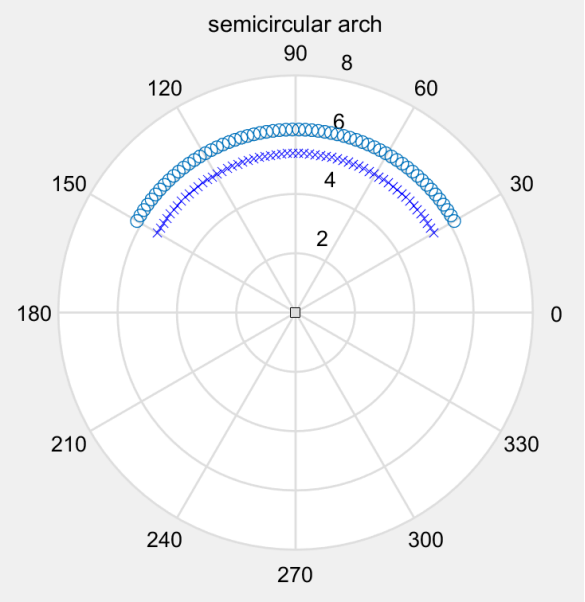

# Appendix B – 3DEC code of the segmental arch (60°) with 51blocks (Dynamic load, 30-degree friction angle)

```
; Start the *3ddat file with the new command
new
;
;Define the geometry with command prism
polyhedron prism a 5.200625,9.007747,-0.401250 4.799375,8.312761,-0.401250
4.627687,8.409549,-0.401250 5.014583,9.112626,-0.401250 b
5.200625,9.007747,0.401250 4.799375,8.312761,0.401250
4.627687,8.409549,0.401250 5.014583,9.112626,0.401250
polyhedron prism a 5.014583,9.112626,-0.401250 4.627687,8.409549,-0.401250
4.454048,8.502791,-0.401250 4.826427,9.213664,-0.401250 b
5.014583,9.112626,0.401250 4.627687,8.409549,0.401250
4.454048,8.502791,0.401250 4.826427,9.213664,0.401250
polyhedron prism a 4.826427,9.213664,-0.401250 4.454048,8.502791,-0.401250
4.278531,8.592449,-0.401250 4.636236,9.310817,-0.401250 b
4.826427,9.213664,0.401250 4.454048,8.502791,0.401250
4.278531,8.592449,0.401250 4.636236,9.310817,0.401250
polyhedron prism a 4.636236,9.310817,-0.401250 4.278531,8.592449,-0.401250
4.101210,8.678483,-0.401250 4.444091,9.404045,-0.401250 b
4.636236,9.310817,0.401250 4.278531,8.592449,0.401250
4.101210,8.678483,0.401250 4.444091,9.404045,0.401250
polyhedron prism a 4.444091,9.404045,-0.401250 4.101210,8.678483,-0.401250
3.922161,8.760859,-0.401250 4.250071,9.493308,-0.401250 b
4.444091,9.404045,0.401250 4.101210,8.678483,0.401250
3.922161,8.760859,0.401250 4.250071,9.493308,0.401250
polyhedron prism a 4.250071,9.493308,-0.401250 3.922161,8.760859,-0.401250
3.741457,8.839542,-0.401250 4.054260,9.578569,-0.401250 b
4.250071,9.493308,0.401250 3.922161,8.760859,0.401250
3.741457,8.839542,0.401250 4.054260,9.578569,0.401250
polyhedron prism a 4.054260,9.578569,-0.401250 3.741457,8.839542,-0.401250
3.559176,8.914497,-0.401250 3.856740,9.659791,-0.401250 b
4.054260,9.578569,0.401250 3.741457,8.839542,0.401250
3.559176,8.914497,0.401250 3.856740,9.659791,0.401250
polyhedron prism a 3.856740,9.659791,-0.401250 3.559176,8.914497,-0.401250
3.375395,8.985695,-0.401250 3.657594,9.736940,-0.401250 b
3.856740,9.659791,0.401250 3.559176,8.914497,0.401250
3.375395,8.985695,0.401250 3.657594,9.736940,0.401250
```

polyhedron prism a 3.657594,9.736940,-0.401250 3.375395,8.985695,-0.401250
3.190191,9.053104,-0.401250 3.456905,9.809985,-0.401250 b
3.657594,9.736940,0.401250 3.375395,8.985695,0.401250
3.190191,9.053104,0.401250 3.456905,9.809985,0.401250
polyhedron prism a 3.456905,9.809985,-0.401250 3.190191,9.053104,-0.401250
3.003641,9.116696,-0.401250 3.254760,9.878894,-0.401250 b
3.456905,9.809985,0.401250 3.190191,9.053104,0.401250
3.003641,9.116696,0.401250 3.254760,9.878894,0.401250
polyhedron prism a 3.254760,9.878894,-0.401250 3.003641,9.116696,-0.401250
2.815826,9.176444,-0.401250 3.051242,9.943637,-0.401250 b
3.254760,9.878894,0.401250 3.003641,9.116696,0.401250
2.815826,9.176444,0.401250 3.051242,9.943637,0.401250
polyhedron prism a 3.051242,9.943637,-0.401250 2.815826,9.176444,-0.401250
2.626823,9.232324,-0.401250 2.846437,10.004189,-0.401250 b
3.051242,9.943637,0.401250 2.815826,9.176444,0.401250
2.626823,9.232324,0.401250 2.846437,10.004189,0.401250
polyhedron prism a 2.846437,10.004189,-0.401250 2.626823,9.232324,-0.401250
2.436712,9.284311,-0.401250 2.640433,10.060523,-0.401250 b
2.846437,10.004189,0.401250 2.626823,9.232324,0.401250
2.436712,9.284311,0.401250 2.640433,10.060523,0.401250
polyhedron prism a 2.640433,10.060523,-0.401250 2.436712,9.284311,-0.401250
2.245575,9.332384,-0.401250 2.433315,10.112615,-0.401250 b
2.640433,10.060523,0.401250 2.436712,9.284311,0.401250
2.245575,9.332384,0.401250 2.433315,10.112615,0.401250
polyhedron prism a 2.433315,10.112615,-0.401250 2.245575,9.332384,-0.401250
2.053490,9.376523,-0.401250 2.225171,10.160444,-0.401250 b
2.433315,10.112615,0.401250 2.245575,9.332384,0.401250
2.053490,9.376523,0.401250 2.225171,10.160444,0.401250
polyhedron prism a 2.225171,10.160444,-0.401250 2.053490,9.376523,-0.401250
1.860540,9.416708,-0.401250 2.016090,10.203989,-0.401250 b
2.225171,10.160444,0.401250 2.053490,9.376523,0.401250
1.860540,9.416708,0.401250 2.016090,10.203989,0.401250
polyhedron prism a 2.016090,10.203989,-0.401250 1.860540,9.416708,-0.401250
1.666805,9.452923,-0.401250 1.806158,10.243232,-0.401250 b
2.016090,10.203989,0.401250 1.860540,9.416708,0.401250
1.666805,9.452923,0.401250 1.806158,10.243232,0.401250
polyhedron prism a 1.806158,10.243232,-0.401250 1.666805,9.452923,-0.401250
1.472368,9.485153,-0.401250 1.595465,10.278156,-0.401250 b
1.806158,10.243232,0.401250 1.666805,9.452923,0.401250
1.472368,9.485153,0.401250 1.595465,10.278156,0.401250
polyhedron prism a 1.595465,10.278156,-0.401250 1.472368,9.485153,-0.401250
1.277310,9.513384,-0.401250 1.384099,10.308747,-0.401250 b

1.595465,10.278156,0.401250 1.472368,9.485153,0.401250
1.277310,9.513384,0.401250 1.384099,10.308747,0.401250
polyhedron prism a 1.384099,10.308747,-0.401250 1.277310,9.513384,-0.401250
1.081714,9.537604,-0.401250 1.172150,10.334992,-0.401250 b
1.384099,10.308747,0.401250 1.277310,9.513384,0.401250
1.081714,9.537604,0.401250 1.172150,10.334992,0.401250
polyhedron prism a 1.172150,10.334992,-0.401250 1.081714,9.537604,-0.401250
0.885661,9.557803,-0.401250 0.959706,10.356880,-0.401250 b
1.172150,10.334992,0.401250 1.081714,9.537604,0.401250
0.885661,9.557803,0.401250 0.959706,10.356880,0.401250
polyhedron prism a 0.959706,10.356880,-0.401250 0.885661,9.557803,-0.401250
0.689235,9.573973,-0.401250 0.746858,10.374401,-0.401250 b
0.959706,10.356880,0.401250 0.885661,9.557803,0.401250
0.689235,9.573973,0.401250 0.746858,10.374401,0.401250
polyhedron prism a 0.746858,10.374401,-0.401250 0.689235,9.573973,-0.401250
0.492518,9.586106,-0.401250 0.533695,10.387549,-0.401250 b
0.746858,10.374401,0.401250 0.689235,9.573973,0.401250
0.492518,9.586106,0.401250 0.533695,10.387549,0.401250
polyhedron prism a 0.533695,10.387549,-0.401250 0.492518,9.586106,-0.401250
0.295594,9.594198,-0.401250 0.320307,10.396317,-0.401250 b
0.533695,10.387549,0.401250 0.492518,9.586106,0.401250
0.295594,9.594198,0.401250 0.320307,10.396317,0.401250
polyhedron prism a 0.320307,10.396317,-0.401250 0.295594,9.594198,-0.401250
0.098545,9.598244,-0.401250 0.106784,10.400702,-0.401250 b
0.320307,10.396317,0.401250 0.295594,9.594198,0.401250
0.098545,9.598244,0.401250 0.106784,10.400702,0.401250
polyhedron prism a 0.106784,10.400702,-0.401250 0.098545,9.598244,-0.401250 -
0.098545,9.598244,-0.401250 -0.106784,10.400702,-0.401250 b
0.106784,10.400702,0.401250 0.098545,9.598244,0.401250 -
0.098545,9.598244,0.401250 -0.106784,10.400702,0.401250
polyhedron prism a -0.106784,10.400702,-0.401250 -0.098545,9.598244,-0.401250 -
0.295594,9.594198,-0.401250 -0.320307,10.396317,-0.401250 b -
0.106784,10.400702,0.401250 -0.098545,9.598244,0.401250 -
0.295594,9.594198,0.401250 -0.320307,10.396317,0.401250
polyhedron prism a -0.320307,10.396317,-0.401250 -0.295594,9.594198,-0.401250 -
0.492518,9.586106,-0.401250 -0.533695,10.387549,-0.401250 b -
0.320307,10.396317,0.401250 -0.295594,9.594198,0.401250 -
0.492518,9.586106,0.401250 -0.533695,10.387549,0.401250
polyhedron prism a -0.533695,10.387549,-0.401250 -0.492518,9.586106,-0.401250 -
0.689235,9.573973,-0.401250 -0.746858,10.374401,-0.401250 b -
0.533695,10.387549,0.401250 -0.492518,9.586106,0.401250 -
0.689235,9.573973,0.401250 -0.746858,10.374401,0.401250

polyhedron prism a -0.746858,10.374401,-0.401250 -0.689235,9.573973,-0.401250 -0.885661,9.557803,-0.401250 -0.959706,10.356880,-0.401250 b -0.746858,10.374401,0.401250 -0.689235,9.573973,0.401250 -0.885661,9.557803,0.401250 -0.959706,10.356880,0.401250
polyhedron prism a -0.959706,10.356880,-0.401250 -0.885661,9.557803,-0.401250 -1.081714,9.537604,-0.401250 -1.172150,10.334992,-0.401250 b -0.959706,10.356880,0.401250 -0.885661,9.557803,0.401250 -1.081714,9.537604,0.401250 -1.172150,10.334992,0.401250
polyhedron prism a -1.172150,10.334992,-0.401250 -1.081714,9.537604,-0.401250 -1.277310,9.513384,-0.401250 -1.384099,10.308747,-0.401250 b -1.172150,10.334992,0.401250 -1.081714,9.537604,0.401250 -1.277310,9.513384,0.401250 -1.384099,10.308747,0.401250
polyhedron prism a -1.384099,10.308747,-0.401250 -1.277310,9.513384,-0.401250 -1.472368,9.485153,-0.401250 -1.595465,10.278156,-0.401250 b -1.384099,10.308747,0.401250 -1.277310,9.513384,0.401250 -1.472368,9.485153,0.401250 -1.595465,10.278156,0.401250
polyhedron prism a -1.595465,10.278156,-0.401250 -1.472368,9.485153,-0.401250 -1.666805,9.452923,-0.401250 -1.806158,10.243232,-0.401250 b -1.595465,10.278156,0.401250 -1.472368,9.485153,0.401250 -1.666805,9.452923,0.401250 -1.806158,10.243232,0.401250
polyhedron prism a -1.806158,10.243232,-0.401250 -1.666805,9.452923,-0.401250 -1.860540,9.416708,-0.401250 -2.016090,10.203989,-0.401250 b -1.806158,10.243232,0.401250 -1.666805,9.452923,0.401250 -1.860540,9.416708,0.401250 -2.016090,10.203989,0.401250
polyhedron prism a -2.016090,10.203989,-0.401250 -1.860540,9.416708,-0.401250 -2.053490,9.376523,-0.401250 -2.225171,10.160444,-0.401250 b -2.016090,10.203989,0.401250 -1.860540,9.416708,0.401250 -2.053490,9.376523,0.401250 -2.225171,10.160444,0.401250
polyhedron prism a -2.225171,10.160444,-0.401250 -2.053490,9.376523,-0.401250 -2.245575,9.332384,-0.401250 -2.433315,10.112615,-0.401250 b -2.225171,10.160444,0.401250 -2.053490,9.376523,0.401250 -2.245575,9.332384,0.401250 -2.433315,10.112615,0.401250
polyhedron prism a -2.433315,10.112615,-0.401250 -2.245575,9.332384,-0.401250 -2.436712,9.284311,-0.401250 -2.640433,10.060523,-0.401250 b -2.433315,10.112615,0.401250 -2.245575,9.332384,0.401250 -2.436712,9.284311,0.401250 -2.640433,10.060523,0.401250
polyhedron prism a -2.640433,10.060523,-0.401250 -2.436712,9.284311,-0.401250 -2.626823,9.232324,-0.401250 -2.846437,10.004189,-0.401250 b -2.640433,10.060523,0.401250 -2.436712,9.284311,0.401250 -2.626823,9.232324,0.401250 -2.846437,10.004189,0.401250
polyhedron prism a -2.846437,10.004189,-0.401250 -2.626823,9.232324,-0.401250 -2.815826,9.176444,-0.401250 -3.051242,9.943637,-0.401250 b -

2.846437,10.004189,0.401250 -2.626823,9.232324,0.401250 -
2.815826,9.176444,0.401250 -3.051242,9.943637,0.401250
polyhedron prism a -3.051242,9.943637,-0.401250 -2.815826,9.176444,-0.401250 -
3.003641,9.116696,-0.401250 -3.254760,9.878894,-0.401250 b -
3.051242,9.943637,0.401250 -2.815826,9.176444,0.401250 -
3.003641,9.116696,0.401250 -3.254760,9.878894,0.401250
polyhedron prism a -3.254760,9.878894,-0.401250 -3.003641,9.116696,-0.401250 -
3.190191,9.053104,-0.401250 -3.456905,9.809985,-0.401250 b -
3.254760,9.878894,0.401250 -3.003641,9.116696,0.401250 -
3.190191,9.053104,0.401250 -3.456905,9.809985,0.401250
polyhedron prism a -3.456905,9.809985,-0.401250 -3.190191,9.053104,-0.401250 -
3.375395,8.985695,-0.401250 -3.657594,9.736940,-0.401250 b -
3.456905,9.809985,0.401250 -3.190191,9.053104,0.401250 -
3.375395,8.985695,0.401250 -3.657594,9.736940,0.401250
polyhedron prism a -3.657594,9.736940,-0.401250 -3.375395,8.985695,-0.401250 -
3.559176,8.914497,-0.401250 -3.856740,9.659791,-0.401250 b -
3.657594,9.736940,0.401250 -3.375395,8.985695,0.401250 -
3.559176,8.914497,0.401250 -3.856740,9.659791,0.401250
polyhedron prism a -3.856740,9.659791,-0.401250 -3.559176,8.914497,-0.401250 -
3.741457,8.839542,-0.401250 -4.054260,9.578569,-0.401250 b -
3.856740,9.659791,0.401250 -3.559176,8.914497,0.401250 -
3.741457,8.839542,0.401250 -4.054260,9.578569,0.401250
polyhedron prism a -4.054260,9.578569,-0.401250 -3.741457,8.839542,-0.401250 -
3.922161,8.760859,-0.401250 -4.250071,9.493308,-0.401250 b -
4.054260,9.578569,0.401250 -3.741457,8.839542,0.401250 -
3.922161,8.760859,0.401250 -4.250071,9.493308,0.401250
polyhedron prism a -4.250071,9.493308,-0.401250 -3.922161,8.760859,-0.401250 -
4.101210,8.678483,-0.401250 -4.444091,9.404045,-0.401250 b -
4.250071,9.493308,0.401250 -3.922161,8.760859,0.401250 -
4.101210,8.678483,0.401250 -4.444091,9.404045,0.401250
polyhedron prism a -4.444091,9.404045,-0.401250 -4.101210,8.678483,-0.401250 -
4.278531,8.592449,-0.401250 -4.636236,9.310817,-0.401250 b -
4.444091,9.404045,0.401250 -4.101210,8.678483,0.401250 -
4.278531,8.592449,0.401250 -4.636236,9.310817,0.401250
polyhedron prism a -4.636236,9.310817,-0.401250 -4.278531,8.592449,-0.401250 -
4.454048,8.502791,-0.401250 -4.826427,9.213664,-0.401250 b -
4.636236,9.310817,0.401250 -4.278531,8.592449,0.401250 -
4.454048,8.502791,0.401250 -4.826427,9.213664,0.401250
polyhedron prism a -4.826427,9.213664,-0.401250 -4.454048,8.502791,-0.401250 -
4.627687,8.409549,-0.401250 -5.014583,9.112626,-0.401250 b -
4.826427,9.213664,0.401250 -4.454048,8.502791,0.401250 -
4.627687,8.409549,0.401250 -5.014583,9.112626,0.401250

```
polyhedron prism a -5.014583,9.112626,-0.401250 -4.627687,8.409549,-0.401250 -
4.799375,8.312761,-0.401250 -5.200625,9.007747,-0.401250 b -
5.014583,9.112626,0.401250 -4.627687,8.409549,0.401250 -
4.799375,8.312761,0.401250 -5.200625,9.007747,0.401250
;
;Define the support blocks with the same command
polyhedron prism a -5.9330,9.2763,-0.401250 -5.5000,9.5263,-0.401250 -
4.5000,7.7942,-0.401250 -4.9330,7.5442,-0.401250 b -5.9330,9.2763,0.401250 -
5.5000,9.5263,0.401250 -4.5000,7.7942,0.401250 -4.9330,7.5442,0.401250
polyhedron prism a 5.9330,9.2763,-0.401250 5.5000,9.5263,-0.401250
4.5000,7.7942,-0.401250 4.9330,7.5442,-0.401250 b 5.9330,9.2763,0.401250
5.5000,9.5263,0.401250 4.5000,7.7942,0.401250 4.9330,7.5442,0.401250
;Save the geometry with command save
save structure.sav
;
;Define the loading block 13 with the same command
polyhedron prism a -2.4333,10.1127,-0.401250 -2.4333,11.1127,-0.401250 -
2.6404,11.0606,-0.401250 -2.6404,10.0606,-0.401250 b -2.4333,10.1127,0.401250 -
2.4333,11.1127,0.401250 -2.6404,11.0606,0.401250 -2.6404,10.0606,0.401250
;
;Generate
gen edge 0.2
;
;Creat ranges
range name loadingblock id 35492
range name supportblock1 id 34869
range name supportblock2 id 34246
;
;Fix the support blocks
fix range supportblock1
fix range supportblock2
;
;Define the material properties of the blocks and joints
prop mat=1 density=2700. ymod 35.e9 prat 0.25
prop mat=2 density=100. ymod 35.e9 prat 0.25
change mat 2 range loadingblock
prop jmat=1 jkn 1.e11 jks 1.e11 jfri 30.
;
;Plot the structure_single-ring arch
plot block
;
;Apply gravity
```

```
gravity 0.0,-9.81,0.0
;
;history the unbalanced forces of the system
hist unbal id=1
cycle 1
plot hist 1 yaxis label 'Unbalanced force'
;
;Find the equilibrium under selfweight
cycle 50000
plot contour ydisp above au
plot contour xdisp above au
plot jointcontour sforce
plot jointcontour nforce
;
;Apply live loads_additional loading block with increasing density until the structure
collapsed
;plot block
;plot contour ydisp above au
;plot contour ydisp above au
;plot jointcontour sforce
;plot jointcontour nforce
prop mat=2 density=2089900. ymod 35.e9 prat 0.25
solve ratio 1.e-11
```

# Appendix C – 3DEC code of the segmental arch (60°) with 51blocks (Quasi-static load, 45-degree friction angle)

```
; Start the *3ddat file with the saved document "arch3.sav", which defines the geometry of the structure
restore arch3.sav
;Define the loading block 21 with the same command
polyhedron prism a -4.0543,9.5786,-0.401250 -4.0543,10.5786,-0.401250 -4.2501,10.4934,-0.401250 -4.2501,9.4934,-0.401250 b -4.0543,9.5786,0.401250 -4.0543,10.5786,0.401250 -4.2501,10.4934,0.401250 -4.2501,9.4934,0.401250
gen edge 0.2
;Creat ranges
range name loadingblock id 35492
range name supportblock1 id 34869
range name supportblock2 id 34246
;
;Fix the support blocks
fix range supportblock1
fix range supportblock2
;
;Define the material properties of the blocks and joints
prop mat=1 density=2700. ymod 35.e9 prat 0.25
prop mat=2 density=100. ymod 35.e9 prat 0.25
change mat 2 range loadingblock
prop jmat=1 jkn 1.e11 jks 1.e11 jfri 45.
;
;Plot the structure_single-ring arch
plot block
;
;Apply gravity
gravity 0.0,-9.81,0.0
;
;history the unbalanced forces of the system
hist unbal id=1
cycle 1
;
;Find the equilibrium under selfweight
cycle 50000
```

```
;
;Apply live loads_additional loading block with increasing density until the structure collapsed
prop mat=2 density=20000. ymod 35.e9 prat 0.25
solve ratio 1.e-9
prop mat=2 density=40000. ymod 35.e9 prat 0.25
solve ratio 1.e-9
prop mat=2 density=60000. ymod 35.e9 prat 0.25
solve ratio 1.e-9
prop mat=2 density=80000. ymod 35.e9 prat 0.25
solve ratio 1.e-9
prop mat=2 density=100000. ymod 35.e9 prat 0.25
solve ratio 1.e-9
prop mat=2 density=120000. ymod 35.e9 prat 0.25
solve ratio 1.e-9
prop mat=2 density=140000. ymod 35.e9 prat 0.25
solve ratio 1.e-9
prop mat=2 density=160000. ymod 35.e9 prat 0.25
solve ratio 1.e-9
prop mat=2 density=180000. ymod 35.e9 prat 0.25
solve ratio 1.e-9
prop mat=2 density=200000. ymod 35.e9 prat 0.25
solve ratio 1.e-9
prop mat=2 density=220000. ymod 35.e9 prat 0.25
solve ratio 1.e-9
prop mat=2 density=240000. ymod 35.e9 prat 0.25
solve ratio 1.e-9
prop mat=2 density=260000. ymod 35.e9 prat 0.25
solve ratio 1.e-9
prop mat=2 density=280000. ymod 35.e9 prat 0.25
solve ratio 1.e-9
prop mat=2 density=300000. ymod 35.e9 prat 0.25
solve ratio 1.e-9
prop mat=2 density=320000. ymod 35.e9 prat 0.25
solve ratio 1.e-9
prop mat=2 density=340000. ymod 35.e9 prat 0.25
solve ratio 1.e-9
prop mat=2 density=360000. ymod 35.e9 prat 0.25
solve ratio 1.e-9
prop mat=2 density=380000. ymod 35.e9 prat 0.25
solve ratio 1.e-9
prop mat=2 density=400000. ymod 35.e9 prat 0.25
```

```
solve ratio 1.e-9
prop mat=2 density=420000. ymod 35.e9 prat 0.25
solve ratio 1.e-9
prop mat=2 density=440000. ymod 35.e9 prat 0.25
solve ratio 1.e-9
prop mat=2 density=460000. ymod 35.e9 prat 0.25
solve ratio 1.e-9
prop mat=2 density=480000. ymod 35.e9 prat 0.25
solve ratio 1.e-9
prop mat=2 density=500000. ymod 35.e9 prat 0.25
solve ratio 1.e-9
prop mat=2 density=520000. ymod 35.e9 prat 0.25
solve ratio 1.e-9
prop mat=2 density=540000. ymod 35.e9 prat 0.25
solve ratio 1.e-9
prop mat=2 density=560000. ymod 35.e9 prat 0.25
solve ratio 1.e-9
prop mat=2 density=580000. ymod 35.e9 prat 0.25
solve ratio 1.e-9
prop mat=2 density=600000. ymod 35.e9 prat 0.25
solve ratio 1.e-9
prop mat=2 density=620000. ymod 35.e9 prat 0.25
solve ratio 1.e-9
prop mat=2 density=640000. ymod 35.e9 prat 0.25
solve ratio 1.e-9
prop mat=2 density=660000. ymod 35.e9 prat 0.25
solve ratio 1.e-9
prop mat=2 density=680000. ymod 35.e9 prat 0.25
solve ratio 1.e-9
prop mat=2 density=700000. ymod 35.e9 prat 0.25
solve ratio 1.e-9
prop mat=2 density=720000. ymod 35.e9 prat 0.25
solve ratio 1.e-9
prop mat=2 density=722000. ymod 35.e9 prat 0.25
solve ratio 1.e-9
prop mat=2 density=724000. ymod 35.e9 prat 0.25
solve ratio 1.e-9
prop mat=2 density=726000. ymod 35.e9 prat 0.25
solve ratio 1.e-9
prop mat=2 density=728000. ymod 35.e9 prat 0.25
solve ratio 1.e-9
prop mat=2 density=728100. ymod 35.e9 prat 0.25
```

```
solve ratio 1.e-9
prop mat=2 density=728200. ymod 35.e9 prat 0.25
solve ratio 1.e-9
prop mat=2 density=728300. ymod 35.e9 prat 0.25
solve ratio 1.e-9
prop mat=2 density=728400. ymod 35.e9 prat 0.25
solve ratio 1.e-9
prop mat=2 density=728500. ymod 35.e9 prat 0.25
solve ratio 1.e-9
```

# Appendix D – 3DEC code of the segmental arch (60°) with 51blocks (travelling load, 40-degree friction angle)

```
; Start the *3ddat file with the saved document “arch3.sav", which defines the geometry of the structure
restore arch3.sav
;Define the loading block 20 with the same command
polyhedron prism a -3.8568,9.6598,-0.401250 -3.8568,10.6598,-0.401250 -4.0543,10.5786,-0.401250 -4.0543,9.5786,-0.401250 b -3.8568,9.6598,0.401250 -3.8568,10.6598,0.401250 -4.0543,10.5786,0.401250 -4.0543,9.5786,0.401250
;Define the loading block 21 with the same command
polyhedron prism a -4.0543,9.5786,-0.401250 -4.0543,10.5786,-0.401250 -4.2501,10.4934,-0.401250 -4.2501,9.4934,-0.401250 b -4.0543,9.5786,0.401250 -4.0543,10.5786,0.401250 -4.2501,10.4934,0.401250 -4.2501,9.4934,0.401250
;Define the loading block 22 with the same command
polyhedron prism a -4.2501,9.4934,-0.401250 -4.2501,10.4934,-0.401250 -4.4432,10.4021,-0.401250 -4.4432,9.4021,-0.401250 b -4.2501,9.4934,0.401250 -4.2501,10.4934,0.401250 -4.4432,10.4021,0.401250 -4.4432,9.4021,0.401250
;Define the loading block 23 with the same command
polyhedron prism a -4.4432,9.4021,-0.401250 -4.4432,10.4021,-0.401250 -4.6343,10.3069,-0.401250 -4.6343,9.3069,-0.401250 b -4.4432,9.4021,0.401250 -4.4432,10.4021,0.401250 -4.6343,10.3069,0.401250 -4.6343,9.3069,0.401250
;Define the loading block 24 with the same command
polyhedron prism a -4.6343,9.3069,-0.401250 -4.6343,10.3069,-0.401250 -4.8265,10.2137,-0.401250 -4.8265,9.2137,-0.401250 b -4.6343,9.3069,0.401250 -4.6343,10.3069,0.401250 -4.8265,10.2137,0.401250 -4.8265,9.2137,0.401250
;Define the loading block 25 with the same command
polyhedron prism a -4.8265,9.2137,-0.401250 -4.8265,10.2137,-0.401250 -5.0146,10.1127,-0.401250 -5.0146,9.1127,-0.401250 b -4.8265,9.2137,0.401250 -4.8265,10.2137,0.401250 -5.0146,10.1127,0.401250 -5.0146,9.1127,0.401250
;Define the loading block 26 with the same command
polyhedron prism a -5.0146,9.1127,-0.401250 -5.0146,10.1127,-0.401250 -5.2006,10.0078,-0.401250 -5.2006,9.0078,-0.401250 b -5.0146,9.1127,0.401250 -5.0146,10.1127,0.401250 -5.2006,10.0078,0.401250 -5.2006,9.0078,0.401250
;
gen edge 0.2
;
;Creat ranges
range name loadingblock20 id 35492
range name loadingblock21 id 36199
```

```
range name loadingblock22 id 36948
range name loadingblock23 id 37697
range name loadingblock24 id 38446
range name loadingblock25 id 39195
range name loadingblock26 id 39944
range name supportblock1 id 34869
range name supportblock2 id 34246
;
;Fix the support blocks
fix range supportblock1
fix range supportblock2
;
;Define the material properties of the blocks and joints
prop mat=1 density=2700. ymod 35.e9 prat 0.25
prop mat=2 density=10. ymod 35.e9 prat 0.25
prop mat=3 density=10. ymod 35.e9 prat 0.25
prop mat=4 density=10. ymod 35.e9 prat 0.25
prop mat=5 density=10. ymod 35.e9 prat 0.25
prop mat=6 density=10. ymod 35.e9 prat 0.25
prop mat=7 density=10. ymod 35.e9 prat 0.25
prop mat=8 density=10. ymod 35.e9 prat 0.25
change mat 2 range loadingblock20
change mat 3 range loadingblock21
change mat 4 range loadingblock22
change mat 5 range loadingblock23
change mat 6 range loadingblock24
change mat 7 range loadingblock25
change mat 8 range loadingblock26
prop jmat=1 jkn 1.e11 jks 1.e11 jfri 40.
;
;Plot the structure_single-ring arch
plot block
;
;Apply gravity
gravity 0.0,-9.81,0.0
;
;history the unbalanced forces of the system
hist unbal id=1
cycle 1
;
;Find the equilibrium under selfweight
cycle 100000
```

```
;
;Apply travelling loads_additional loading block with increasing and decreasing densities until the total load is applied to the critical position, check when the structure collapse
prop mat=8 density=713954.374 ymod 35.e9 prat 0.25
solve ratio 1.e-10
;
prop mat=8 density=611960.892 ymod 35.e9 prat 0.25
prop mat=7 density=100640.783 ymod 35.e9 prat 0.25
solve ratio 1.e-10
;
prop mat=8 density=509967.410 ymod 35.e9 prat 0.25
prop mat=7 density=201281.566 ymod 35.e9 prat 0.25
solve ratio 1.e-10
;
prop mat=8 density=407973.928 ymod 35.e9 prat 0.25
prop mat=7 density=301922.349 ymod 35.e9 prat 0.25
solve ratio 1.e-10
;
prop mat=8 density=305980.446 ymod 35.e9 prat 0.25
prop mat=7 density=402563.132 ymod 35.e9 prat 0.25
solve ratio 1.e-10
;
prop mat=8 density=203986.964 ymod 35.e9 prat 0.25
prop mat=7 density=503203.915 ymod 35.e9 prat 0.25
solve ratio 1.e-10
;
prop mat=8 density=101993.482 ymod 35.e9 prat 0.25
prop mat=7 density=603844.698 ymod 35.e9 prat 0.25
solve ratio 1.e-10
;
prop mat=8 density=10. ymod 35.e9 prat 0.25
prop mat=7 density=704485.481 ymod 35.e9 prat 0.25
solve ratio 1.e-10
;
prop mat=7 density=603844.698 ymod 35.e9 prat 0.25
prop mat=6 density=99741.26 ymod 35.e9 prat 0.25
solve ratio 1.e-10
;
prop mat=7 density=503203.915 ymod 35.e9 prat 0.25
prop mat=6 density=199482.52 ymod 35.e9 prat 0.25
solve ratio 1.e-10
```

```
;
prop mat=7 density=402563.132 ymod 35.e9 prat 0.25
prop mat=6 density=299223.78 ymod 35.e9 prat 0.25
solve ratio 1.e-10
;
prop mat=7 density=301922.349 ymod 35.e9 prat 0.25
prop mat=6 density=398965.04 ymod 35.e9 prat 0.25
solve ratio 1.e-10
;
prop mat=7 density=201281.566 ymod 35.e9 prat 0.25
prop mat=6 density=498706.3 ymod 35.e9 prat 0.25
solve ratio 1.e-10
;
prop mat=7 density=100640.783 ymod 35.e9 prat 0.25
prop mat=6 density=598447.56 ymod 35.e9 prat 0.25
solve ratio 1.e-10
;
prop mat=7 density=10. ymod 35.e9 prat 0.25
prop mat=6 density=698188.82 ymod 35.e9 prat 0.25
solve ratio 1.e-10
;
prop mat=6 density=598447.56 ymod 35.e9 prat 0.25
prop mat=5 density=98498.378 ymod 35.e9 prat 0.25
solve ratio 1.e-10
;
prop mat=6 density=498706.3 ymod 35.e9 prat 0.25
prop mat=5 density=196996.756 ymod 35.e9 prat 0.25
solve ratio 1.e-10
;
prop mat=6 density=398965.04 ymod 35.e9 prat 0.25
prop mat=5 density=295495.134 ymod 35.e9 prat 0.25
solve ratio 1.e-10
;
prop mat=6 density=299223.78 ymod 35.e9 prat 0.25
prop mat=5 density=393993.512 ymod 35.e9 prat 0.25
solve ratio 1.e-10
;
prop mat=6 density=199482.52 ymod 35.e9 prat 0.25
prop mat=5 density=492491.89 ymod 35.e9 prat 0.25
solve ratio 1.e-10
;
prop mat=6 density=99741.26 ymod 35.e9 prat 0.25
```

```
prop mat=5 density=590990.268 ymod 35.e9 prat 0.25
solve ratio 1.e-10
;
prop mat=6 density=10. ymod 35.e9 prat 0.25
prop mat=5 density=689488.646 ymod 35.e9 prat 0.25
solve ratio 1.e-10
;
prop mat=5 density=590990.268 ymod 35.e9 prat 0.25
prop mat=4 density=97787.565 ymod 35.e9 prat 0.25
solve ratio 1.e-10
;
prop mat=5 density=492491.89 ymod 35.e9 prat 0.25
prop mat=4 density=195575.13 ymod 35.e9 prat 0.25
solve ratio 1.e-10
;
prop mat=5 density=393993.512 ymod 35.e9 prat 0.25
prop mat=4 density=293362.695 ymod 35.e9 prat 0.25
solve ratio 1.e-10
;
prop mat=5 density=295495.134 ymod 35.e9 prat 0.25
prop mat=4 density=391150.26 ymod 35.e9 prat 0.25
solve ratio 1.e-10
;
prop mat=5 density=196996.756 ymod 35.e9 prat 0.25
prop mat=4 density=488937.825 ymod 35.e9 prat 0.25
solve ratio 1.e-10
;
prop mat=5 density=98498.378 ymod 35.e9 prat 0.25
prop mat=4 density=586725.39 ymod 35.e9 prat 0.25
solve ratio 1.e-10
;
prop mat=5 density=10. ymod 35.e9 prat 0.25
prop mat=4 density=684512.955 ymod 35.e9 prat 0.25
solve ratio 1.e-10
;
prop mat=4 density=586725.39 ymod 35.e9 prat 0.25
prop mat=3 density=96888.599 ymod 35.e9 prat 0.25
solve ratio 1.e-10
;
prop mat=4 density=488937.825 ymod 35.e9 prat 0.25
prop mat=3 density=193777.198 ymod 35.e9 prat 0.25
solve ratio 1.e-10
```

```
;
prop mat=4 density=391150.26 ymod 35.e9 prat 0.25
prop mat=3 density=290665.797 ymod 35.e9 prat 0.25
solve ratio 1.e-10
;
prop mat=4 density=293362.695 ymod 35.e9 prat 0.25
prop mat=3 density=387554.396 ymod 35.e9 prat 0.25
solve ratio 1.e-10
;
prop mat=4 density=195575.13 ymod 35.e9 prat 0.25
prop mat=3 density=484442.995 ymod 35.e9 prat 0.25
solve ratio 1.e-10
;
prop mat=4 density=97787.565 ymod 35.e9 prat 0.25
prop mat=3 density=581331.594 ymod 35.e9 prat 0.25
solve ratio 1.e-10
;
prop mat=4 density=10. ymod 35.e9 prat 0.25
prop mat=3 density=678220.193 ymod 35.e9 prat 0.25
solve ratio 1.e-10
;
prop mat=3 density=581331.594 ymod 35.e9 prat 0.25
prop mat=2 density=96054.621 ymod 35.e9 prat 0.25
solve ratio 1.e-10
;
prop mat=3 density=484442.995 ymod 35.e9 prat 0.25
prop mat=2 density=192109.242 ymod 35.e9 prat 0.25
solve ratio 1.e-10
;
prop mat=3 density=387554.396 ymod 35.e9 prat 0.25
prop mat=2 density=288163.863 ymod 35.e9 prat 0.25
solve ratio 1.e-10
;
prop mat=3 density=290665.797 ymod 35.e9 prat 0.25
prop mat=2 density=384218.484 ymod 35.e9 prat 0.25
solve ratio 1.e-10
;
prop mat=3 density=193777.198 ymod 35.e9 prat 0.25
prop mat=2 density=480273.105 ymod 35.e9 prat 0.25
solve ratio 1.e-10
;
prop mat=3 density=96888.599 ymod 35.e9 prat 0.25
```

```
prop mat=2 density=576327.726 ymod 35.e9 prat 0.25
solve ratio 1.e-10
;
prop mat=3 density=10. ymod 35.e9 prat 0.25
prop mat=2 density=672382.347 ymod 35.e9 prat 0.25
solve ratio 1.e-10
```

# Appendix E – Setting of blocks' densities in 3DEC running travelling load

*The unit of density is kg/m$^3$.

1) Arch1

| material no. | 7 | 6 | 5 | 4 | 3 | 2 |
|---|---|---|---|---|---|---|
| loading block no. | 8 | 7 | 1 | 2 | 3 | 4 |
| 1 | 18412.55 | 10 | 10 | 10 | 10 | 10 |
| 2 | 15782.18 | 2538.785 | 10 | 10 | 10 | 10 |
| 3 | 13151.82 | 5077.569 | 10 | 10 | 10 | 10 |
| 4 | 10521.46 | 7616.354 | 10 | 10 | 10 | 10 |
| 5 | 7891.092 | 10155.14 | 10 | 10 | 10 | 10 |
| 6 | 5260.728 | 12693.92 | 10 | 10 | 10 | 10 |
| 7 | 2630.364 | 15232.71 | 10 | 10 | 10 | 10 |
| 8 | 10 | 17771.49 | 10 | 10 | 10 | 10 |
| 9 | 10 | 15232.71 | 2484.325 | 10 | 10 | 10 |
| 10 | 10 | 12693.92 | 4968.65 | 10 | 10 | 10 |
| 11 | 10 | 10155.14 | 7452.974 | 10 | 10 | 10 |
| 12 | 10 | 7616.354 | 9937.299 | 10 | 10 | 10 |
| 13 | 10 | 5077.569 | 12421.62 | 10 | 10 | 10 |
| 14 | 10 | 2538.785 | 14905.95 | 10 | 10 | 10 |
| 15 | 10 | 10 | 17390.27 | 10 | 10 | 10 |
| 16 | 10 | 10 | 14905.95 | 2441.199 | 10 | 10 |
| 17 | 10 | 10 | 12421.62 | 4882.398 | 10 | 10 |
| 18 | 10 | 10 | 9937.299 | 7323.597 | 10 | 10 |
| 19 | 10 | 10 | 7452.974 | 9764.796 | 10 | 10 |
| 20 | 10 | 10 | 4968.65 | 12206 | 10 | 10 |
| 21 | 10 | 10 | 2484.325 | 14647.19 | 10 | 10 |
| 22 | 10 | 10 | 10 | 17088.39 | 10 | 10 |
| 23 | 10 | 10 | 10 | 14647.19 | 2408.352 | 10 |
| 24 | 10 | 10 | 10 | 12206 | 4816.703 | 10 |
| 25 | 10 | 10 | 10 | 9764.796 | 7225.055 | 10 |
| 26 | 10 | 10 | 10 | 7323.597 | 9633.406 | 10 |
| 27 | 10 | 10 | 10 | 4882.398 | 12041.76 | 10 |
| 28 | 10 | 10 | 10 | 2441.199 | 14450.11 | 10 |
| 29 | 10 | 10 | 10 | 10 | 16858.46 | 10 |
| 30 | 10 | 10 | 10 | 10 | 14450.11 | 2385.735 |
| 31 | 10 | 10 | 10 | 10 | 12041.76 | 4771.469 |
| 32 | 10 | 10 | 10 | 10 | 9633.406 | 7157.204 |

| | | | | | | |
|---|---|---|---|---|---|---|
| 33 | 10 | 10 | 10 | 10 | 7225.055 | 9542.938 |
| 34 | 10 | 10 | 10 | 10 | 4816.703 | 11928.67 |
| 35 | 10 | 10 | 10 | 10 | 2408.352 | 14314.41 |
| 36 | 10 | 10 | 10 | 10 | 10 | 16700.14 |

2) Arch2

| material no. | 5 | 4 | 3 | 2 |
|---|---|---|---|---|
| loading block no. | 13 | 12 | 11 | 10 |
| 1 | 118247.22 | 10 | 10 | 10 |
| 2 | 106422.498 | 11581.074 | 10 | 10 |
| 3 | 94597.776 | 23162.148 | 10 | 10 |
| 4 | 82773.054 | 34743.222 | 10 | 10 |
| 5 | 70948.332 | 46324.296 | 10 | 10 |
| 6 | 59123.61 | 57905.37 | 10 | 10 |
| 7 | 47298.888 | 69486.444 | 10 | 10 |
| 8 | 35474.166 | 81067.518 | 10 | 10 |
| 9 | 23649.444 | 92648.592 | 10 | 10 |
| 10 | 11824.722 | 104229.666 | 10 | 10 |
| 11 | 10 | 115810.74 | 10 | 10 |
| 12 | 10 | 104229.666 | 11361.905 | 10 |
| 13 | 10 | 92648.592 | 22723.81 | 10 |
| 14 | 10 | 81067.518 | 34085.715 | 10 |
| 15 | 10 | 69486.444 | 45447.62 | 10 |
| 16 | 10 | 57905.37 | 56809.525 | 10 |
| 17 | 10 | 46324.296 | 68171.43 | 10 |
| 18 | 10 | 34743.222 | 79533.335 | 10 |
| 19 | 10 | 23162.148 | 90895.24 | 10 |
| 20 | 10 | 11581.074 | 102257.145 | 10 |
| 21 | 10 | 10 | 113619.05 | 10 |
| 22 | 10 | 10 | 102257.145 | 11090.021 |
| 23 | 10 | 10 | 90895.24 | 22180.042 |
| 24 | 10 | 10 | 79533.335 | 33270.063 |
| 25 | 10 | 10 | 68171.43 | 44360.084 |
| 26 | 10 | 10 | 56809.525 | 55450.105 |
| 27 | 10 | 10 | 45447.62 | 66540.126 |
| 28 | 10 | 10 | 34085.715 | 77630.147 |
| 29 | 10 | 10 | 22723.81 | 88720.168 |
| 30 | 10 | 10 | 11361.905 | 99810.189 |
| 31 | 10 | 10 | 10 | 110900.21 |

3) Arch3 (friction angle = 30° )

| material no. | 3 | 2 |
|---|---|---|

| loading block no. | 26 | 25 |
|---|---|---|
| 1 | 440441.55 | 10 |
| 2 | 396397.395 | 43460.015 |
| 3 | 352353.24 | 86920.03 |
| 4 | 308309.085 | 130380.045 |
| 5 | 264264.93 | 173840.06 |
| 6 | 220220.775 | 217300.075 |
| 7 | 176176.62 | 260760.09 |
| 8 | 132132.465 | 304220.105 |
| 9 | 88088.31 | 347680.12 |
| 10 | 44044.155 | 391140.135 |
| 11 | 10 | 434600.15 |

4) Arch3 (friction angle = 40° )

| material no. | 8 | 7 | 6 | 5 | 4 | 3 | 2 |
|---|---|---|---|---|---|---|---|
| loading block no. | 26 | 25 | 24 | 23 | 22 | 21 | 20 |
| 1 | 713954.4 | 10 | 10 | 10 | 10 | 10 | 10 |
| 2 | 611960.9 | 100640.8 | 10 | 10 | 10 | 10 | 10 |
| 3 | 509967.4 | 201281.6 | 10 | 10 | 10 | 10 | 10 |
| 4 | 407973.9 | 301922.3 | 10 | 10 | 10 | 10 | 10 |
| 5 | 305980.4 | 402563.1 | 10 | 10 | 10 | 10 | 10 |
| 6 | 203987 | 503203.9 | 10 | 10 | 10 | 10 | 10 |
| 7 | 101993.5 | 603844.7 | 10 | 10 | 10 | 10 | 10 |
| 8 | 10 | 704485.5 | 10 | 10 | 10 | 10 | 10 |
| 9 | 10 | 603844.7 | 99741.26 | 10 | 10 | 10 | 10 |
| 10 | 10 | 503203.9 | 199482.5 | 10 | 10 | 10 | 10 |
| 11 | 10 | 402563.1 | 299223.8 | 10 | 10 | 10 | 10 |
| 12 | 10 | 301922.3 | 398965 | 10 | 10 | 10 | 10 |
| 13 | 10 | 201281.6 | 498706.3 | 10 | 10 | 10 | 10 |
| 14 | 10 | 100640.8 | 598447.6 | 10 | 10 | 10 | 10 |
| 15 | 10 | 10 | 698188.8 | 10 | 10 | 10 | 10 |
| 16 | 10 | 10 | 598447.6 | 98498.38 | 10 | 10 | 10 |
| 17 | 10 | 10 | 498706.3 | 196996.8 | 10 | 10 | 10 |
| 18 | 10 | 10 | 398965 | 295495.1 | 10 | 10 | 10 |
| 19 | 10 | 10 | 299223.8 | 393993.5 | 10 | 10 | 10 |
| 20 | 10 | 10 | 199482.5 | 492491.9 | 10 | 10 | 10 |
| 21 | 10 | 10 | 99741.26 | 590990.3 | 10 | 10 | 10 |
| 22 | 10 | 10 | 10 | 689488.6 | 10 | 10 | 10 |
| 23 | 10 | 10 | 10 | 590990.3 | 97787.57 | 10 | 10 |
| 24 | 10 | 10 | 10 | 492491.9 | 195575.1 | 10 | 10 |
| 25 | 10 | 10 | 10 | 393993.5 | 293362.7 | 10 | 10 |
| 26 | 10 | 10 | 10 | 295495.1 | 391150.3 | 10 | 10 |

| | | | | | | | |
|---|---|---|---|---|---|---|---|
| 27 | 10 | 10 | 10 | 196996.8 | 488937.8 | 10 | 10 |
| 28 | 10 | 10 | 10 | 98498.38 | 586725.4 | 10 | 10 |
| 29 | 10 | 10 | 10 | 10 | 684513 | 10 | 10 |
| 30 | 10 | 10 | 10 | 10 | 586725.4 | 96888.6 | 10 |
| 31 | 10 | 10 | 10 | 10 | 488937.8 | 193777.2 | 10 |
| 32 | 10 | 10 | 10 | 10 | 391150.3 | 290665.8 | 10 |
| 33 | 10 | 10 | 10 | 10 | 293362.7 | 387554.4 | 10 |
| 34 | 10 | 10 | 10 | 10 | 195575.1 | 484443 | 10 |
| 35 | 10 | 10 | 10 | 10 | 97787.57 | 581331.6 | 10 |
| 36 | 10 | 10 | 10 | 10 | 10 | 678220.2 | 10 |
| 37 | 10 | 10 | 10 | 10 | 10 | 581331.6 | 96054.62 |
| 38 | 10 | 10 | 10 | 10 | 10 | 484443 | 192109.2 |
| 39 | 10 | 10 | 10 | 10 | 10 | 387554.4 | 288163.9 |
| 40 | 10 | 10 | 10 | 10 | 10 | 290665.8 | 384218.5 |
| 41 | 10 | 10 | 10 | 10 | 10 | 193777.2 | 480273.1 |
| 42 | 10 | 10 | 10 | 10 | 10 | 96888.6 | 576327.7 |
| 43 | 10 | 10 | 10 | 10 | 10 | 10 | 672382.3 |

5) Arch3 (friction angle = 45° )

| material no. | 8 | 7 | 6 | 5 | 4 | 3 | 2 |
|---|---|---|---|---|---|---|---|
| loading block no. | 26 | 25 | 24 | 23 | 22 | 21 | 20 |
| 1 | 713867 | 10 | 10 | 10 | 10 | 10 | 10 |
| 2 | 611886 | 100628.5 | 10 | 10 | 10 | 10 | 10 |
| 3 | 509905 | 201256.9 | 10 | 10 | 10 | 10 | 10 |
| 4 | 407924 | 301885.4 | 10 | 10 | 10 | 10 | 10 |
| 5 | 305943 | 402513.8 | 10 | 10 | 10 | 10 | 10 |
| 6 | 203962 | 503142.3 | 10 | 10 | 10 | 10 | 10 |
| 7 | 101981 | 603770.8 | 10 | 10 | 10 | 10 | 10 |
| 8 | 10 | 704399.2 | 10 | 10 | 10 | 10 | 10 |
| 9 | 10 | 603770.8 | 99729.05 | 10 | 10 | 10 | 10 |
| 10 | 10 | 503142.3 | 199458.1 | 10 | 10 | 10 | 10 |
| 11 | 10 | 402513.8 | 299187.1 | 10 | 10 | 10 | 10 |
| 12 | 10 | 301885.4 | 398916.2 | 10 | 10 | 10 | 10 |
| 13 | 10 | 201256.9 | 498645.2 | 10 | 10 | 10 | 10 |
| 14 | 10 | 100628.5 | 598374.3 | 10 | 10 | 10 | 10 |
| 15 | 10 | 10 | 698103.3 | 10 | 10 | 10 | 10 |
| 16 | 10 | 10 | 598374.3 | 98486.32 | 10 | 10 | 10 |
| 17 | 10 | 10 | 498645.2 | 196972.6 | 10 | 10 | 10 |
| 18 | 10 | 10 | 398916.2 | 295459 | 10 | 10 | 10 |
| 19 | 10 | 10 | 299187.1 | 393945.3 | 10 | 10 | 10 |
| 20 | 10 | 10 | 199458.1 | 492431.6 | 10 | 10 | 10 |
| 21 | 10 | 10 | 99729.05 | 590917.9 | 10 | 10 | 10 |

| | | | | | | | |
|---|---|---|---|---|---|---|---|
| 22 | 10 | 10 | 10 | 689404.2 | 10 | 10 | 10 |
| 23 | 10 | 10 | 10 | 590917.9 | 97775.59 | 10 | 10 |
| 24 | 10 | 10 | 10 | 492431.6 | 195551.2 | 10 | 10 |
| 25 | 10 | 10 | 10 | 393945.3 | 293326.8 | 10 | 10 |
| 26 | 10 | 10 | 10 | 295459 | 391102.4 | 10 | 10 |
| 27 | 10 | 10 | 10 | 196972.6 | 488878 | 10 | 10 |
| 28 | 10 | 10 | 10 | 98486.32 | 586653.6 | 10 | 10 |
| 29 | 10 | 10 | 10 | 10 | 684429.1 | 10 | 10 |
| 30 | 10 | 10 | 10 | 10 | 586653.6 | 96876.74 | 10 |
| 31 | 10 | 10 | 10 | 10 | 488878 | 193753.5 | 10 |
| 32 | 10 | 10 | 10 | 10 | 391102.4 | 290630.2 | 10 |
| 33 | 10 | 10 | 10 | 10 | 293326.8 | 387506.9 | 10 |
| 34 | 10 | 10 | 10 | 10 | 195551.2 | 484383.7 | 10 |
| 35 | 10 | 10 | 10 | 10 | 97775.59 | 581260.4 | 10 |
| 36 | 10 | 10 | 10 | 10 | 10 | 678137.2 | 10 |
| 37 | 10 | 10 | 10 | 10 | 10 | 581260.4 | 96042.86 |
| 38 | 10 | 10 | 10 | 10 | 10 | 484383.7 | 192085.7 |
| 39 | 10 | 10 | 10 | 10 | 10 | 387506.9 | 288128.6 |
| 40 | 10 | 10 | 10 | 10 | 10 | 290630.2 | 384171.4 |
| 41 | 10 | 10 | 10 | 10 | 10 | 193753.5 | 480214.3 |
| 42 | 10 | 10 | 10 | 10 | 10 | 96876.74 | 576257.2 |
| 43 | 10 | 10 | 10 | 10 | 10 | 10 | 672300 |

# Appendix F – Summary of failure loads in three programs

Note: the unit of failure load is kN
*Friction angle or masonry strength is shown in the row.

semicircular arch with 51 blocks

| position | 3-Dec | | | Archie-M | | RING | | | |
|---|---|---|---|---|---|---|---|---|---|
| | *30° | *40° | *45° | *5MPa | *10MPa | *20° | *30° | *40° | *45° |
| 0.500L | 48.149 | 48.409 | 48.409 | 41.5944 | 44.9298 | 6.42 | 49.5 | 49.5 | 49.5 |
| 0.467L | 43.972 | 43.972 | 43.972 | 39.6324 | 42.6735 | 6.4 | 46 | 46 | 46 |
| 0.434L | 43.399 | 43.399 | 43.399 | 39.0438 | 41.8887 | 6.94 | 44.6 | 44.6 | 44.6 |
| 0.401L | 44.021 | 44.021 | 44.021 | 37.8666 | 40.4172 | 7.74 | 45 | 45 | 45 |
| 0.368L | 45.968 | 45.968 | 45.968 | 38.9457 | 41.3001 | 8.72 | 46.9 | 46.9 | 46.9 |
| 0.336L | 49.662 | 49.662 | 49.662 | 41.7906 | 44.145 | 9.95 | 50.5 | 50.5 | 50.5 |

semicircular arch with 77 blocks

| position | 3-Dec | | | Archie-M | RING | | |
|---|---|---|---|---|---|---|---|
| | *30° | *40° | *45° | *5MPa | *30° | *40° | *45° |
| 0.500L | 47.359 | 47.359 | 47.359 | 4.24 | 47.9 | 47.9 | 47.9 |
| 0.456L | 41.515 | 41.515 | 41.515 | 3.92 | 44.3 | 44.3 | 44.3 |
| 0.434L | 41.832 | 41.832 | 41.832 | 3.84 | 43.9 | 43.9 | 43.9 |
| 0.412L | 44.814 | 44.814 | 44.814 | 3.97 | 46.2 | 46.2 | 46.2 |
| 0.369L | 51.096 | 51.096 | 51.096 | 4.26 | 51.3 | 51.3 | 51.3 |
| 0.327L | 61.534 | 61.534 | 61.534 | 4.74 | 59.9 | 59.9 | 59.9 |
| 0.286L | 78.108 | 78.108 | 78.108 | 5.86 | 73.1 | 73.1 | 73.1 |

120-degree embrace segmental arch with 51 blocks

| position | 3-Dec | | | Archie-M | | RING | | | |
|---|---|---|---|---|---|---|---|---|---|
| | *30 | *40 | *45 | *5MPa | *10MPa | *20 | *30 | *40 | *45 |
| 0.500L | 2105.879 | 2535.919 | 2634.944 | 459.108 | 689.643 | 176 | 3950 | 3950 | 3950 |
| 0.475L | 945.408 | 998.651 | 1013.806 | 373.761 | 512.082 | 166 | 921 | 921 | 921 |
| 0.449L | 566.18 | 575.928 | 577.917 | 318.825 | 405.153 | 159 | 544 | 544 | 544 |
| 0.424L | 402.088 | 403.672 | 404.266 | 282.528 | 340.407 | 154 | 399 | 399 | 399 |
| 0.399L | 319.359 | 319.949 | 320.146 | 240.345 | 276.642 | 151 | 324 | 324 | 324 |
| 0.374L | 270.428 | 270.428 | 270.428 | 212.877 | 238.383 | 149 | 280 | 280 | 280 |
| 0.349L | 258.668 | 259.083 | 259.083 | 196.2 | 216.801 | 149 | 253 | 253 | 253 |
| 0.329L | 222.476 | 222.476 | 222.476 | 189.333 | 206.991 | 142 | 240 | 240 | 240 |
| 0.301L | 217.847 | 217.654 | 217.654 | 175.599 | 189.333 | 150 | 225 | 225 | 225 |
| 0.277L | 207.589 | 206.651 | 206.651 | 166.77 | 178.542 | 150 | 220 | 220 | 220 |
| 0.254L | 209.576 | 209.576 | 209.576 | 162.846 | 173.637 | 151 | 219 | 219 | 219 |

| | | | | | | | | | |
|---|---|---|---|---|---|---|---|---|---|
| 0.230L | 208.663 | 208.663 | 208.663 | 163.827 | 173.637 | 154 | 222 | 222 | 222 |
| 0.208L | 217.202 | 217.906 | 217.202 | 161.865 | 169.713 | 158 | 228 | 228 | 228 |
| 0.186L | - | - | - | 160.884 | 168.8301 | 165 | 238 | 238 | 238 |
| 0.176L | - | - | - | 164.808 | 172.656 | - | - | - | - |
| 0.166L | - | - | - | 165.789 | 172.8522 | - | - | - | - |
| 0.156L | - | - | - | 166.77 | 174.618 | - | - | - | - |
| 0.146L | - | - | - | 172.656 | 180.9945 | - | - | - | - |

120-degree embrace segmental arch with 59 blocks

| position | 3-Dec | | | Archie-M | RING | | |
|---|---|---|---|---|---|---|---|
| | *30° | *40° | *45° | *5MPa | *30° | *40° | *45° |
| 0.500L | 1790.323 | 2158.229 | 2244.896 | 46.8 | 3390 | 3390 | 3390 |
| 0.478L | 931.867 | 1010.83 | 1031.346 | 39.4 | 984 | 984 | 984 |
| 0.456L | 693.154 | 624.522 | 625.556 | 35.7 | 594 | 594 | 594 |
| 0.434L | 436.575 | 442.579 | 443.094 | 29.3 | 437 | 437 | 437 |
| 0.391L | 293.363 | 293.363 | 293.363 | 24.4 | 303 | 303 | 303 |
| 0.348L | 236.769 | 236.769 | 236.769 | 19.9 | 248 | 248 | 248 |
| 0.306L | 210.027 | 210.027 | 210.027 | 17.9 | 224 | 224 | 224 |
| 0.265L | 204.736 | 204.736 | 204.736 | 17.2 | 216 | 216 | 216 |
| 0.225L | 209.553 | 209.553 | 209.553 | 16.4 | 220 | 220 | 220 |
| 0.187L | - | - | - | 16.4 | 236 | 236 | 236 |
| 0.150L | - | - | - | 17.3 | 271 | 271 | 271 |

60-degree embrace segmental arch with 51 blocks

| position | 3-Dec | | | Archie-M | | RING | | | |
|---|---|---|---|---|---|---|---|---|---|
| | *30 | *40 | *45 | *5MPa | *10MPa | *20 | *30 | *40 | *45 |
| 0.500L | 18245.47 | 30191.77 | 33568.7 | 546.417 | 1098.72 | | | | |
| 0.479L | 16282.6 | 28885.45 | 32880.34 | 534.645 | 1030.05 | | | | |
| 0.457L | 15950.73 | 28874.61 | 32865.27 | 500.31 | 981 | | | | |
| 0.436L | 12172.76 | 19553.96 | 24398.72 | 457.146 | 922.14 | | | | |
| 0.415L | 11268.73 | 18551.31 | 24487.5 | 446.355 | 922.14 | | Geometrically | | |
| 0.393L | 9886.435 | 17112.86 | 20513.29 | 410.058 | 824.04 | | locked | | |
| 0.372L | 9068.377 | 14194.13 | 17419.1 | 423.792 | 863.28 | | | | |
| 0.351L | 8342.006 | 12607.72 | 15942.85 | 385.533 | 774.99 | | | | |
| 0.330L | 7209.718 | 10947.69 | 13155.64 | 355.122 | 765.18 | | | | |
| 0.309L | 6181.294 | 8613.69 | 10032.31 | 321.768 | 608.22 | 48000 | | | |
| 0.288L | 5090.703 | 7103.116 | 7784.126 | 321.768 | 647.46 | 3840 | | | |
| 0.267L | 4179.421 | 5523.241 | 5749.044 | 328.635 | 598.41 | 2280 | | | |
| 0.246L | 3407.373 | 3920.786 | 4087.902 | 283.509 | 529.74 | 1550 | | | |
| 0.226L | 2547.754 | 2873.399 | 2956.594 | 305.091 | 519.93 | 1250 | 7300 | 7300 | 7300 |
| 0.205L | 1929.915 | 2093.563 | 2106.622 | 311.958 | 559.17 | 1010 | 2520 | 2520 | 2520 |

| | | | | | | | | | |
|---|---|---|---|---|---|---|---|---|---|
| 0.185L | 1489.915 | 1597.733 | 1621.604 | 333.54 | 559.17 | 880 | 1660 | 1660 | 1660 |
| 0.164L | 1253.101 | 1279.671 | 1287.467 | 311.958 | 519.93 | 777 | 1320 | 1320 | 1320 |
| 0.144L | 1256.903 | 1118.967 | 1121.811 | 348.255 | 588.6 | 716 | 1110 | 1180 | 1180 |
| 0.124L | 977.286 | 1045.782 | 1047.193 | 392.4 | 657.27 | 670 | 965 | 1140 | 1140 |
| 0.104L | 869.924 | 1040.643 | 1043.287 | 415.944 | 686.7 | 600 | 873 | 1210 | 1210 |
| 0.085L | 793.071 | 1121.244 | 1122.939 | 502.272 | 804.42 | 550 | 812 | 1250 | 1450 |
| 0.065L | 740.42 | 1147.743 | 1346.594 | 716.13 | 1152.675 | 509 | 761 | 1210 | 1590 |
| 0.046L | 701.265 | 1105.952 | 1454.234 | 1006.506 | 1667.7 | 477 | 722 | 1170 | 1590 |
| 0.027L | 657.638 | 1054.137 | 1410.208 | 2183.706 | 3619.89 | 453 | 696 | 1150 | 1600 |
| 0.008L | 644.489 | 1052.581 | 1450.582 | - | - | 465 | 719 | 1200 | 1660 |

RING - semicircular arch with 51 blocks – backfill depth

| position | 30° friction angle | | | 40° friction angle | | | 50° friction angle | | |
|---|---|---|---|---|---|---|---|---|---|
| | depth 0 | depth 500 | depth 1000 | depth 0 | depth 500 | depth 1000 | depth 0 | depth 500 | depth 1000 |
| 0.500L | 49.5 | 49.5 | 49.5 | 49.5 | 49.5 | 49.5 | 49.5 | 49.5 | 49.5 |
| 0.467L | 46 | 46 | 46 | 46 | 46 | 46 | 46 | 46 | 46 |
| 0.434L | 44.6 | 44.6 | 44.6 | 44.6 | 44.6 | 44.6 | 44.6 | 44.6 | 44.6 |
| 0.401L | 45 | 45 | 45 | 45 | 45 | 45 | 45 | 45 | 45 |
| 0.368L | 46.9 | 46.9 | 46.9 | 46.9 | 46.9 | 46.9 | 46.9 | 46.9 | 46.9 |
| 0.336L | 50.5 | 50.5 | 50.5 | 50.5 | 50.5 | 50.5 | 50.5 | 50.5 | 50.5 |

RING - 120° embrace segmental arch with 51 blocks - backfill depth

| positi on | 30° friction angle | | | 40° friction angle | | | 50° friction angle | | |
|---|---|---|---|---|---|---|---|---|---|
| | depth 0 | depth 500 | depth 1000 | depth 0 | depth 500 | depth 1000 | depth 0 | depth 500 | depth 1000 |
| 0.500L | 3950 | 3950 | 3950 | 3950 | 3950 | 3950 | 3950 | 3950 | 3950 |
| 0.475L | 921 | 921 | 921 | 921 | 921 | 921 | 921 | 921 | 921 |
| 0.449L | 544 | 544 | 544 | 544 | 544 | 544 | 544 | 544 | 544 |
| 0.424L | 399 | 399 | 399 | 399 | 399 | 399 | 399 | 399 | 399 |
| 0.399L | 324 | 324 | 324 | 324 | 324 | 324 | 324 | 324 | 324 |
| 0.374L | 280 | 280 | 280 | 280 | 280 | 280 | 280 | 280 | 280 |
| 0.349L | 253 | 253 | 253 | 253 | 253 | 253 | 253 | 253 | 253 |
| 0.329L | 240 | 240 | 240 | 240 | 240 | 240 | 240 | 240 | 240 |
| 0.301L | 225 | 225 | 225 | 225 | 225 | 225 | 225 | 225 | 225 |
| 0.277L | 220 | 220 | 220 | 220 | 220 | 220 | 220 | 220 | 220 |
| 0.254L | 219 | 219 | 219 | 219 | 219 | 219 | 219 | 219 | 219 |
| 0.230L | 222 | 222 | 222 | 222 | 222 | 222 | 222 | 222 | 222 |
| 0.208L | 228 | 228 | 228 | 228 | 228 | 228 | 228 | 228 | 228 |
| 0.186L | 238 | 238 | 238 | 238 | 238 | 238 | 238 | 238 | 238 |